Research Article

Shubham Sharma*, P. Sudhakara*, Michal Petru*, Jujhar Singh, and S. Rajkumar

Effect of nanoadditives on the novel leather fiber/recycled poly(ethylene-vinyl-acetate) polymer composites for multifunctional applications: Fabrication, characterizations, and multiobjective optimization using central composite design

https://doi.org/10.1515/ntrev-2022-0067
received November 25, 2021; accepted January 31, 2022

Abstract: The current study intended to investigate the viability and efficacy of performance measurement by incorporating one of the most hazardous leather wastes, that is, leather buffing dust and nanofillers as reinforcing constituents within recycled poly(ethylene-vinyl acetate) as a matrix with maximum leather fiber-loading of 1:1, using a mill followed by hot-press molding. The samples were tested to evaluate the physicomechanical characteristics including tensile, compressive strength, density, abrasion-resistance, adhesion-strength, hardness, tear-resistance, compression and resilience, damping, and water-absorption as per the standard ASTM/SATRA/ISO testing methods. The thermoanalytical methods, namely thermalgravimetric analysis and differential scanning calorimetry, have been employed to simulate the performance, including the effectiveness of blended-mix through glass-transition and crystallization temperature. Furthermore, morphological properties of the fabricated composites have been explored using scanning electron microscopy and energy-dispersive spectroscopy analysis. In addition, the attenuated total reflection-Fourier-transform infrared spectroscopy was performed to examine the physicochemical molecular structure, chemical bonding, and functional groups of the neat recycled EVA (ethylene-vinyl acetate) copolymer and leather buffing dust/recycled EVA polymer composites. Throughout this study, the physicomechanical characteristics of leather buffing dust/recycled EVA composites were ameliorated by optimizing the operating parameters of the hot-press compression molding process through the central composite design approach in response surface methodology. The obtained results of the fabricated novel composites were certainly splendid for a value-added application in footwear, structural, floor-covering, and transportation domains.

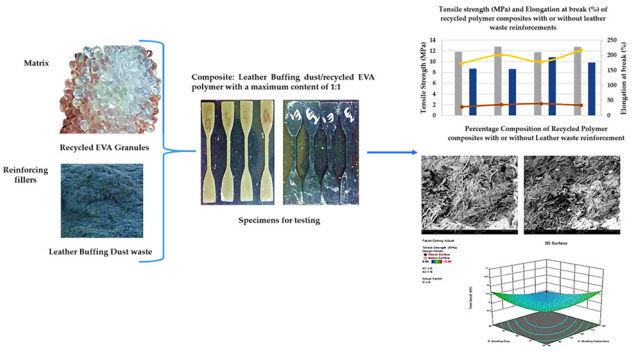

Graphical abstract

Keywords: recycled EVA, leather buffing dust, rolling and compression molding, central composite designs, footwear, and leather ancillaries(s) application

* **Corresponding author: Shubham Sharma,** PhD Research Scholar, Department of Mechanical Engineering, IK Gujral Punjab Technical University, Jalandhar-Kapurthala Road, Kapurthala 144603, Punjab, India; CSIR-Central Leather Research Institute, Regional Center Department, Jalandhar 144021, India, e-mail: shubham543sharma@gmail.com, tel: +91-7009239473
* **Corresponding author: P. Sudhakara,** CSIR-Central Leather Research Institute, RCED, Jalandhar 144021, India, e-mail: sudhakarp@clri.res.in
* **Corresponding author: Michal Petru,** Faculty of Mechanical Engineering, Technical University of Liberec, Studentská 2, 461 17 Liberec, Czech Republic, e-mail: michal.petru@tul.cz
Jujhar Singh: Department of Mechanical Engineering, IKGPTU, Jalandhar-Kapurthala Road, Kapurthala 144603, Punjab, India
S. Rajkumar: Department of Mechanical Engineering, Faculty of Manufacturing, Institute of Technology, Hawassa University, Hawassa, Ethiopia

Open Access. © 2022 Shubham Sharma *et al.*, published by De Gruyter. This work is licensed under the Creative Commons Attribution 4.0 International License.

Abbreviations

ARCFC	acrylate resin-based cotton fabric composites
CCD	central composite design
CF	carbon fiber
CP	catalytic pyrolysis
CRT	compression and resilience test
DMA	dynamic mechanical analysis
GF	glass fiber
HDI	hexamethylene diisocyanate
HDPE	high-density polyethylene
KF	Kevlar fiber
NFRCs	natural-fiber-reinforced composites
nHA	nanohydroxyapatite
PA66	polyamide 66
PBS	poly-butylene succinate
PE	polyethylene
PEEK	polyetheretherketone
PLA	poly-lactic acid
PMMA	poly(methyl-methacrylate)
PP	polypropylene
PPEO	poly(ethylene-oxide)
PS	polystyrene
PVC	polyvinyl chloride
RSM	response-surface methodology
TPT	trimethylolpropane triacrylate
ZrP	α-zirconium phosphate

1 Introduction

Leather is an essential global commodity. The leather sector plays a prominent role in the economy, with an estimated world trade value of leather, and leather products exceeding $200 billion per year. The leather sector gained significance in developing countries because of its export earnings and employment opportunities. However, the industry is frequently under threat due to solid and liquid wastes generated during the manufacture of leather [1]. The method of leather production generates large amounts of liquid and solid waste such as shavings, trimmings, buffing dust, process effluents, and sludge. The most popular approach to handling solid waste is land disposal [1,2].

Numerous waste-management alternatives strive to produce valuation to wastes *via* new technologies as well as materials [4–6]. An essential feature of the leather is its fibrous structure which possesses good tear resistance, flexibility, thermal insulation, resistance to water, and shape maintenance. Whenever solid leather-waste fibers were incorporated as particulate-reinforcing constituents in the polymer matrices, it offered exceptional characteristics to the material which made it acceptable for a multitude of applications. Outstanding thermal strength, resistance to tear, excellent resistance to stretching/flexing and perforation, resistance to fire as well as flames, resistance to chemical-attack, resistance to microorganisms, resistance to dry and wet abrasion, and permeation/penetrability and flowability to absorb a substantial volume of water-vapors are among some of the physicomechanical characteristics which make leather a distinctive choice for upholstery. The thermostatic characteristics of leather (leather gets cool during summer and warm during winters). Furthermore, leather possesses outstanding molding characteristics, enabling it to be made stiffer or flexible/pliable/softer. Vulcanizing characteristics and dimensional stability, both are offered by leather fibers. Moreover, leather is indeed a high thermal insulator and a low heat conductor. Whenever worn, leather indeed has elastic – viscous characteristics. Therefore, the addition of this leather waste (leather buffing dust in particular) into any suitable polymer matrix may produce composites of superior properties for a wide range of uses such as footwear, leather ancillaries, automotive, transportation, and packaging applications. The approach toward making useful products from waste material would have a synergetic effect on the environment as well as create value addition to the wastes generated from the leather and polymer industry, respectively. Many researchers have tried to convert solid leather wastes into different biocomposite materials such as films, sheets, and fibers by employing environment-friendly polymers as matrix materials [4,7–25].

The advancement, as well as the development of thermoplastic elastomeric (TPE)-based footwear and apparel, is dramatically booming. TPEs have paved the way for myriad variables and criteria to address customer demand [3,26–28]. Throughout the industrial footwear sector, ethylene-vinyl acetate (EVA) polymer is being used for inserts/soles, and midsoles contributing with a range of 18–28% of the overall. EVA has low compression set, abrasion, and tearing characteristics before incorporating a blend of natural rubber (NR) and butadiene rubber (BR), which offers superior mechanical properties, minimizes slippage, shrinkage, and provides a fierce compression set. In comparison to EVA/BR and EVA/NR, EVA/BR/NR offers outstanding physical and compression attributes, as well as a significant diminution in slippage. The EVA midsole is perhaps the most frequently utilized vibration-damping-based cushion

material for commercial athletic footwear and is employed to manufacture hiking boots, basketball shoes, and nearly any other sporting footwear. EVA is exceptionally lightweight, defies compression set, is readily accessible in nearly any color, and is conveniently manufactured.

For this study, leather buffing dust, one of the significant leather solid wastes, and recycled EVA polymer was identified, as it was produced in large quantities worldwide. Leather buffing dust is classified as a hazardous solid waste as it has trivalent chromium, which may be converted into toxic hexavalent chromium under abnormal conditions. The traditional disposal methods such as landfill and incineration cannot eliminate the hazardousness and easily create secondary pollution. Therefore, impregnation of this leather waste with recycled EVA polymer matrix may be an optimal solution to eliminate the hazardousness to a great extent. As learned from the literature survey, the combination of both recycled TPE polymers and leather solid waste is expected to produce composites with superior properties. To date, no work/data on the recycled EVA thermoplastic elastomer polymer matrix-based composites with a high amount of leather fiber as a filler of 1:1 ratio are available in the literature. Usually, the impregnation of leather with the polymer in higher quantities is a complex process. However, in this study, suitable additives such as lubricants/oils, paraffin, and naphthalene have been utilized to improve the homogeneity/proper blending of polymer and leather, thus producing composites of superior properties for desired multifunctional, value-added applications. A prominent implication of this study with the targeted objectives has been depicted in Table 1.

The manufacturing of prepared composite sheets has also been tested and validated to attain optimal results using the RSM approach. Three independent control parameters of hot-press molding *viz.* molding temperature (90–120°C), time (20–40 min), and pressure (5–7 tons) were optimized in connection with the physicomechanical characteristics of the leather buffing dust-reinforced recycled EVA polymer composites in the study. A series of experimental trial runs were designed by utilizing the CCD methodology depending on different formulations

Table 1: Objectives of this study

S. no.	Objectives
1	Basic characterizations of raw materials involving • Evaluation percentage of moisture content • Evaluation of the functional group analysis
2	To characterize Studies on the swelling behavior of the leather-filled composites in aqueous media. This is an important aspect of the materials developed as they may find applications in footwear materials for which properties such as water vapor absorption and desorption are important • Water-absorption behavior • Chrome-oxide detection and • Chemical composition analysis (Fourier-transform infrared spectroscopy (FTIR) with attenuated total reflection (ATR), UV-Vis spectroscopy) of the fabricated composite
3	To evaluate the Physicomechanical properties (tensile strength, compressive strength, density/volume displacement method); abrasion resistance, adhesion, hardness, and tear resistance); • Multiobjective optimization of the hot-press compression molding process operating parameters through central composite designs (CCD) approach in response surface methodology (RSM); • Thermal properties using thermogravimetric analysis (TGA) and differential scanning calorimeter to check the stability of the composites against the thermal load as the geometrical stability of the material under structural loading is significantly affected by material loss owing to thermal degradation
4	To examine the • Compression deformation properties and resilience energy using compression and resilience test (CRT, utilizing constant-stress method); • Elemental analysis (energy-dispersive analysis of X-ray, EDAX); fracture mechanism (studies on the distribution of leather fibers in the polymer matrix using scanning electron microscopic (SEM) analysis);
5	Comparison of the results with existing literature and to recommend the scope of the fabricated composites for suitable applications such as in leather ancillaries, footwear, packaging, automotive, construction, transportation, and machinery industries

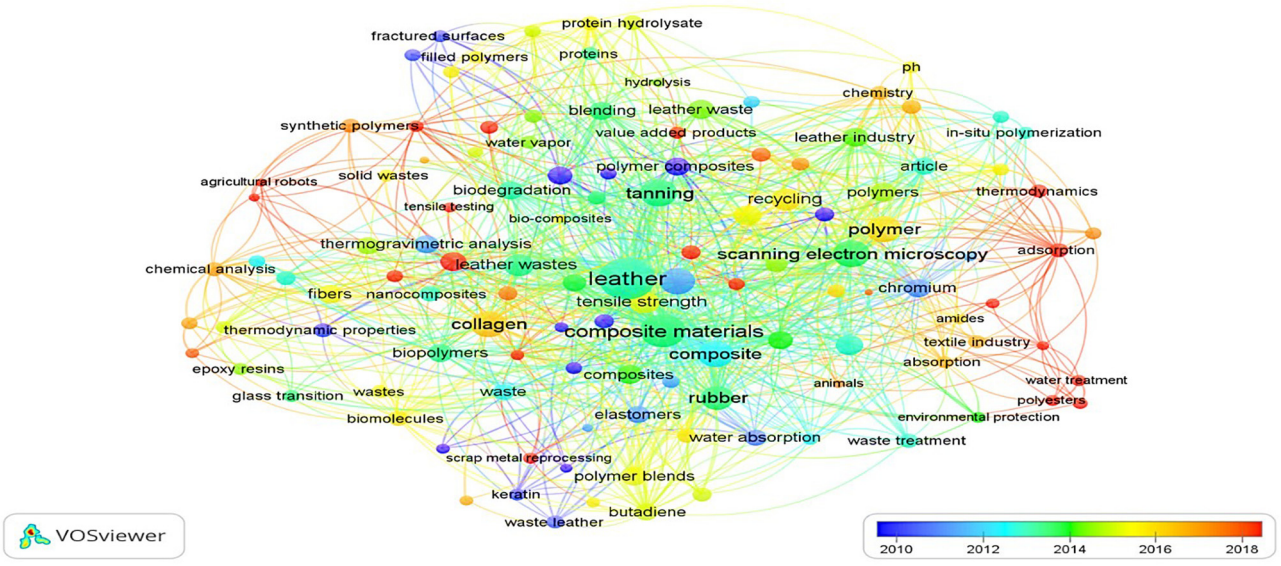

Figure 1: Mapping scientometrics analysis chart.

of the compression molding in design-expert software. The iterative optimal parametric levels have confirmed an adequate favorable response to the predictive mathematical model. As depicted in Figure 1, using the Vosviewer analytic framework, a bioinformatics mapping chart has also been developed, clearly showing that this study is reported for the first time.

Figure 2 illustrates the proposed research methodology to carry out the research work for leather buffing dust/recycled EVA polymeric composites.

2 Experimental set-up

2.1 Materials

Recycled EVA granules were obtained from one of the footwear industries, Laxmi Polymer, Bahadurgarh, Haryana, India. The solid leather wastes (buffing dust with a particulate size of 2–5 mm) were collected from the local tanneries of the leather complex in Jalandhar, Punjab, India, as illustrated in Figure 3(a) and (b). Fillers and plasticizers in a nanoscale range such as zinc octadecenoate and octadecanoic acid were procured from the impact agencies in Jalandhar, Punjab, India, which acts as a lubricant and allows solid leather fibers to blend appropriately with the recycled polymer matrix. During post-processing and finishing operation in the hot-press, polyvinyl alcohol (PVA), and polytetrafluoroethylene/teflon (PTFE) sheet, wrapped around steel molds are used as a mold-releasing agent which was obtained from the Sigma Aldrich Chemicals.

2.2 Preparation of composites

2.2.1 Fabrication of leather buffing dust/recycled EVA thermoplastic elastomer polymer composites

The formulations of leather polymer composites with recycled EVA polymer and buffing dust are taken in a 1:1 ratio (wt%). Figure 4 depicts the methodology of this study in a sequential manner.

The leather wastes were dried under direct sunlight for 5 h. It was found that the initial weight got reduced by 9% due to buffing dust. Also, the average particle size of leather buffing dust was 500 microns when measured using a particle size analyzer with propanol as a dispersant. The two-roll mill, commonly used for rubber compounding, was used to mix the components. To obtain optimum huge-shear blending, the two rolls were directed and positioned facing one another with a user-specified preset, customizable/configurable nip or gap to enable the materials to permeate or penetrate across at 368.15 K. The gap between the rollers has been maintained at 1–1.5 mm. The rear roll commonly turns faster than a front roll. Here, the rear roll has been made to rotate at a speed of 15 rpm and the front roll at 10 rpm. Dyes were prepared to fabricate the required flexible sheet of dimensions

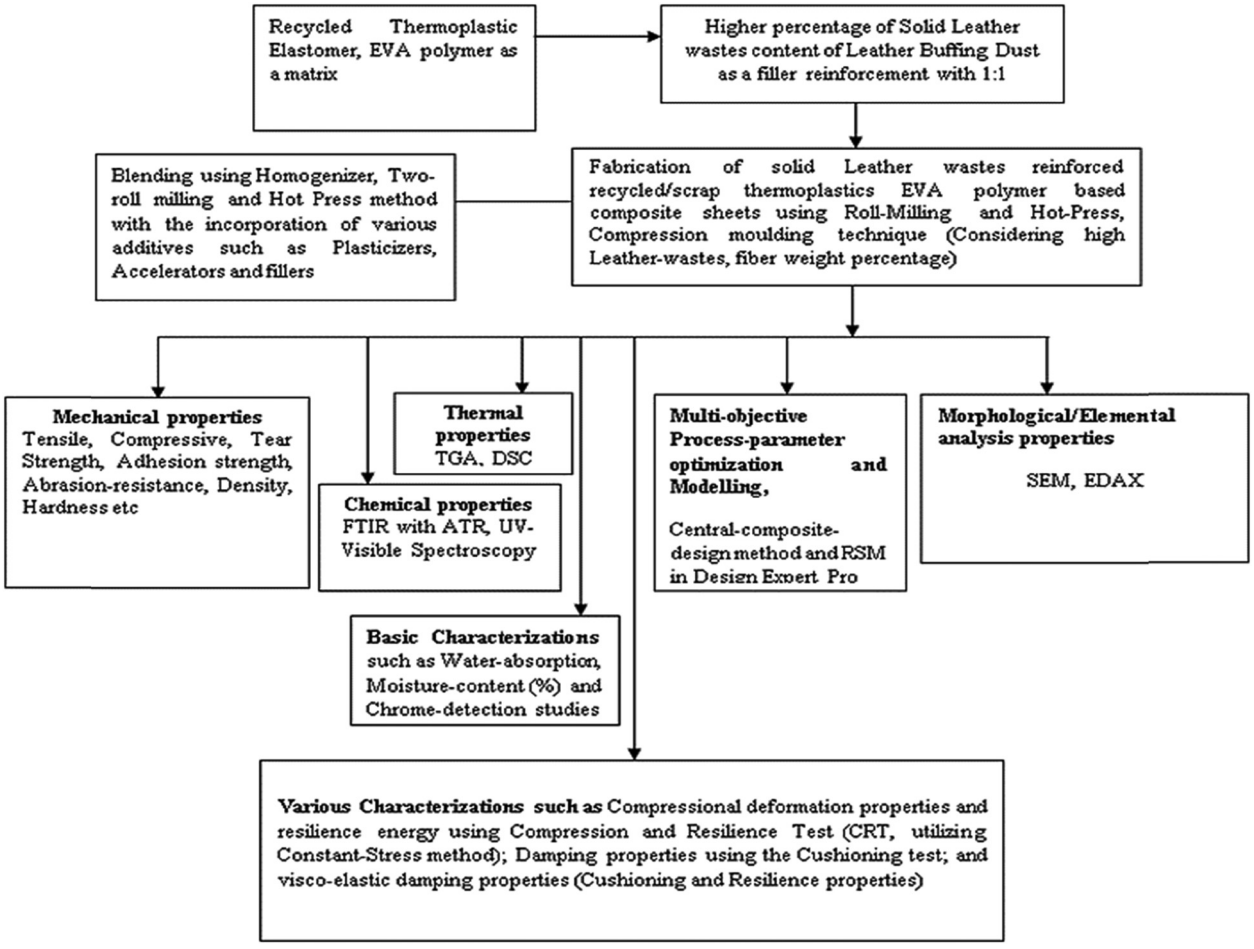

Figure 2: Research methodology was adopted in this study to achieve the set goals.

Figure 3: (a) Leather buffing dust employed as a reinforcing particulate; (b) recycled EVA granules as a matrix.

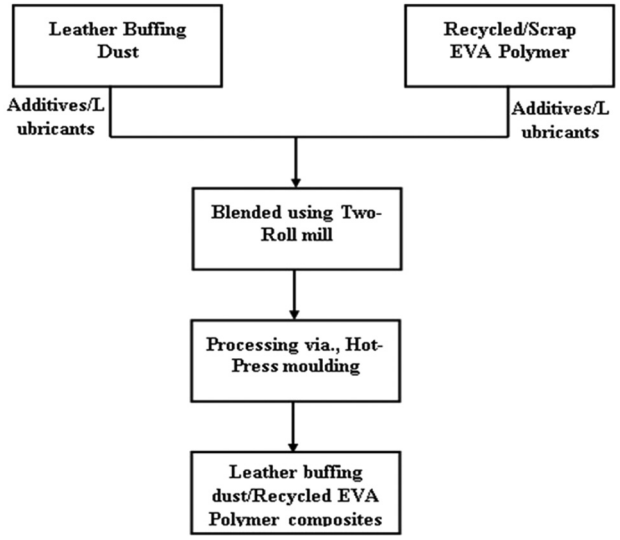

Figure 4: Flow chart representing the processing of solid leather wastes/recycled EVA thermoplastic elastomer polymer composites.

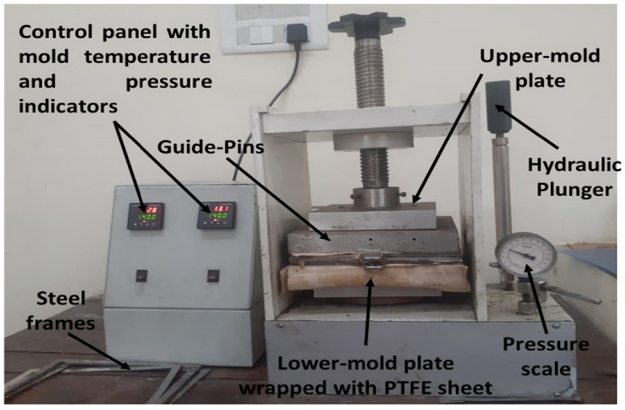

Figure 5: Hot-press compression molding.

185 mm × 185 mm × 3.5 mm. Materials were introduced in lower dyes following compounding. The dyes were heated to temperatures of 368.15 K. The upper dye is then compressed against the lower dye by applying a load of 20 tons, and it has been allowed to cool in the dye for 30 min. The compounded composite material was taken out of the dye with the aid of the ejector pin.

For the fabrication of flexible composites, mixing was done with the help of two roll mills at a particular temperature and pressure. The homogeneous mixture was transferred to a hot-press containing preheated molds with 20 cm × 20 cm length and breadth with variation in thickness of 1, 2, 3, and 5 mm as exhibited in Figure 5. Fillers and plasticizers were also used to optimize the processing parameters. The fine particulate matter-blended mix was transmitted to the hot-press, dye mold to achieve desired flexible viscoelastic damping

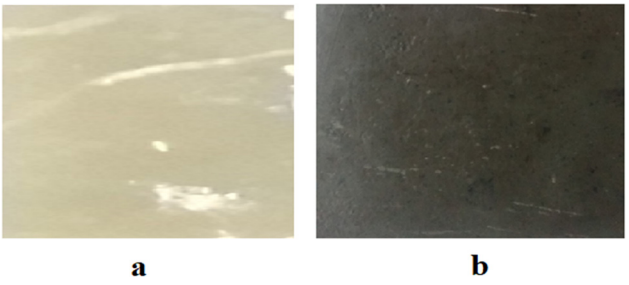

Figure 6: (a) Recycled EVA polymer without any leather waste fiber content or neat recycled EVA polymer; (b) fabricated leather buffing dust/recycled EVA thermoplastic composites.

composite sheets. The wet sheet formed was further pressed using a hydraulic press to remove additional water. The prepared leather fibrous composites were dried and hot-pressed between 90 and 120°C for 20–40 min at 77–108 psi as exhibited in Figure 6(a) and (b).

2.3 Specimen standards

ASTM/SATRA/ISO provides standards for characterization and performance of leather fibrous composite materials. The properties of materials vary with specimen preparation, specimen dimensions, and speed and environment of testing. In this study, a series of experimentation was the requirement; therefore, 3–5 samples were tested in each category, and various test methods and specimen standards used in this study are illustrated in Table 2. The specimens for each test were prepared as per ASTM/SATRA/ISO specifications, as illustrated in Table 2.

The fabricated SATRA testing standards were kept in a computerized Universal-testing machine (UTM). The specimen was kept at a proper spacing in the UTM and was pulled till it failed at the testing speed of 60 mm/min to calculate the elongation and strength of the material.

2.4 Characterizations

The neat recycled EVA polymer without any leather fiber and leather buffing dust/recycled EVA composites was cut into strips of various dimensions to suit the specimen standards as per ASTM/SATRA/ISO. The test-ready specimens were finally tested for their thickness, at least four randomly selected points were measured, and the results were averaged. The specimen dimensions for various mechanical tests as per ASTM/SATRA/ISO standards are indicated in Table 2. The specifications of the testing

Table 2: Standard test methods and specimen standards used in this study

S. no.	Test-type	ASTM/ISO/SATRA TM standards or sample dimensions
1	Tensile strength of polymer using INSTRON equipment, model 3369J7257, with an optical extensometer	SATRA TM-137 1995
2	Compressive strength of polymer using INSTRON equipment, model 3369J7257, with an optical extensometer	ASTM D-3410
3	Tear strength and extension of polymer using INSTRON equipment, model 3369J7257, with an optical extensometer	SATRA TM-218 1999/ISO 20344:2011
4	Adhesion strength of polymer	SATRA TM-401 2000
5	Compression set constant-relaxation method (CRT) stress	SATRA TM-64 1996
6	Abrasion resistance using rotating drum method, model STM-140, UK	ISO 20871:2001/TM-174:2016/ISO-20344 (8.3)/ISO 4649:20871
7	Density of polymers by displacement volume	SATRA TM-134:2010/ISO-2781:2018
8	Hardness of rubber and durometer method plastics	SATRA TM-205:2016/ISO 868:2013
9	Moisture content (%)	SATRA TM347:1996 and EN ISO 4684:2005
10	Water-absorption behavior of polymer composites	ASTM-D-570
11	Detection of chromium content using UV-Visible spectrophotometry	IUC 8 and 18 test standards
12	TGA TA Instruments, model Q-50	Powder form (1–5 g)
13	Differential scanning calorimetry (DSC) TA Instruments, model Q-200	Powder form (1–5 g)
14	FTIR–ATR using JASCO, FTIR-model 4700	Powder/Pellets form (1–5 g)
15	SEM analysis using Phenom-World Pro at an accelerating voltage of 10 kV	Powder form up to 32 mm (Ø)
16	Elemental composition analysis using Thermo Fisher Scientific model Quanta200	Powder form (2–7 g)

equipment, test method, test significance, and specimen details are discussed later in the respective sections.

It was indispensable to determine the physicochemical characteristics of leather buffing dust, which was used to manufacture the composites. To do this, the moisture content, the potential for hydrogen (pH), chromium trivalent, and chromium content were measured.

2.4.1 pH and moisture content

The pH of the chrome shaving was determined by soaking 5 g of sample in 100 mL distilled water and was kept in an orbital shaking device for 16–24 h, followed by direct measurement of the pH according to the standard methods of SLC13 (SLC, 1996) [27]. As far as the moisture content is concerned, the leather is initially filtered and milled in a physical sieve shaker to produce fine-grade micron-sized particulates. Leather fibers relatively smaller than 650 microns in size were further separated and heated about a half-hour inside an oven at a temperature of 100°C to extract moisture. Initially, these leather particles were dried to a moisture content of percentage in a small size dry kiln at a temperature range of 95–100°C. The properties were then measured at 23°C and 0.5 relative humidity. The moisture content of samples was determined by the gravimetric method by weighing 3 g of the sample by crucible and putting it in an oven for 5–6 h, and the moisture content will be determined according to the standard method of SLC 3 (SLC, 1996), and findings revealed out to be 9 ± 2% moisture [27].

Further, the moisture content of leather buffing dust was 5.12%; due to uniformly powdered form structure. As a result, drying time had to be extended for leather shaving wastes, or an alternative drying method was to be chosen further.

2.4.2 Chromium trivalent

According to SLC 1996, chromium trivalent was determined by using SLC 8 [27]. A 2 g ground chrome shaving was weighed, 5 mL of sulfuric acid and 10 mL of per chloric acid, or 15 mL of the mixture and 15 mL of nitric acid were added. Heated to boil on a hot plate to a moderate flame, a small funnel was placed on the neck of the flask until the reaction mixture begins to turn to orange, the flame was lowered until the complete change of color, further heated gently for 2 min, cooled for a short time in the air, then rapidly in cold water and diluted to approximately 200 mL. In order to remove the chlorine influence/interference, the mixture has been boiled further for around 10 minutes. Cooled and 15 mL of orthophosphoric acid added to mask if any iron present and 20 mL of 10% potassium iodide, left to stand for 10 min in the dark place.

The sample was titrated against 0.1 N sodium thiosulfate until the solution in the flask turns to light green by using 5 mL of 1% starch indicator (SLC, 1996) [27].

$$Cr_2O_3(\%) = \frac{\text{Titration volume} \times 0.00253 \times 100 \times \text{Correction factor}}{\text{Sample weight}}, \quad (1)$$

where 0.1 N sodium thiosulfate = 0.00253 g Cr_2O_3.

2.4.3 Chemical characteristics of leather buffing dust/recycled EVA composites

UV-visible spectrophotometry offers the most suitable, effective, and accurate method for analyzing the chromium levels, Cr(VI) in solid leather wastes (leather buffing dust)/recycled EVA TPE polymer composite according to IUC 8 and 18 test standards [28,29].

The chromium content of the control sample and the leather fibrous composites was determined by using IUC 8 and 18 test standards/ISO 17072-1:2011(E): IULTCS/IUC 27-1:2011(E) test method [28,29]. To the accurately weighed 2 g of grounded leather board sample in the conical flask, artificial perspiration acid that was prepared by mixing 5 g of sodium chloride, 2.2 g of sodium dihydrogen orthophosphate dehydrate, 0.5 g L-histidine monohydrochloride monohydrate per liter, 100 mL of the acid artificial-perspiration acid solution was added and at 37 ± 2°C the sample was shaken slowly in a water bath for 4 h ± 5 min. The extracted solution was filtered with a filter paper, and then it was filtered with a membrane filter. For the direct measurement of the elements, a suitable amount of extract was taken for analysis, and 5% (by volume) of nitric acid was added. This addition was considered in the dilution factor. Blank samples were carried out with the sample to control contaminants with the same procedure. An aliquot of acid perspiration is placed in a sample container and treated as a sample, in all respects, including all analytical procedures. After sample preparation, the chromium content was selected using a UV-vis spectrophotometry instrument (SICAN 2600 Series). Chromium trivalent content control sample and composite sheets were determined by using IUC 8 test method [29]. A 2 g sample was taken, and 20 mL of nitric acid was added, followed by 20 mL of a mixture of per chloric acid and sulfuric acid with 70 to 30 ratios. The mixture was heated until the orange color is observed. The digested sample was cooled, and 100 mL of distilled water was added, heated for a further 10 min to remove excess chlorine. To avoid interference of iron, 15 mL of orthophosphoric acid was added. Around 20 mL of 10% potassium iodide was added and kept in the dark place for 10 min to prevent light interference to iodine. The sample was titrated against 0.1 N sodium thiosulfate using starch indicator until sky blue was observed (IUC/SLC, 1996) [27–29]. The pH of the leather buffing dust/recycled EVA composite was determined by soaking 5 g of grinded sample in 100 mL distilled water and keeping it in an orbital shaking device for 16–24 h, followed by direct measurement of the pH according to the standard methods of SLC 13 (SLC, 1996) [27–29].

Table 3: Absorbance values obtained with phosphate buffer testing procedure

Samples	Absorbance
Blank	0.0848
Neat recycled EVA polymer without any leather buffing dust	0.0089
Recycled EVA polymer with leather buffing dust (1:1)	0.0087
Standard	0.0782

Table 4: Absorbance values obtained with water testing procedure

Samples	Absorbance
Blank	0.0196
Neat recycled EVA polymer without any leather buffing dust	0.0118
Recycled EVA polymer with leather buffing dust (1:1)	0.013
Standard	0.0814

Results revealed from Tables 3 and 4 show that the concentration of hexavalent chromium was not found in the measured leather buffing dust and reinforced recycled EVA TPE polymer composite samples.

2.4.4 Physicomechanical characteristics

2.4.4.1 Tensile strength

The tensile strength does not directly influence the properties and expectations of the soling materials, yet it is one of the parameters to be judged as a general characteristic. Tensile strength refers to break load per unit cross-sectional area. Break load is the quantum of force that can break a material under specific conditions. After measuring its width and thickness, a rectangular or dumbbell-shaped test specimen is filled with both the jaws in a tensile tester, as depicted in Figure 7. The force is applied to pull the specimen to determine the tensile strength. By dividing the force with the cross-sectional

Figure 7: (a–b): Dumb-bell shaped tensile strength testing specimens.

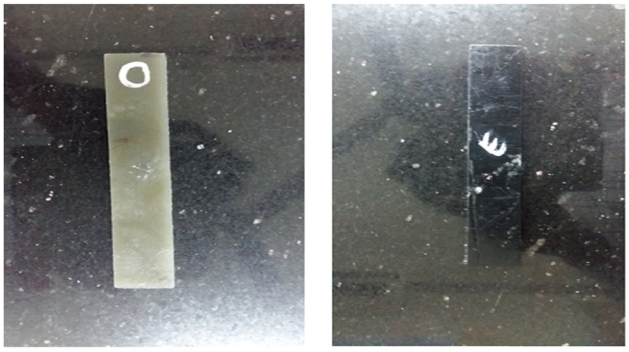

Figure 8: (a–b): Compressive strength testing specimens.

area using the same apparatus, the "percentage of elongation at break" is calculated by noting down the initial and final length when it breaks the percentage of elongation. The mathematically calculated, *i.e.* "elongation at break" is an essential parameter for determining the flexibility which indirectly influences the durability too. According to SATRA TM-137 1995, the tensile test on composite sheets was performed using computer-controlled INSTRON equipment, model 3369J7257, with an optical extensometer gauge length of 50 mm [34]. The leather composite samples were then clamped to the tensile tester. The speed of separation of jaws was kept at 100 ± 20 mm per min. The load at which the leather composite samples broke was noted. The distance between the two separating jaws of the tensile tester before starting the instrument (L_1) and at the time of the breaking of the test specimen (L_2) was noted. The tensile strength and percentage elongation at break were then calculated. This physical characteristic is indispensably employed to estimate the strength of leather and footwear-related products. Four samples were tested in each case (including tensile, flexural, compressive, tear strength), and the average values were reported in each case.

$$\text{Tensile strength}\left(\frac{\text{N}}{\text{mm}^2}\right) = \frac{\text{Breaking load}}{\text{Thickness} \times \text{Width}}, \quad (2)$$

$$\text{Elongation at break (\%)} = \frac{L_2 - L_1}{L_1} \times 100, \quad (3)$$

where L_2 = final length of the leather composite sample and L_1 = initial length of the leather composite sample.

2.4.4.2 Compressive strength

According to ASTM D-3410, the compression test on composites was conducted using computer-controlled INSTRON equipment, model 3369J7257, with an optical extensometer of gauge-length 50 mm and a test-speed of 50 mm/min as shown in Figure 8 [35]. This machine is used for testing materials under tension or compression. The two columns of the main frame provide precise guidance to the moving cross head. The loading unit consists of two cross heads for fixing the test specimen, and a drive unit provides load at the required speed. The speed of the moving cross head can be adjusted, controlled, or varied. The load cells value of 5 kN and so on are interchangeable and are mounted above or below the cross heads depending upon the nature of the tests. The speed with which the load is applied can be controlled. The ultimate physicomechanical characteristics of the composites were computed by considering the average of several observational measurement techniques.

2.4.4.3 Tear resistance

Tear test specimens were prepared as per SATRA TM-218 1999/ISO 20344:2011 [36]. The tear resistance result shows the ability of resistance toward the tearing load of prepared leather polymer composites. The tests were

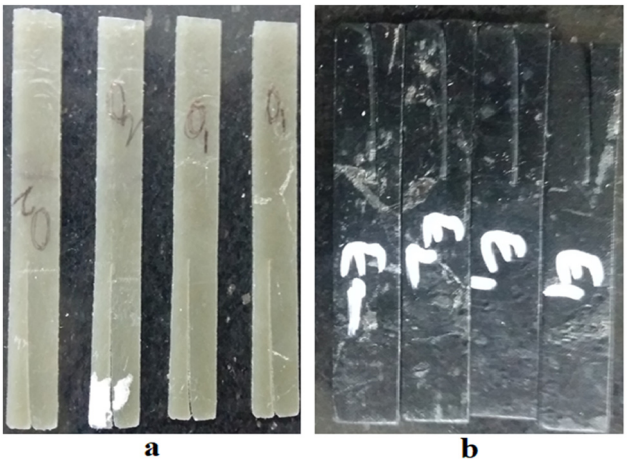

Figure 9: (a–b): Tear-resistance testing specimens.

conducted at a speed of 50 mm/min. Four test specimens of each composition were tested as depicted in Figure 9.

2.4.4.4 Hardness

The hardness of soling materials is judged by measuring the penetration of a rigid ball into the test pieces under specific conditions by an apparatus known as a hardness tester. The shore A hardness of the composites was examined by utilizing a hardness tester, model Digitest, following the SATRA TM-205:2016/ISO 868:2013 test method [37].

2.4.4.5 Density

Density is related to the weight of the materials and is expressed as mass per unit volume. This indicates how material becomes heavier or lighter. The higher the density, the heavier the materials and vice versa. The test specimen of uniform thickness is taken either in a circular or square-shaped container to measure the density of flat materials by employing SATRA TM-134:2010/ISO-2781:2018. Both thickness and diameter/length were measured, and accordingly, the volume was ascertained. Subsequently, the test specimen was estimated for their mass, and density was determined by dividing mass by volume. It is somehow difficult to measure the volume of a molded unit sole dye to the uneven surface. However, the volume in this sample sole was taken in both normal and immersed condition in the water. Loss of weight in water determines the volume of water replaced, which is equivalent to the sole unit, and then density can be calculated by using the formula,

$$\rho_{\text{sample}} = \frac{m_{\text{air}}}{m_{\text{air}} - m_{\text{water}}} \times (\rho_{\text{water}} - \rho_{\text{air}}), \qquad (4)$$

where ρ_{sample} = density of the sample, m_{air} = mass of air, m_{water} = mass of water, ρ_{water} = density of water, and ρ_{air} = density of air.

The specimens were obtained in either form with a volume to determine volume and mass, and then compute a density by utilizing the equation.

2.4.4.6 Adhesion strength

The adhesion strength of the leather fibrous/recycled EVA polymeric composites was evaluated using SATRA TM 401 2000 at room temperature to examine the bonding strength of the linings [38].

2.4.4.7 CRT

The CRT of the recycled polymeric composites was evaluated by using SATRA TM 64:1996 at room temperature to find out the compressional deformation properties of leather waste/recycled EVA polymer composites as exhibited in Figure 10 [39].

2.4.4.8 Abrasion resistance

The wear resistance of the leather buffing dust/recycled EVA composites was determined using DuPont-based unidirectional rotary drum abrasion model STM-140, UK tester using ISO20871:2001 standards [40]. Composites of the appropriate dimensions were affixed to the abrasive wheel at thirty revolutions per minute. Tests were conducted for 1,000 cycles. The loss of weight due to the abrasive paper was measured by a revolving cylinder filled with an emery abrasive paper, 50-mesh. The specimen holding limb moved parallel to the (horizontal) cylinder axes and was powered by a 1,500 g weight, offering a 2.03943 kgf, as contact normal force. Alternatively, leather composite samples were cut using the standard dye, weighed, and clamped rigidly in the abrasive disc against an emery paper. The machine was started, and weight loss was noted after 500, 1,000, 1,500, and 2,000 revolutions. Weight loss in the samples before and after abrasion testing thus provides volumetric wear loss.

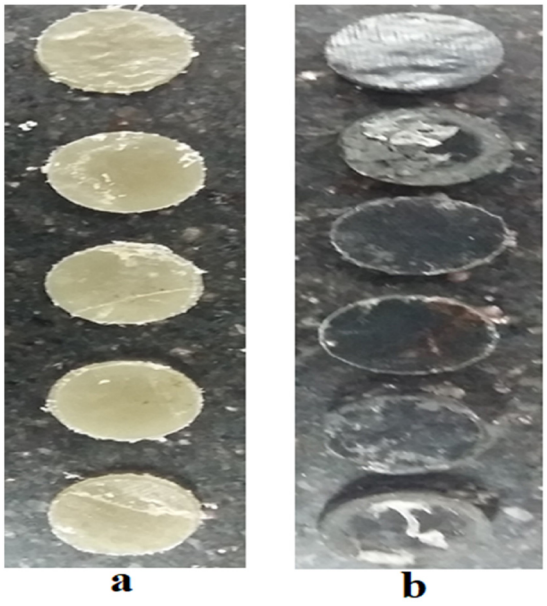

Figure 10: (a–b): CRT testing specimens.

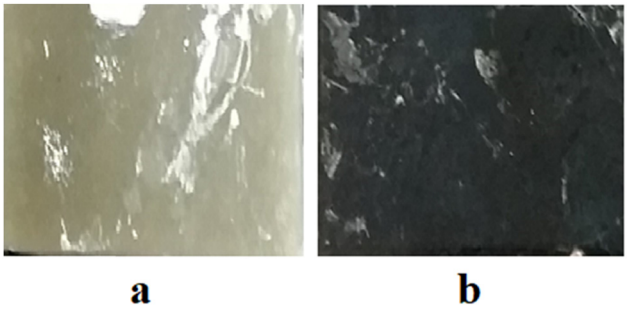

Figure 11: (a–b): Water absorption test specimens.

2.4.4.9 Water-absorption test

In this study, the specimen of size 25 mm × 25 mm from the sheet of the composite plate is maintained, as depicted in Figure 11. The composite plate was then cleaned properly and further measured the sample of specimen going under the test and kept the initial weight for comparison as per the ASTM-D-570 standards. One liter of fresh water was taken in a jar and the sample was completely immersed in water for 12 h. After that, the sample was taken out of the water, and the percentage of water absorption was calculated at different times by measuring the change in weight of the sample.

$$\text{Percentage water} - \text{Absorption in time, } t = \frac{\text{Volume (mL) of water absorbed in time, } t}{\text{Weight (g) of leather specimens}} \times 100. \quad (5)$$

2.4.5 Thermal properties

The thermal stability of the leather-filled composites would depend on the thermal stability of leather. Since both leather fibers and the matrix are highly polar, the interactions between the two might lead to changes in the melting behavior of the leather fibers. Hence, thermogravimetry and DSC techniques were used to study the degradation aspects of the leather-filled composites concerning temperature and the melting behavior of neat recycled EVA polymer without any leather fiber and leather fiber (buffing dust) mixed with recycled EVA polymer composites at different temperatures.

2.4.5.1 TGA

TGA was conducted to examine the thermostability of neat recycled EVA polymer without any leather fiber and leather buffing dust/recycled EVA composites using a TGA/DSC analyzer (TA Instruments, Waters Austria, model Q50). A sample of 5 mg was processed in an aluminum pan and heated from 30 to 800°C at a heating rate of 20°C/min in an N_2 atmospheric condition. The temperature corresponding to 5% weight loss in the TGA thermogram is considered as a minimum weight loss of the sample. The TGA thermogram of neat recycled EVA polymer and leather buffing dust/recycled EVA composites thus developed gives quantitative information on the weight loss, decomposition, and products formed on decomposition.

2.4.5.2 DSC

The samples were pre-dried in an air circulating oven at 100°C for 10 min, after which they were conditioned at room temperature for 24 h. Thermal stability of neat recycled EVA polymer without any leather fiber and leather buffing dust/recycled EVA composites were followed by a TGA analyzer (TA Instruments, Waters Austria, model Q50).

DSC gives information about thermal transitions in polymers such as melting, glass transition, and oxidation. Also, the miscibility of the polymeric blend system can be examined by analyzing shifts or changes in crystallization peaks.

A TA Instruments, Waters Austria, model Q200, DSC2A-00837 (192.168.1.11) differential scanning calorimeter attached with a 990 thermal analyzer was used to follow the melting behavior as well as thermal transitions of neat recycled EVA and leather fibers when blending with recycled EVA polymer. About 20 mg of the sample was packed into an aluminum pan, and placed in the DSC cell. An empty aluminum pan was used as a reference. DSC study was carried out at a heating rate of 10°C/min under temperature ranging from −20 to 400°C and the analysis was performed under nitrogen atmosphere.

2.4.6 Fourier-transform infra-red spectroscopy (FTIR)

The FTIR-JASCO, model 4700typeA, was used to analyze the chemical property of the neat recycled EVA polymer and leather buffing dust/recycled EVA polymer samples. The FTIR spectra for collagen hydrolysate were recorded with KBr pellet using SHIMAZU IR affinity −IS spectrometer. Samples were ground into a fine powder, and this powder was mixed with KBr and placed in the IR cell, which was kept in the cell compartment with a normal slit. The reference was taken as air and IR spectra were recorded. It was recorded in the transmittance vibrational

modes with a resolution of 4 cm^{-1}, scan speed of 2 mm/s in the wave-number span of 600–4,000 cm^{-1} at room temperature. This technique measures the surface composition, bonding, and structure and provides a limited compositional profile.

2.4.7 Morphological and elemental analysis

To understand the morphological changes that might take place in leather fibers during molding at high temperatures and the possible changes at the interface between the matrix and the fiber, SEM with EDAX, Phenom-World make, PhenomPro model at an accelerating voltage of 10 kV was used. SEM was used to study the surface morphology of leather fibers, cross-sectional morphology of leather fibers reinforced recycled EVA polymer composites, degree of fiber alignment, degree of adhesion, the fusion of leather fibers with recycled EVA polymer, the uniformity of fiber dispersion, and the extent of fiber polymer adhesion. EDAX explores the stoichiometric compounds as well as the percent chemical purity of the specimens to ascertain the occurrence/existence of chemical elemental compositions.

Untreated leather fibers (buffing dust), without any other additives, were incorporated into the recycled EVA polymer matrix and mixed at room temperature or 120°C on the combined mixing mill and hot-press molding. After keeping the mixed samples for 24 h, the neat recycled EVA polymer without any leather fiber content and leather buffing dust/recycled EVA polymer composites were used for SEM morphological examinations.

2.5 Optimization by design of experiments (DOEs)

An experiment can be defined as a systematic procedure performed under controlled conditions to find out the effect of input parameters on the output of a process. To completely understand a process, the experiments are generally carried out for evaluating which input process parameters have a significant effect on the process performance and also for determining what values of input parameters should be used to get the desired output. DOE, generally referred to as experimental design, is systematic and possesses the major advantages which include a significant reduction in the number of experimental runs, recognition of important input parameters which affect the process performance, ease of determining the optimum combinations of input parameters for achieving desired output, and the estimation of experimental errors [30–33].

In this research, RSM was chosen as an experimental design technique because it has several advantages over other experimental design techniques. It establishes a true functional relationship among individual processing variables as well as response variables throughout the least set of trial runs. The data points are reasonably distributed throughout the experimental region. Perhaps it aids in determining the appropriate model as well as lack of fit. The experimentation followed by regression analysis helps to model response parameters to various input parameters.

The optimization analysis of the hot-press and compression process parameters was conducted *via* CCD modeling of RSM employing Design-Expert-13.0 (Statease Inc., USA) tool for the selected three process-operating factors. Table 5 illustrates the three parameters that were selected as molding temperature, pressure, and time.

The genric standardized response surface model is represented in equation (6).

$$Y = b_0 + \sum_{i=1}^{3} b_i X_i + \sum_{i=1}^{3} b_{ii} X_i^2 + \sum_{i=1}^{2} \sum_{j>1}^{3} b_{ij} X_i X_j + \ldots, \quad (6)$$

where "Y" represented the response variables (tensile, tear, adhesion strength, compression modulus, hardness, and abrasion resistance), b_0 portrayed the constant, was the residual (error) term, b_i expressed the linear coefficients, b_{ii} described the quadratic co-efficient, b_{ij} represented the interaction co-efficient, and X_i portrayed the dimensionless coded independent factor.

The processing temperature, time, and pressure play important roles in the physicomechanical properties, abrasion resistance, and adhesion peel strength characteristics of leather buffing dust/recycled EVA polymer composites. The molding temperature ought to be substantial to liquefy the recycled EVA thermoplastic, yet not fervent that it utterly deteriorates/degrades the leather buffing dust fibers. The compression molding pressure should be sufficiently adequate to prevent short shots

Table 5: Parameters for experimental design

Factors	Variation levels		
	Low (−1)	**Medium (0)**	**High (+1)**
Molding temperature (°C)	90	110	120
Molding time (min)	20	30	40
Molding pressure (tons)	5	6	7

(*i.e.* partially loaded pores/holes/openings), yet not massively enough to inflict flash at the surfaces.

The physicomechanical performance of the testing sample steadily improved as the pressure-holding molding period elapsed until it reached a certain limit. Any further rise in molding time did not influence physicomechanical efficacy. The physicomechanical output(s) held steady at the thresholds since then and uniformity blending as well as surface-finishing – both enhanced as the pressure-holding period was prolonged. Considering the tensile, tear, adhesion strength, compression modulus, hardness, and abrasion resistance as paramount variables, the optimum pressure-holding period for the physicomechanical characteristics of the samples were ascertained at 30 min.

Thus, the processing temperature, time, and pressure were potentially significant factors. In general, increasing fiber loading in leather buffing dust/recycled EVA polymer composites would improve the stiffness and the strength of flexible polymeric composites. However, in practice, the hot-press molding process would limit the number of leather fibers to be compressed because of fiber cluttering, a narrow gate, and a sprue of the leather fibers recycled EVA polymer mixture. In addition, leather buffing dust/recycled EVA polymer composites with fiber contents of 1:1 may require different compression molding conditions.

Three-factor experiments were conducted to study the effects on the properties of leather buffing dust/recycled EVA polymer composites, molding temperature, molding pressure, and molding time.

3 Results and discussions

Recycled or scrap EVA thermoplastic polymer is one of the most widely used cost–beneficial extenders in thermoplastic products. Many industrial thermoplastic polymer products can accept the scrap EVA polymer in their formulations for some applications either for economic reasons or for improved processability. For noncritical applications, scrap EVA polymer in large quantities can be incorporated into virgin thermoplastic polymers. However, the presence of scrap EVA polymer could significantly reduce the physical properties of the product. The principal reason for the reduction in strength properties when scrap EVA polymer is incorporated is because there is little interfacial bonding between the scrap EVA polymer, which is already in the cross-linked state, and the virgin thermoplastics.

If suitable means are identified to maximize the scrap EVA polymer consumption in such formulations, which would subsequently make the recycling of the end product after their service life effective, environmental problems associated with the scrap or recycled EVA polymer disposal could be minimized. The addition of waste leather along with scrap or recycled EVA polymer is one such approach that could increase the scrap or recycled EVA polymer consumption in virgin polymer formulations and make the recyclability of the end products energy-efficient.

When fibrous materials such as leather wastes are added to scrap or recycled EVA polymer matrix, tensile strength drops even if the fibers are strongly bonded to the matrix. This reduction in tensile strength occurs even at low fiber concentrations because the matrix is not constrained enough by fibers to resist deformation, resulting in high matrix strain. This leads to local stresses leading to either breaking or de-bonding of the fibers from the matrix with the formation of the voids. The voids grow in size as the strain increases at lower stresses, breaking and debonding occurs at the fiber–matrix interface leading to failure of the composite. The stress required for debonding depends on the extent of adhesion between the fibers and matrix. At intermediate fiber concentrations, the matrix is sufficiently constrained, and hence the strength of the composite increases moderately. Due to the extremely high viscosity of the compounds at higher fiber concentrations, imperfections occur because of poor flow behavior, which in turn results in poor mechanical properties.

Leather is a closely knitted structure of collagen fibers. SEM has been used to study the degree of adhesion between leather fibers and scrap or recycled EVA polymer. Morphology of recycled EVA thermoplastic polymer mixed with leather fibers at a temperature of 80–100°C has been found to exhibit a highly diffused interface between the fibers and the matrix. The fibers were completely covered by the matrix, and extensive fusion of the fibers with the matrix was observed as they were incorporated in the matrix at high temperatures [41]. In this study, though the leather was employed in particulate form, it is expected to be an integral part of the scrap EVA thermoplastic polymer.

The physicomechanical studies of blends are prominent characteristics because the products made have to bear the mechanical stress exerted when used by the consumer. The physicomechanical characteristics of the composites prepared in this study were evaluated.

The experimental method gave remarkable outcomes with leather buffing wastes and recycled EVA polymer (injection/extruder waste grades) for manufacturing footwear soles.

3.1 Chromium(VI) and chemical composition

The presence of Cr(VI) in the solid leather wastes/recycled EVA thermoplastic polymer composites was measured using UV-vis spectroscopy as a fast tool of its determination. Results exhibit the absentia of Cr(VI) in leather buffing dust/recycled or commercial low-cost thermoplastic elastomer-based polymer composites.

3.2 RSM analysis of physicomechanical characteristics using CCD

Experiment planning is one of the major and important steps for deriving accurate and clear results. It is an activity that impacts the whole research input behavior on the output responses. So, a well-designed research problem leads to conclude the significant impact of input characteristics on the output results to fulfill the objectives of the research. Further, it draws the correlation between input, and output variables efficiently if it is planned in a better manner. In addition to this, data collection and analysis become simpler while having good DOE.

This study took into account input variables such as molding temperature, time, and pressure, as well as their effect on output variables such as tensile strength, tear strength, compression modulus, adhesion strength, abrasion resistance, and hardness. The optimization equations for the modeling equations were created using the RSM technique. Table 5 shows the coded, and actual values of input variables at various levels as indicated by RSM. The conversion of original values of the variables into coded form was one of the essential features of this approach. Seventeen trials were executed as per the RSM design matrix, as in Table 6. To eradicate bias, the experimental run was randomly assigned. At each location, the tensile strength, tear strength, compression modulus, adhesion strength, abrasion resistance, and hardness were calculated.

Table 6 shows the results of calculating the tensile strength, tear strength, compression modulus, adhesion strength, abrasion resistance, and hardness for each of the 17 experiments. With the aid of the software Design Expert, a statistical review of the experimental data was carried out (Dx-13.0). In terms of input parameters, a regression equation for tensile strength, tear strength, compression modulus, adhesion strength, abrasion resistance, and hardness was found. For experimental data, analysis of variance (ANOVA) was used to determine the significance of input variables as well as the degree of trust in their influence. In terms of model adequacy, precision, and lack of fit, the statistical inference was drawn. The influences of input factors such as (molding

Table 6: Arrangement of experimental design matrix in terms of coded values (levels) based on the CCD for six input process parameters for leather buffing dust reinforced recycled EVA polymer composites

Standard order	Process parameters (coded values)			Response parameters					
	Molding temperature (°C) (A)	Molding time (min) (B)	Molding pressure (tons) (C)	Tensile strength (MPa)	Compression modulus (MPa)	Tear strength (N/mm)	Hardness (HRR)	Abrasion resistance (mm^3)	Adhesion strength (N/mm)
1	105	30	6	8.65	74.12	7.08	85.12	331.23	1.69
2	120	40	5	8.68	75.32	7.18	88.03	323.41	1.34
3	105	30	6	8.73	77.34	8.96	86.78	336.71	1.28
4	130.227	30	6	9.63	74.34	8.77	86.77	347.86	0.89
5	105	30	4.31821	9.67	74.56	7.18	84.45	313.8	0.92
6	90	40	7	10.23	77.09	8.19	83.32	323.19	0.69
7	120	20	7	10.56	73.34	8.25	91.11	367.91	0.87
8	105	13.1821	6	9.85	80.12	7.17	88.09	311.6	0.88
9	79.7731	30	6	9.79	76.45	8.76	90.45	338.65	1.26
10	120	40	7	9.52	77.86	8.88	88.67	343.56	0.84
11	120	20	5	9.54	76.12	7.37	89.56	377.22	0.58
12	90	40	5	9.63	75.49	8.65	93.67	343.61	0.77
13	105	30	6	9.71	75.03	7.41	86.65	351.45	1.45
14	105	46.8179	6	9.69	79.23	6.34	85.69	366.33	1.67
15	90	20	7	10.02	77.06	7.13	88.34	319.56	1.56
16	105	30	7.68179	10.41	71.12	6.06	92.56	354.34	1.79
17	90	20	5	9.61	73.23	7.21	86.71	361.2	0.86

DOF: Degree of freedom.

temperature, molding pressure, and molding time) on response characteristics (tensile strength, tear strength, compression modulus, adhesion strength, abrasion resistance, and hardness) were discussed.

3.2.1 Development of leather buffing dust reinforced recycled EVA polymer composites: mathematical modeling

To examine the impact of the variable on tensile, tear, adhesion strength, compression modulus, hardness, and abrasion resistance of leather buffing dust/recycled EVA polymer composites, the primary influence including the interaction of processing variables on response-characteristic(s), ANOVA, and regression-model was discussed. The contour analysis was performed to assess the optimum arrangement of processing factors. Besides, multiple regression analysis was employed to develop a quantitative statistical model for the variation of tensile, tear, adhesion strength, compression modulus, hardness, and abrasion resistance with substantial operating control factors. Table 6 demonstrates a maximum of 17 experimental data trail runs.

3.2.1.1 ANOVA as well as model-fitting for tensile strength

As depicted in Table 7, the model F-value of 136.26 indicates that the proposed model is statistically significant. An F-value of this magnitude has a 0.01% probability of occurring owing to noise. Model terms with P-values lower than 0.0500 are significant. Throughout this context, A and A^2 are considerable significantly model terms. If the value is higher than 0.1000, the model terms are not significantly relevant. If the model has a lot of insignificant terms, then, the model reduction can ameliorate the model (not considering those needed to assist and facilitate the hierarchy).

The R^2 (adjusted) of 0.9334 is fairly comparative or equivalent to the R^2 (predicted) of 0.8912 and therefore, the disparity/variation is less than 0.2. The signal-to-noise ratio was computed by Adeq precision. A signal-to-noise ratio of 22.1602 implies that the signal is adequately effective, and one can utilize this model to navigate the design, and model-layout space, as shown in Table 8.

3.2.1.2 Evolution of mathematical model from ANOVA for tensile strength

For specified levels of each variable, the expression in terms of the actual variables can be utilized to make accurate prophecies for the response. In addition, for each factor, the levels should be stated in the original units. The aforesaid equation can be employed to evaluate the relative implications of each factor as the coefficients were measured to accommodate within each factor's units, and the intercept is at the core of design spaces. The quadratic regression mathematical models developed based on RSM for correlating the tensile strength in

Table 8: Fit statistics for tensile strength

Std. dev.	4.27	R^2	0.9075
Mean	143	Adjusted R^2	0.9334
CV%	2.86	Predicted R^2	0.8912
		Adeq precision	22.1602

Table 7: ANOVA for tensile strength

Source	Sum of squares	DOF	Mean square	*F*-value	*P*-value	
Model	927.24	9	95.14	136.26	<0.0001	Significant
A-Molding temperature	221.62	1	221.62	227.11	<0.0001	
B-Molding time	65.43	1	65.43	45.28	0.0341	
C-Molding pressure	44.01	1	44.01	22.62	0.0159	
AB	202.09	1	202.09	172.16	0.0051	
AC	29.27	1	29.27	22.44	0.0097	
BC	45.96	1	45.96	65.13	0.0055	
A^2	337.11	1	337.11	344.24	<0.0001	
B^2	22.16	1	22.16	22.23	0.0043	
C^2	10.45	1	10.45	9.12	0.0138	
Residual	6.42	7	0.75			
Lack of fit	4.31	5	1.01	7.13	0.0548	Non-significant
Pure error	1.16	2	0.42			
Cor total	917.04	19				

terms of coded values, and actual values with hot-press processing parameters after eliminating the nonsignificant terms are specified as follows:

$$\begin{aligned}\text{Tensile strength} = {} & + 30.83951 - 0.186493 \text{ moulding temperature} \\ & + 0.036478 \text{ moulding time} \\ & - 4.29069 \text{ moulding pressure} \\ & - 0.001775 \text{ moulding temperature} \times \text{moulding time} \\ & + 0.007083 \text{ moulding temperature} \\ & \times \text{moulding pressure} \\ & + 0.000125 \text{ moulding time} \times \text{moulding pressure} \\ & + 0.000905 \text{ moulding temperature}^2 \\ & + 0.002249 \text{ moulding time}^2 \\ & + 0.320373 \text{ moulding pressure}^2. \end{aligned} \quad (7)$$

The data have been analyzed to further validate that the residual distributions were normal. Figure 12(a) reveals that the residuals' data are normally distributed using a normality distribution plot. The residuals depict the variation among the actual measured value of a response as well as the values predicted by the theoretical mathematical model. The presence of a minimal residual value implies that the modeling predictions are satisfactorily acceptable [42–47]. Figure 12(a) exhibits the datasets, which are substantially remarkable and relatively closer toward the straight-line position. Considering normal observations, a few scatter were discerned, signifying that now the dataset findings are normally distributed.

The fitted model was confirmed to ascertain its adequate resemblance to the actual measured values. Till the model exhibits a suitable fit, optimizing the fitted response surface is expected to yield inadequate as well as deceptive outcomes [42–47]. The diagnostic graphs, like anticipated against actually obtained experimentation data, validated the model's appropriateness or viability. The charts demonstrated a correlation between expected and observed values. Figure 12(b) illustrates the analytic diagnosis diagrams of the response characteristics like tensile strength. The dataset values on this chart reclined significantly closer to the straight line suggesting that the real facts and the evidence presented from the models were in excellent satisfactory accordance. As per the findings, the models employed throughout this investigation were liable for predicting process operational conditions for the production of leather buffing dust reinforced, recycled EVA polymeric composites.

The analytical diagnosis charts of multiobjective optimization of compression molding based process-operating parameters on tensile strength are shown in Figure 12(a)–(c) to further evaluate the adequacy as well as the validity of the regression D-optimum modeling

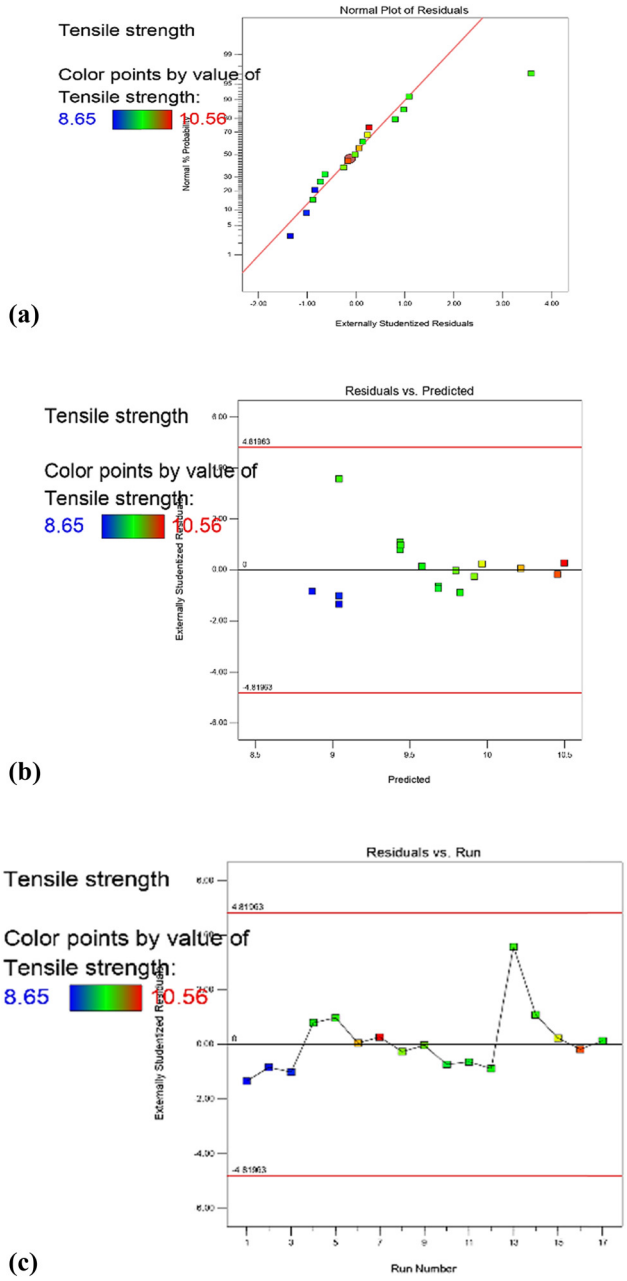

Figure 12: (a) Normal percent probability graph for tensile strength. (b) Residual *vs* predicted graph for tensile strength. (c) Residual *vs* run graph for tensile strength.

framework for the predictive model. The empirical outliers had an excellent distribution within the specified desired spectrum, as shown in Figure 12(c). The anticipated projected tensile strength values of the compression molding were contrasted and evaluated with the observed empirical values to determine the prediction's accurateness (Figure 12(c)). The findings indicate that the experimentation-based observed and forecasted values accord significantly, and are notably evidenced by all spots positioned meticulously closer to the diagonal axis line [42–47].

Figure 12(a)–(c) represents the normality test probability distributions for residuals as well as the relationship between an actual and predicted tensile strength of leather buffing dust/recycled EVA polymer composites. A standard normality probability distribution curve for residuals evaluates the model's adequacy by examining the tensile strength data used throughout the model.

The interaction effects of molding time, molding pressure, and molding temperature against the tensile strength were investigated using plotting surface curves. The input parameters were represented by the primary and secondary horizontal axis, while the measured output parameter was tensile strength, which was represented by the vertical axis. The interactions of these factors generate 3D surface curves (3D) as well as contour plots (2D).

Figure 13(a)–(c) demonstrates the dependency of tensile strength on molding time, molding pressure, and molding temperature. The tensile strength decreases as the molding pressure as well as molding time both proliferate, and with the increase in molding temperature, a slight increase in tensile strength is noted.

3.2.1.3 Tensile strength response-based numerical optimization

To ensure the proposed model's validity and efficacy, experimental trials were performed under standardized optimal settings, and the average value of the scientific observations was correlated to the anticipated results.

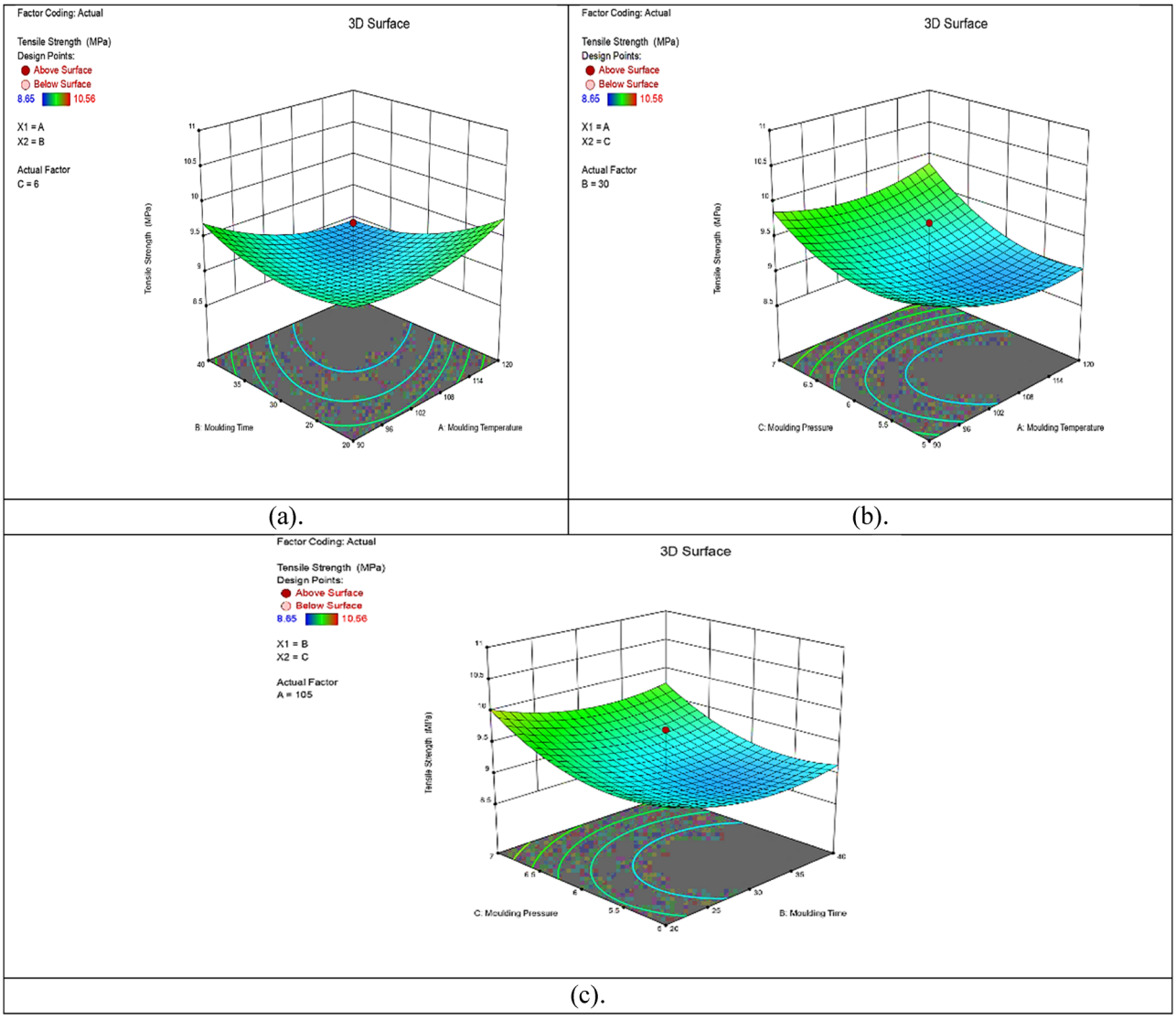

Figure 13: (a–c) 3D interaction plots for tensile strength of leather buffing dust reinforced recycled EVA polymer composites.

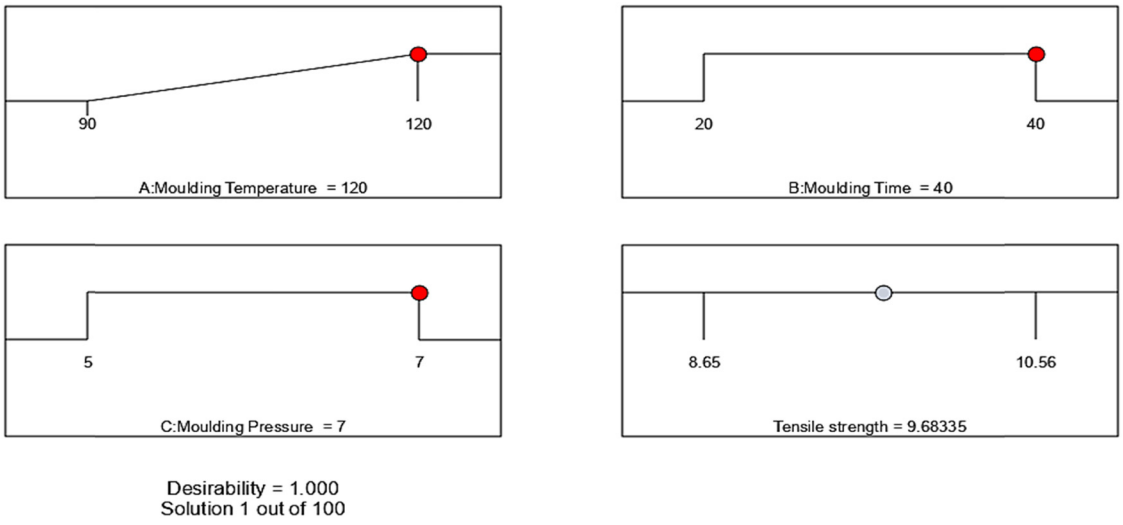

Figure 14: Ramp function graph for tensile strength.

Figure 14 shows the ramp function graph, which indicates that the optimum value of tensile strength (9.68335 MPa) was obtained with molding temperature (120°C), molding time (40 min), and molding pressure parameters (7 tons) with desirability of 1. Besides, a confirmation experiment was also carried out. The tensile strength of leather buffing dust/recycled EVA polymer composites developed at an optimum combination of parameters was found to be 9.485 MPa. The results revealed that the error between the developed model and experimental results was only 2.048%. This proved the applicability, and potential feasibility of the proposed derived mathematical models for efficiently optimizing the tensile strength of leather buffing dust reinforced recycled EVA polymeric composites.

The comparable analysis was also revealed by Kandar and Akil [40], who optimized the parameters of the heat-forming process in the form of molding temperature, molding time, and molding pressure to attain maximum impact strength. For this, woven flax reinforced PLA composites were formulated as per CCD and analyzed using the RSM approach. The authors suggested molding temperature of 200°C, time of 3 min, and pressure of 30 bar as the best set of input conditions to achieve an impact strength value of 48.90 kJ/m^2 [42].

3.2.1.4 ANOVA and model-fitting for compression modulus

As depicted in Table 9, the model *F*-value of 157.42 indicates that the proposed model was statistically significant. An *F*-value of this magnitude has a 0.01% probability

Table 9: ANOVA for compression modulus

Source	Sum of squares	DOF	Mean square	*F*-value	*P*-value	
Model	901.22	9	148.13	157.42	<0.0001	Significant
A-Molding temperature	313.52	1	313.52	291.61	<0.0001	
B-Molding time	56.43	1	56.43	54.68	0.0064	
C-Molding pressure	37.16	1	37.16	38.02	0.0185	
AB	138.62	1	138.62	145.76	<0.0001	
AC	46.03	1	46.03	32.15	0.0087	
BC	34.62	1	34.62	66.73	0.0065	
A^2	359.11	1	359.11	484.24	<0.0001	
B^2	27.27	1	27.27	32.53	0.0043	
C^2	119.65	1	119.65	128.47	<0.0001	
Residual	4.67	7	0.88			
Lack of fit	3.26	5	1.16	6.18	0.0868	Non-significant
Pure error	2.61	2	0.79			
Cor total	973.29	19				

of occurring as a result of noise. Model terms with P-values lower than 0.0500 are significant. Throughout this context, A, AB, A^2, and C^2 are significantly considerable in model terms. If the value is higher than 0.1000, the model terms are not significantly relevant. If the model has a lot of insignificant terms, then, a model reduction can ameliorate the model (not considering those needed to assist and facilitate hierarchy).

The R^2 (adjusted) of 0.9012 is fairly comparative or equivalent to the R^2 (predicted) of 0.8464 and therefore, the disparity/variation is less than 0.2. The signal-to-noise ratio computed using Adeq precision is revealed in Table 10. A signal-to-noise ratio of 23.162 implies that the signal is adequately effective, and one can utilize this model to navigate the design and model layout space.

3.2.1.5 Evolution of mathematical model from ANOVA for compression modulus

The quadratic regression mathematical models were developed based on RSM for correlating the compression modulus in terms of coded values and actual values with hot-press processing parameters after eliminating the non-significant terms is specified as follows,

$$\begin{aligned}\text{Compressive modulus} = {} & + 28.91411 + 0.327079 \text{ moulding temperature} \\ & - 1.16890 \text{ moulding time} \\ & + 15.85595 \text{ moulding pressure} \\ & + 0.001192 \text{ moulding temperature} \\ & \times \text{moulding time} \\ & - 0.047250 \text{ moulding temperature} \\ & \times \text{moulding pressure} \\ & + 0.038625 \text{ moulding time} \times \text{moulding pressure} \\ & - 0.000466 \text{ moulding temperature}^2 \\ & + 0.014085 \text{ moulding time}^2 \\ & - 1.00809 \text{ moulding pressure}^2.\end{aligned} \tag{8}$$

The data have been analyzed to further validate that now the residual distributions were normal. Figure 15 reveals that the residuals' data are normally distributed using a normality distribution plot. The residuals depict the variation among the actual measured value of a response as well as the values predicted by the theoretical mathematical model. The presence of a minimal residual value implies that the modeling predictions are satisfactorily acceptable [42–47]. Figure 15(a) exhibits the datasets, which are substantially remarkable and relatively closer toward the straight-line position. Considering normal observations, a few scatter had also been discerned, signifying that now the dataset findings are normally distributed.

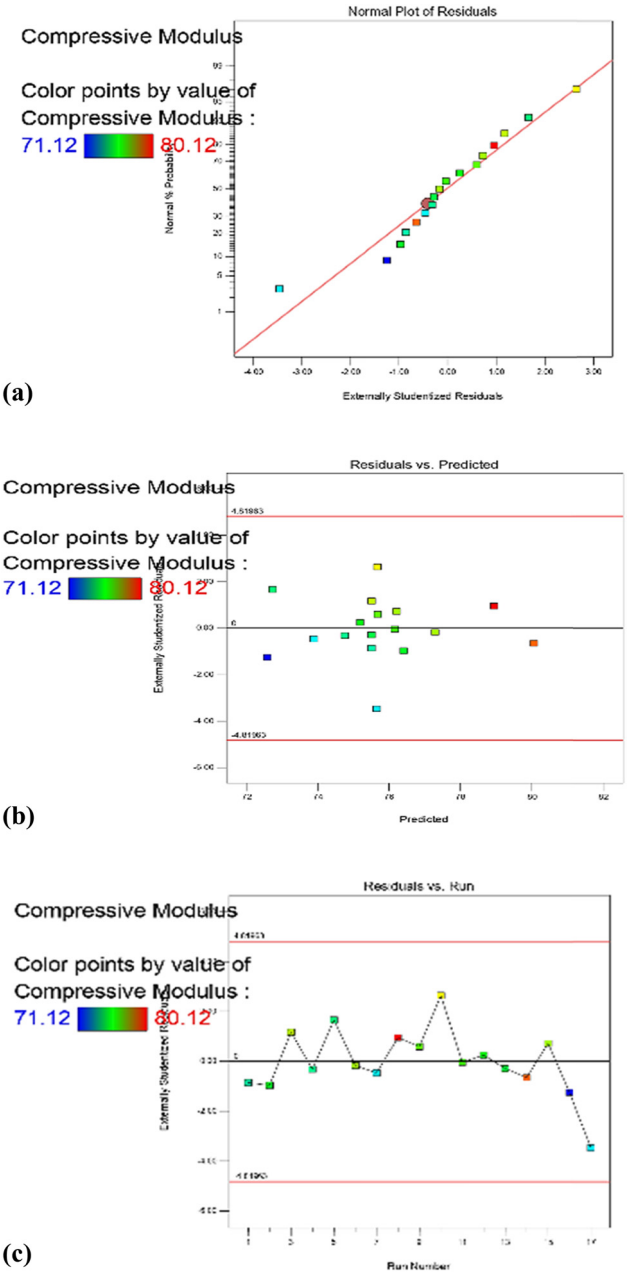

Figure 15: (a) Normal percent probability graph for compression modulus. (b) Residual *vs* predicted graph for compression modulus. (c) Residual *vs* run graph for compression modulus.

Table 10: Fit statistics for compression modulus

Std. dev.	4.27	R^2	0.9143
Mean	129	Adjusted R^2	0.9012
CV%	3.45	Predicted R^2	0.8464
		Adeq precision	23.162

The fitted model was confirmed to ascertain its adequate resemblance to the actual measured values. Till the model exhibits a suitable fit, optimizing the fitted response surface is expected to yield inadequate and deceptive outcomes [42–47]. The diagnostic graphs, like anticipated against actually obtained experimentation data, validated the model's appropriateness or viability. The charts demonstrated a correlation between expected and observed values. Figure 15(b) illustrates the analytic diagnosis diagrams of the response characteristics like compression modulus. The dataset values on this chart reclined significantly closer to the straight line suggesting that the real facts and the evidence presented from the models were in excellent satisfactory accordance. As per the findings, the models employed throughout this investigation were liable for predicting process operational conditions for the production of leather buffing dust reinforced, recycled EVA polymeric composites.

The analytical diagnosis charts of multiobjective optimization of compression molding based process-operating parameters on compression modulus are shown in Figure 15(a)–(c), to further evaluate the adequacy and validity of the regression D-optimum modeling framework for the predictive model. The empirical outliers used to have an excellent distribution within the specified desired spectrum, as shown in Figure 15(c). The anticipated projected compression modulus values of the compression molding were contrasted and evaluated with the observed empirical values to determine the accuracy of prediction (Figure 15(c)). The findings indicate that the experimentation-based observed and forecasted values significantly and evidenced notably by all spots positioned meticulously closer to the diagonal axis line [42–47].

Figure 15(a)–(c) represents the normality test probability distributions for residuals as well as the relationship between an actual and predicted compression modulus of leather buffing dust/recycled EVA polymer composites. A standard normality probability distribution curve for residuals evaluates the model's adequacy by computing the compression modulus data used throughout the model.

The interaction effects of molding time, molding pressure, and molding temperature against the compression modulus are investigated by plotting surface curves. The input parameters are represented by the primary and secondary horizontal axis, while the measured output parameter is a compression modulus, which is represented by the vertical axis. The interactions of these factors generate 3D surface curves (3D) as well as contour plots (2D). Figure 16(a)–(c) shows the dependency of compression modulus on molding time, molding pressure, and molding temperature. The compression modulus is phenomenally decreased with increased molding pressure and is observed that there was no effect of rising temperature on compression modulus. Moreover, molding time did not have much effect on compression modulus.

3.2.1.6 Compression modulus response-based numerical optimization

To ensure the validity and efficacy of the proposed model, the experimental trials were carried out, and under standardized optimal settings, the average value of the empirically scientific observations was correlated to the anticipated prediction results. Figure 17 shows the Ramp function graph, which indicates that the optimum value of compression modulus (76.1649 MPa) is obtained with molding temperature (120°C), molding time (20 min), and molding pressure parameters (5 tons) with the desirability of 1. Besides, a confirmation experiment was also carried out. The compression modulus of leather buffing dust/recycled EVA polymer composites developed at an optimum combination of parameters was found to be 76.71 MPa. The results revealed that the error between the developed model and experimental results was only 0.7156%. This proved the applicability and potential feasibility of the proposed derived mathematical models for efficiently optimizing the compression modulus of leather buffing dust reinforced, recycled EVA polymeric composites.

The associated research was furthermore conducted by Mamoune *et al.* [41] who prepared analytical and semianalytical models for the compression molding process. The suggested model was then applied in resin transfer molding and compression resin transfer molding processes to analyze the effect of size and volumetric contents on the mold filling time. The authors reported that the suggested model could be applied to solve many industrial problems as this process reduced the computational cost time [43].

3.2.1.7 ANOVA and model-fitting for tear strength

As depicted in Table 11, the model F-value of 133.45 indicates that the proposed model is statistically significant. An F-value of this magnitude has a 0.01% probability of occurring as a result of noise. Model terms with P-values lower than 0.0500 are significant. Throughout this context, AB, A^2, and C^2 are considerable significantly model terms. If the value is higher than 0.1000, then the model terms are not significantly relevant. If the model has a lot of insignificant terms, then a model reduction can

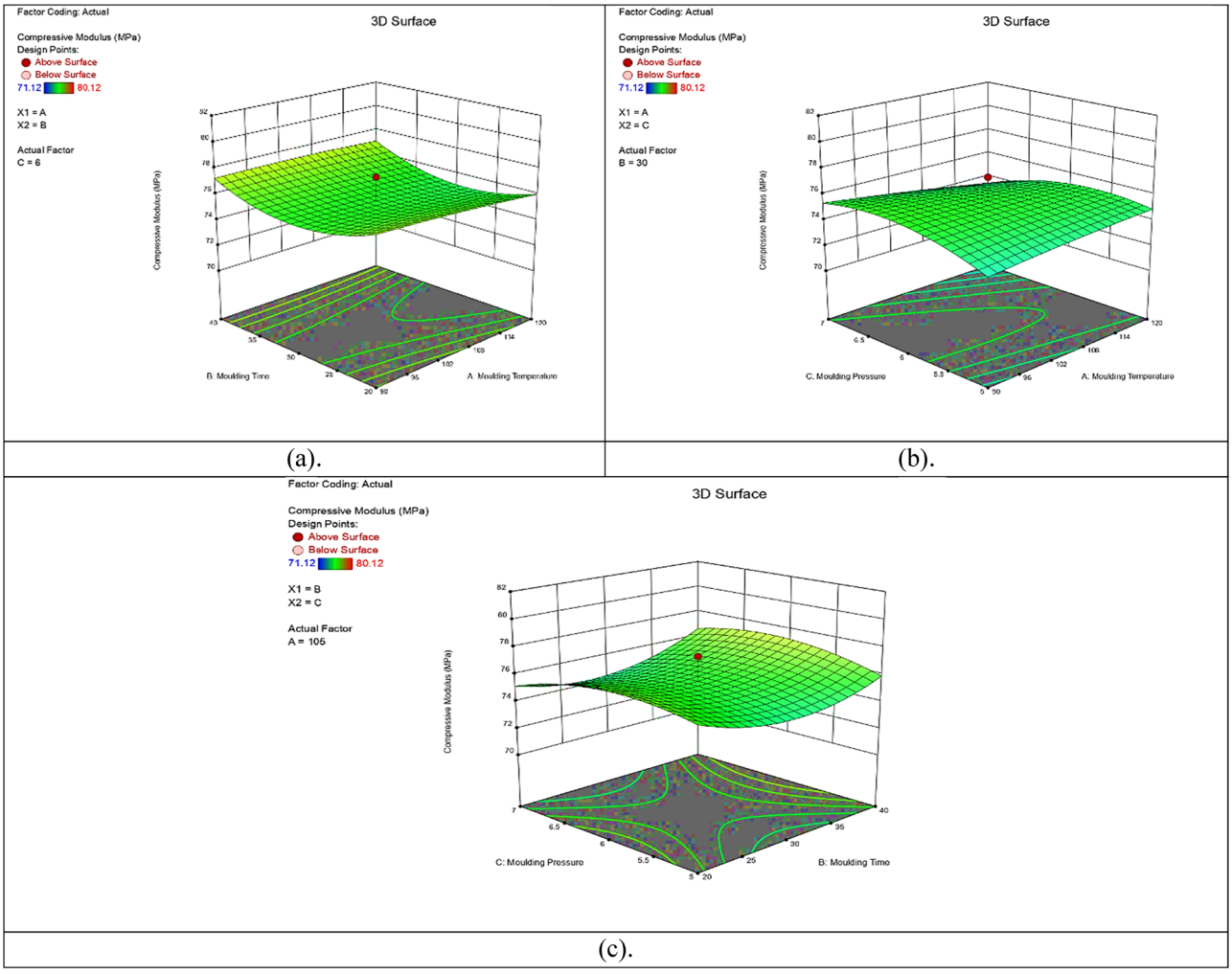

Figure 16: (a–c) 3D interaction plots for compression modulus of leather buffing dust reinforced recycled EVA polymer composites.

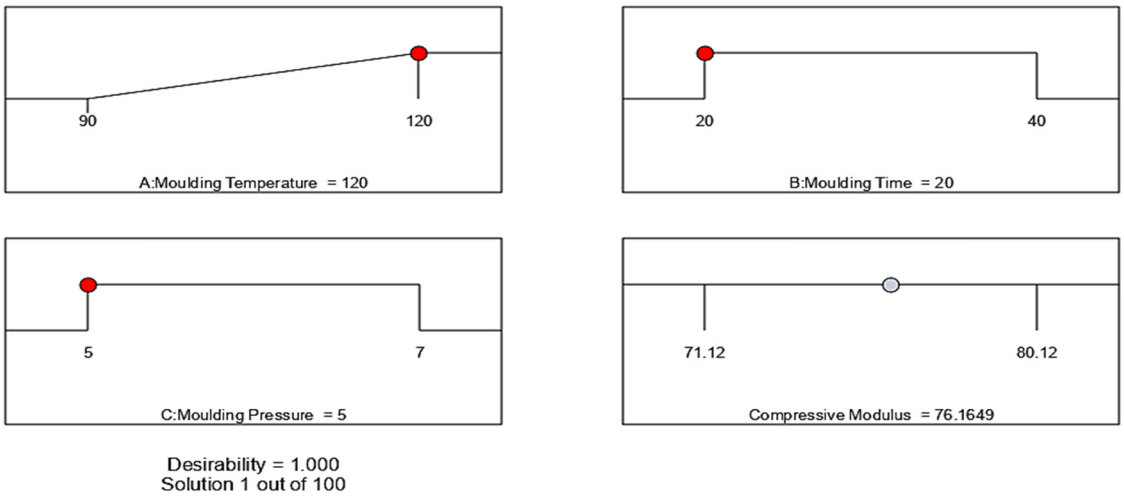

Figure 17: Ramp function graph for compression modulus.

Table 11: ANOVA for tear strength

Source	Sum of squares	DOF	Mean square	*F*-value	*P*-value	
Model	967.82	9	110.29	133.45	<0.0001	Significant
A-Molding temperature	58.12	1	58.12	44.71	0.0175	
B-Molding time	68.08	1	68.08	58.29	0.0064	
C-Molding pressure	77.92	1	77.92	37.02	0.0185	
AB	191.02	1	191.02	146.76	<0.0001	
AC	35.23	1	35.23	29.45	0.0097	
BC	45.68	1	45.68	61.13	0.0045	
A^2	318.61	1	318.61	395.74	<0.0001	
B^2	22.87	1	22.87	38.93	0.0073	
C^2	146.95	1	146.95	143.27	<0.0001	
Residual	3.77	7	0.92			
Lack of fit	3.51	5	1.11	3.84	0.0578	Non-significant
Pure error	2.04	2	0.26			
Cor total	931.19	16				

ameliorate the model (not considering those needed to assist and facilitate hierarchy).

The R^2 (adjusted) of 0.9065 is fairly comparative or equivalent to the R^2 (predicted) of 0.8912 and therefore, the disparity/variation is less than 0.2, as revealed in Table 12. The signal-to-noise ratio was computed by Adeq precision. A signal-to-noise ratio of 24.142 implies that the signal is adequately effective, and one can utilize this model to navigate the design and model layout space.

Table 12: Fit statistics for tear strength

Std. dev.	3.73	R^2	0.9321
Mean	142	Adjusted R^2	0.9065
CV%	2.38	Predicted R^2	0.8912
		Adeq precision	24.142

3.2.1.8 Evolution of the mathematical model from ANOVA for tear strength

The quadratic regression mathematical models developed based on RSM for correlating the tear strength in terms of coded values, and actual values with hot-press processing parameters after eliminating the nonsignificant terms is specified as follows:

$$\begin{aligned}\text{Tear strength} = {} & +27.41110 - 0.519340\ \text{moulding temperature} \\ & + 0.316637\ \text{moulding time} \\ & + 0.850823\ \text{moulding pressure} \\ & - 0.001717\ \text{moulding temperature} \times \text{moulding time} \\ & + 0.026000\ \text{moulding temperature} \\ & \times \text{moulding pressure} \\ & + 0.005500\ \text{moulding time} \times \text{moulding pressure} \\ & + 0.001987\ \text{moulding temperature}^2 \\ & - 0.002635\ \text{moulding time}^2 \\ & - 0.311198\ \text{moulding pressure}^2.\end{aligned} \quad (9)$$

The data have been analyzed to further validate that now the residual distributions were normal. Figure 18(a) reveals that the residuals' data are normally distributed using a normality distribution plot. The residuals depict the variation among the actual measured value of a response as well as the values predicted by the theoretical mathematical model. The presence of a minimal residual value implies that the modeling predictions are satisfactorily acceptable [42–47]. Figure 18(a) exhibits the datasets, which are substantially remarkable and relatively closer toward the straight-line position. Considering normal observations, a few scatter had also been discerned, signifying that now the dataset findings are normally distributed.

The fitted model was confirmed to ascertain its adequate resemblance to the actual measured values. Till the model exhibits a suitable fit optimizing the fitted response surface is expected to yield inadequate as well as deceptive outcomes [42–47]. The diagnostic graphs, like anticipated against actually obtained experimentation data, validated the model's appropriateness or viability. The charts demonstrated a correlation between expected and observed values. Figure 18(b) illustrates the analytic diagnosis of the response characteristics like tear strength.

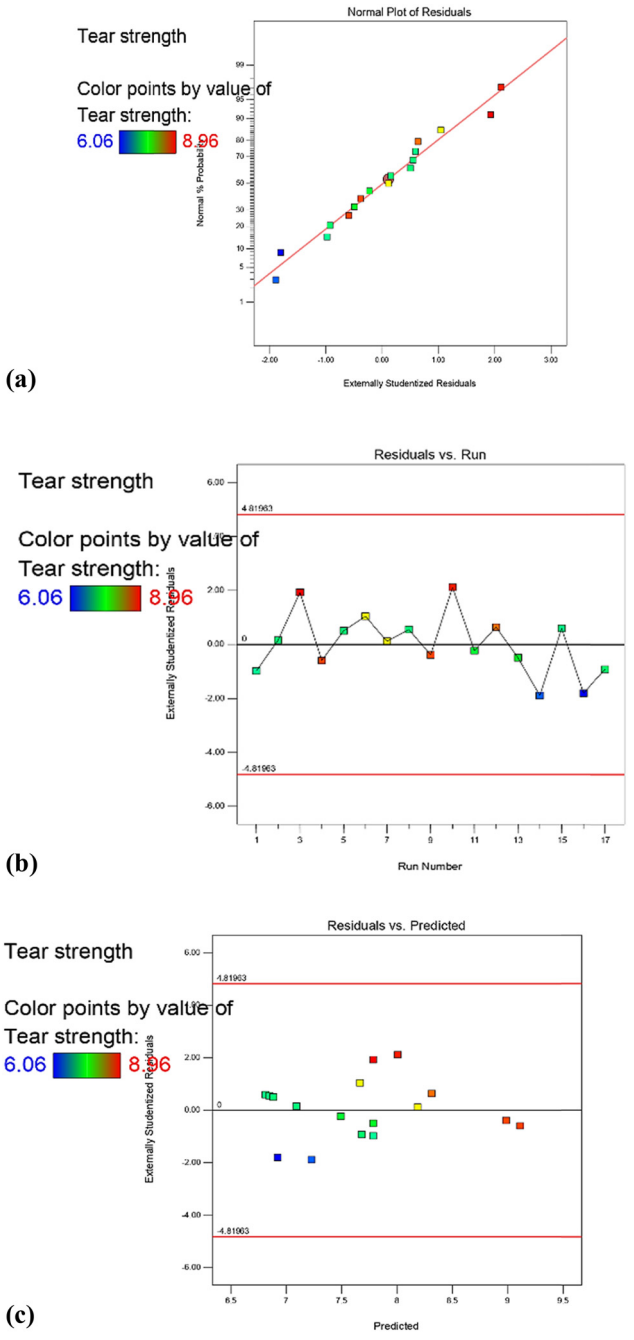

Figure 18: (a) Normal percent probability graph for tear strength. (b) Residual *vs* predicted graph for tear strength. (c) Residual *vs* run graph for tear strength.

The dataset values on this chart reclined significantly closer to the straight line suggesting that the real facts and the evidence presented from the models were in excellent satisfactory accordance. As per the findings, the models employed throughout this investigation were liable for predicting process operational conditions for the production of leather buffing dust reinforced, recycled EVA polymeric composites.

The analytical diagnosis charts of multiobjective optimization of compression molding based process-operating parameters on tear strength are shown in Figure 18(a)–(c) to further evaluate the adequacy and validity of the regression D-optimum modeling framework for the predictive model. The empirical outliers had an excellent distribution within the specified desired spectrum range, as shown in Figure 18(c). The anticipated projected tear strength values of the compression molding were contrasted and evaluated with the observed empirical values to determine the accuracy of prediction (Figure 18(c)). The findings indicate that the experimentation-based observed and forecasted values accord significantly and were evidenced notably by all spots positioned meticulously closer to the diagonal axis line [42–47].

Figure 18(a)–(c) represents the normality test probability distributions for residuals as well as the relationship between an actual and predicted tear strength of leather buffing dust/recycled EVA polymer composites. A standard normality probability distribution curve for residuals evaluates the model's adequacy by examining the tear strength data used throughout the model.

The interaction effects of molding time, molding pressure, and molding temperature against the tear strength are investigated by plotting surface curves. The input parameters are represented by the primary, and secondary horizontal axis, while the measured output parameter is a tear strength, which is represented by the vertical axis. The interactions of these factors generate 3D surface curves (3D) as well as contour plots (2D).

Figure 19(a)–(c) demonstrates the dependency of tear strength on molding time, molding pressure, and molding temperature. An increase in molding pressure, in turn, increases the tear strength to some extent. However, for molding temperature and time, a negligible increase and decrease of tear strength was reported.

3.2.1.9 Tear strength response-based numerical optimization

To ensure the proposed model's validity and efficacy, the experimental trials were performed under standardized optimal settings, and the average value of the empirically scientific observations was correlated to the anticipated prediction results. Figure 20 shows the ramp function graph, which indicates that the optimum value of tear strength (7.49252 N/mm) is obtained with molding temperature (120°C), molding time (20 min), and molding pressure parameters (5 tons) with the desirability of 1. Besides, the confirmation experiment was also carried

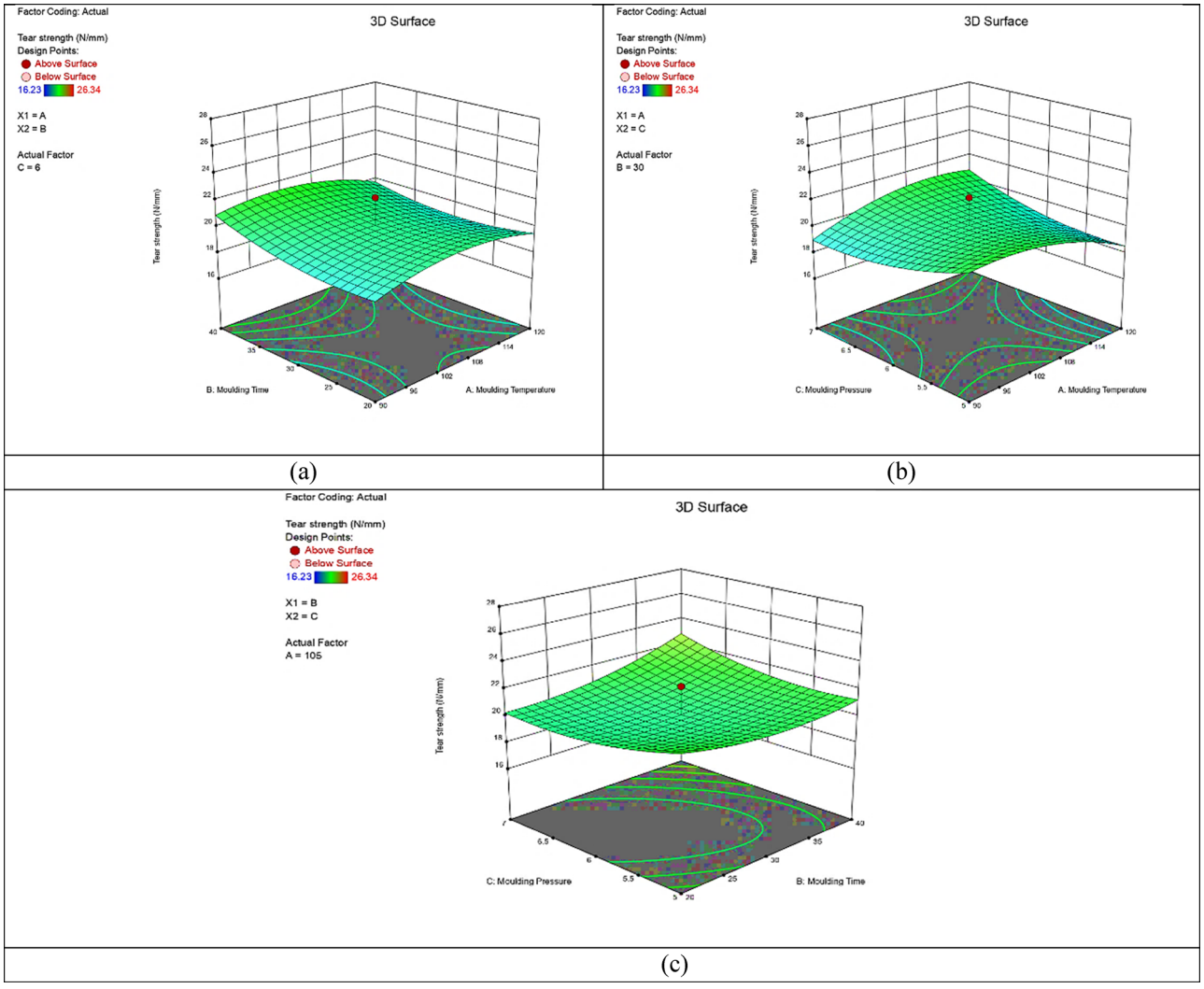

Figure 19: (a–c) 3D interaction plots for tear strength of leather buffing dust reinforced recycled EVA polymer composites.

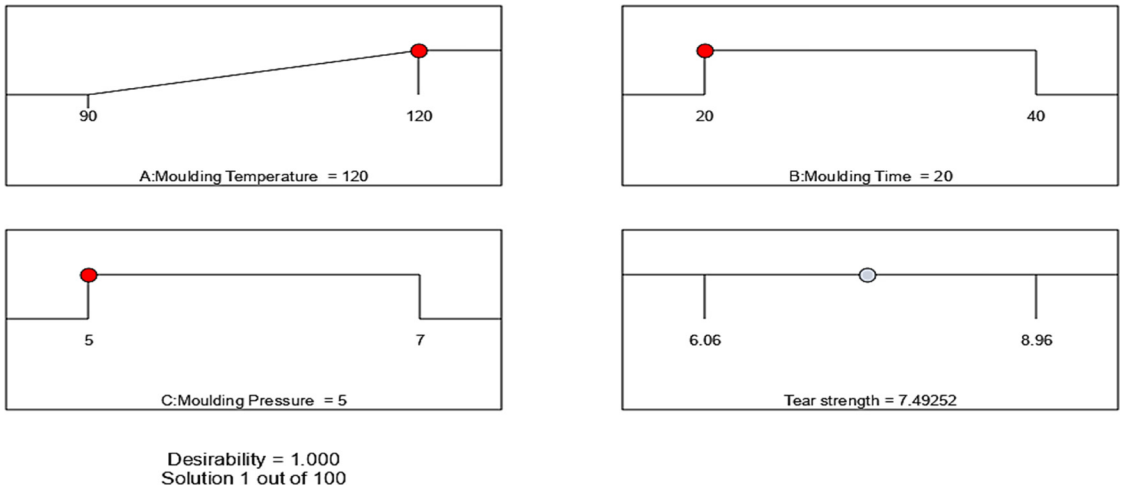

Figure 20: Ramp function graph for tear strength.

out. The tear strength of leather buffing dust/recycled EVA polymer composites developed at an optimum combination of parameters was found to be 7.5425 N/mm. The results revealed that the error between the developed model and experimental results is only 0.6670%. Hence, this proved the applicability, and potential feasibility of the proposed derived mathematical models for efficiently optimizing the tear strength of leather buffing dust reinforced, recycled EVA polymeric composites.

In another comparative investigation, Xie *et al.* [42] optimized compression molding process parameters in the form of compression temperature, pressure, time, and cooling rate for carbon fiber-reinforced thermosetting polymer matrix composites. The authors observed that compression temperature is the most influencing parameter for mechanical properties followed by pressure, the cooling rate, and time. The authors suggested a compression temperature of 150°C, the cooling rate of 3.5°C/min, pressure holding time of 20 min, and pressure opening temperature of 80°C as the best set of input variables to attain better mechanical properties like tensile strength of 785.2 MPa, bending strength of 680.3 MPa, and shear strength of 66.1 MPa [44].

3.2.1.10 ANOVA and model-fitting for hardness

As depicted in Table 13, the model *F*-value of 67.97 indicates that the proposed model is statistically significant. An *F*-value of this magnitude has a 0.01% probability of occurring as a result of noise. Model terms with *P*-values lower than 0.0500 are significant. Throughout this context, A, AB, A^2, and C^2 are considerable significantly model terms. If the value is higher than 0.1000 then, the model terms are not significantly relevant. If the model has a lot of insignificant terms, then model reduction can ameliorate the model (not considering those needed to assist and facilitate hierarchy).

The R^2 (adjusted) of 0.9565 is fairly comparative or equivalent to the R^2 (predicted) of 0.9432 and therefore, the disparity/variation is less than 0.2. The signal-to-noise ratio was computed by Adeq precision. A signal-to-noise ratio of 38.42 implies that the signal is adequately effective, and one can utilize this model to navigate the design and model layout space as revealed in Table 14.

3.2.1.11 Evolution of mathematical model from ANOVA for hardness

The quadratic regression mathematical models developed based on RSM for correlating the hardness in terms of coded values, and actual values with hot-press processing parameters after eliminating the nonsignificant terms is specified as follows:

$$\begin{aligned}\text{Hardness} =& +183.17184 - 1.31962\ \text{moulding temperature} \\ &+ 1.21438\ \text{moulding time} - 15.54521\ \text{moulding pressure} \\ &- 0.004925\ \text{moulding temperature} \times \text{moulding time} \\ &+ 0.090917\ \text{moulding temperature} \times \text{moulding pressure} \\ &- 0.161125\ \text{moulding time} \times \text{moulding pressure} \\ &+ 0.004370\ \text{moulding temperature}^2 \\ &+ 0.003751\ \text{moulding time}^2 \\ &+ 0.946107\ \text{moulding pressure}^2. \end{aligned} \quad (10)$$

Table 13: ANOVA for hardness

Source	Sum of squares	DOF	Mean square	*F*-value	*P*-value	
Model	362.73	9	67.97	85.76	<0.0001	Significant
A-Molding temperature	52.04	1	52.04	114.23	<0.0001	
B-Molding time	2.69	1	2.69	0.2969	0.6027	
C-Molding pressure	3.74	1	3.74	0.4078	0.5434	
AB	87.82	1	87.82	77.23	<0.0001	
AC	14.88	1	14.88	1.64	0.2412	
BC	20.77	1	20.77	2.29	0.1741	
A^2	228.52	1	228.52	314.64	<0.0001	
B^2	1.54	1	1.54	0.1748	0.6684	
C^2	156.86	1	156.86	85.12	<0.0001	
Residual	5.25	7	0.86			
Lack of fit	0.86	5	0.065	0.027	0.568	Non-significant
Pure error	3.21	2	1.33			
Cor total	490.93	19				

Table 14: Fit statistics for hardness

Std. dev.	0.87	R^2	0.9624
Mean	12.42	Adjusted R^2	0.9565
CV%	4.51	Predicted R^2	0.9432
		Adeq precision	38.42

The data were analyzed to further validate that now the residual distributions were normal. Figure 21(a) reveals that the residuals' data are normally distributed using a normality distribution plot. The residuals depict the variation among the actual measured value of a response as well as the values predicted by the theoretical mathematical model. The presence of a minimal residual value implies that the modeling predictions are satisfactory and acceptable [42–47]. Figure 21(a) exhibits the datasets which are substantially remarkable and relatively closer toward the straight-line position. Considering normal observations, a few scatter had also been discerned, signifying that now the dataset findings are normally distributed.

The fitted model was confirmed to ascertain its adequate resemblance to the actual measured values. Till the model exhibits a suitable fit, optimizing the fitted response surface is expected to yield inadequate and deceptive outcomes [42–47]. The diagnostic graphs, as anticipated against actually obtained experimentation data, validated the model's appropriateness or viability. The charts demonstrated a correlation between expected and observed values. Figure 21(b) illustrates the analytic diagnosis of the response characteristics like hardness. The dataset values on this chart reclined significantly closer to the straight line suggesting that the real facts and evidence presented from the models were in excellent accordance. As per the findings, the models employed throughout this investigation were liable for predicting process operational conditions for the production of leather buffing dust-reinforced recycled EVA polymeric composites.

The analytical diagnosis charts of multiobjective optimization of compression molding-based process-operating parameters on hardness have been viewed in Figure 21(a)–(c) to further evaluate the adequacy as well as the validity of the regression D-optimum modeling framework for a predictive model. The empirical outliers used to have an excellent distribution within the specified desired spectrum, as shown in Figure 21(c). The anticipated projected hardness values of the compression molding were contrasted and evaluated with the observed empirical values to determine the accuracy

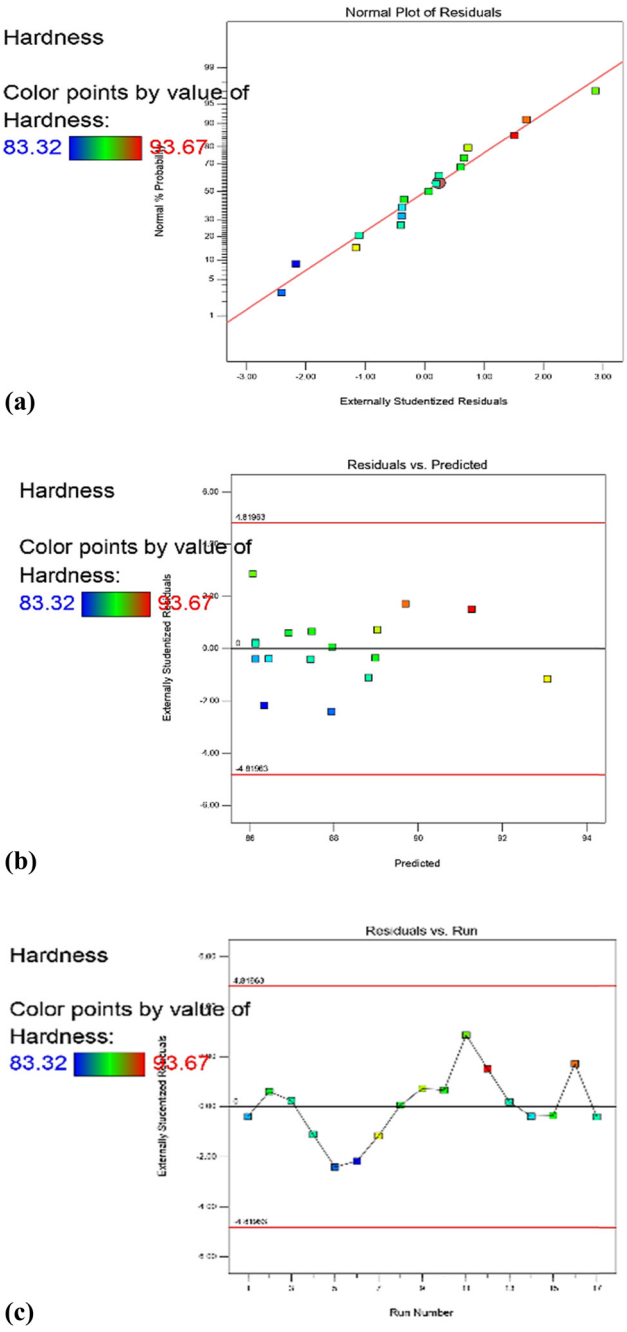

Figure 21: (a) Normal percent probability graph for hardness. (b) Residual *vs* predicted graph for hardness. (c) Residual *vs* run graph for hardness.

of prediction (Figure 21(c)). The findings indicate that the experimentation-based observed and forecasted values accord significantly and notably evidenced by all spots positioned meticulously closer to the diagonal axis line [42–47].

Figure 21(a)–(c) represents normality test probability distributions for residuals as well as the relationship

between an actual and predicted hardness of leather buffing dust/recycled EVA polymer composites. A standard normality probability distribution curve for residuals evaluates the model's adequacy by examining the hardness data used throughout the model.

The interaction effects of molding time, molding pressure, and molding temperature against the hardness are investigated by plotting surface curves. The input parameters are represented by the primary and secondary horizontal axis, while the measured output parameter is hardness, which is represented by the vertical axis. The interactions of these factors generate 3D surface curves (3D) as well as contour plots (2D).

Figure 22(a)–(c) demonstrates the dependency of hardness on molding time, molding pressure, and molding temperature. The hardness was increased to some extent with molding pressure and temperature whereas, with the increase in molding time, a negligible change in hardness can be apparently observed.

3.2.1.12 Hardness response-based numerical optimization

To ensure the proposed model's validity and efficacy, experimental trials were performed under standardized optimal settings, and the average value of the scientific observations was correlated to the anticipated prediction results. Figure 23 shows the ramp function graph, which indicates that the optimum value of hardness (shore A 86.0759) is obtained with molding temperature (120°C), molding time (20 min), and molding pressure parameters (5 tons) with the desirability of 1. Besides, a confirmation experiment was also carried out. Shore A hardness of

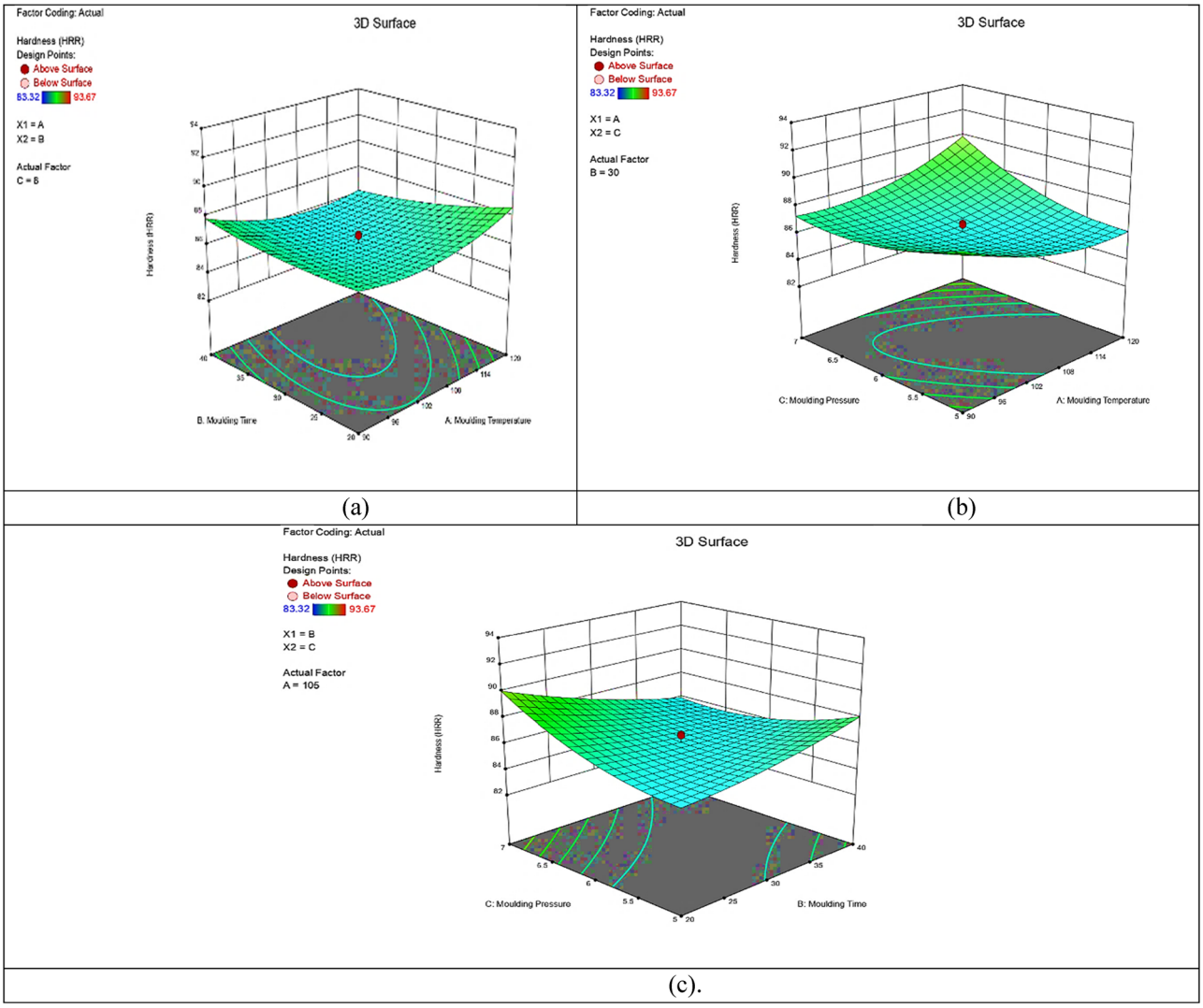

Figure 22: (a–c) 3D interaction plots for the hardness of leather buffing dust reinforced recycled EVA polymer composites.

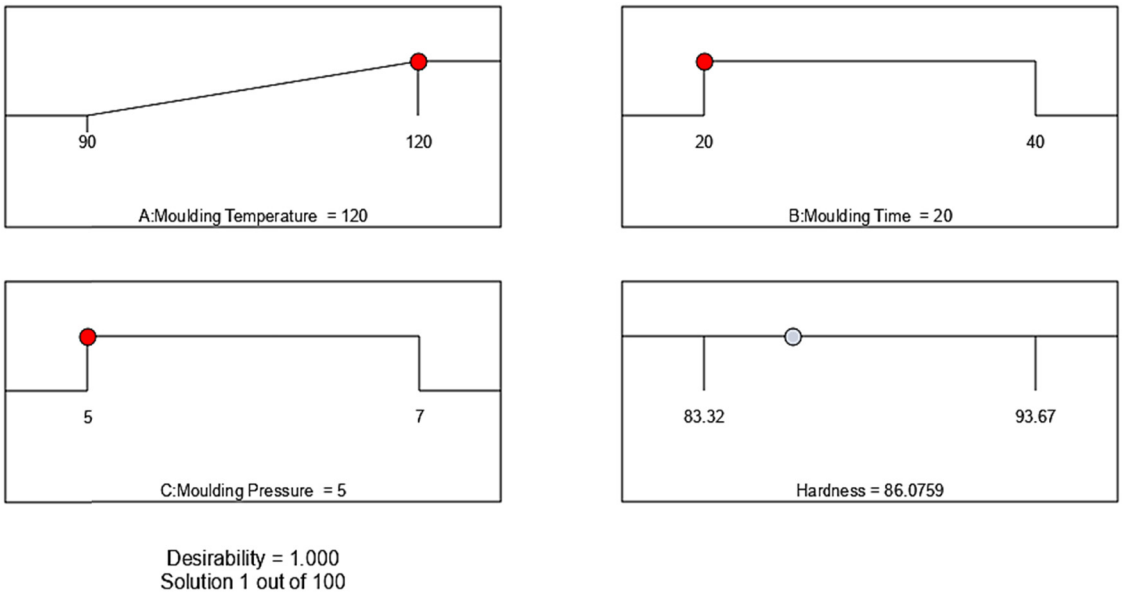

Figure 23: Ramp function graph for hardness.

leather buffing dust/recycled EVA polymer composites, developed at an optimum combination of parameters, was found to be 87.5. The results revealed that the error between the developed model, and experimental results were only 1.65%. Hence, this proved the applicability, and potential feasibility of the proposed derived mathematical models for efficiently optimizing the hardness of leather buffing dust-reinforced recycled EVA polymeric composites.

The related computational studies were also analyzed by Kunnan Singh *et al.* [43] optimized mechanical behavior of polytetrafluoroethylene/glass fiber-reinforced polyoxymethylene composite materials according to RSM technique using CCD. The composition of the polytetrafluoroethylene was varied from 1.7 to 17.3 wt%) and etched time was varied from 2.9 to 17.1 min. The effect of these two parameters was analyzed in the form of hardness, strength, stiffness, and toughness. The authors reported that the toughness of the composites increased but with the loss of hardness, strength, and stiffness [45].

3.2.1.13 ANOVA and model-fitting for abrasion resistance

As depicted in Table 15, the model *F*-value of 16.82 indicates that the proposed model is statistically significant. An *F*-value of this magnitude has a 0.01% probability of occurring as a result of noise. Model terms with *P*-values

Table 15: ANOVA for abrasion resistance

Source	Sum of squares	DOF	Mean square	*F*-value	*P*-value	
Model	2561.82	9	284.65	16.82	<0.0001	Significant
A-Molding temperature	14.44	1	14.44	0.7643	0.3245	
B-Molding time	223.97	1	223.97	14.31	0.0076	
C-Molding pressure	522.61	1	522.61	30.23	0.0054	
AB	36.33	1	36.33	3.13	0.1773	
AC	28.21	1	28.21	2.15	0.3019	
BC	16.04	1	16.04	0.8245	0.3725	
A^2	51.86	1	51.86	62.33	<0.0001	
B^2	119.18	1	119.18	7.03	0.0232	
C^2	387.71	1	387.71	23.57	0.0008	
Residual	151.85	10	12.13			
Lack of fit	20.16	5	6.16	0.2203	0.8261	Non-significant
Pure error	105.17		19.25			
Cor total	2368.24	19				

lower than 0.0500 are significant. Throughout this context, A, B, C, A^2, and B^2 are considerable significantly model terms. If the value is higher than 0.1000 then, the model terms are not significantly relevant. If the model has a lot of insignificant terms, then model reduction can ameliorate the model (not considering those needed to assist and facilitate hierarchy).

The R^2 (adjusted) of 0.9173 is fairly comparative or equivalent to the R^2 (predicted) of 0.8843, and therefore, the disparity/variation is less than 0.2. The signal-to-noise ratio was computed by Adeq precision. A signal-to-noise ratio of 21.9860 implies that the signal is adequately effective, and one can utilize this model to navigate the design and model layout space, as illustrated in Table 16.

3.2.1.14 Evolution of mathematical model from ANOVA for abrasion resistance

The quadratic regression mathematical models developed based on RSM for correlating the abrasion resistance in terms of coded values, and actual values with hot-press processing parameters after eliminating the non-significant terms is specified as follows:

$$\begin{aligned}\text{Abrasion resistance} = {} & +734.11729 - 4.08697 \text{ moulding temperature} \\ & + 1.15894 \text{ moulding time} \\ & - 73.92307 \text{ moulding pressure} \\ & - 0.053500 \text{ moulding temperature} \times \text{moulding time} \\ & + 0.607500 \text{ moulding temperature} \times \text{moulding pressure} \\ & + 0.633500 \text{ moulding time} \times \text{moulding pressure} \\ & + 0.011608 \text{ moulding temperature}^2 \\ & + 0.010950 \text{ moulding time}^2 \\ & - 0.635631 \text{moulding pressure}^2.\end{aligned} \tag{11}$$

The data have been analyzed to further validate that now the residual distributions were normal. Figure 24(a) reveals that the residuals' data are normally distributed using a normality distribution plot. The residuals depict the variation among the actual measured value of a response as well as the values predicted by the theoretical mathematical model. The presence of a minimal residual value implies that the modeling predictions are satisfactorily acceptable [42–47]. Figure 24(a) exhibits the substantially remarkable datasets, and relatively closer toward the straight-line position. Considering normal observations, a few scatter had also been discerned, signifying that now the dataset findings are normally distributed.

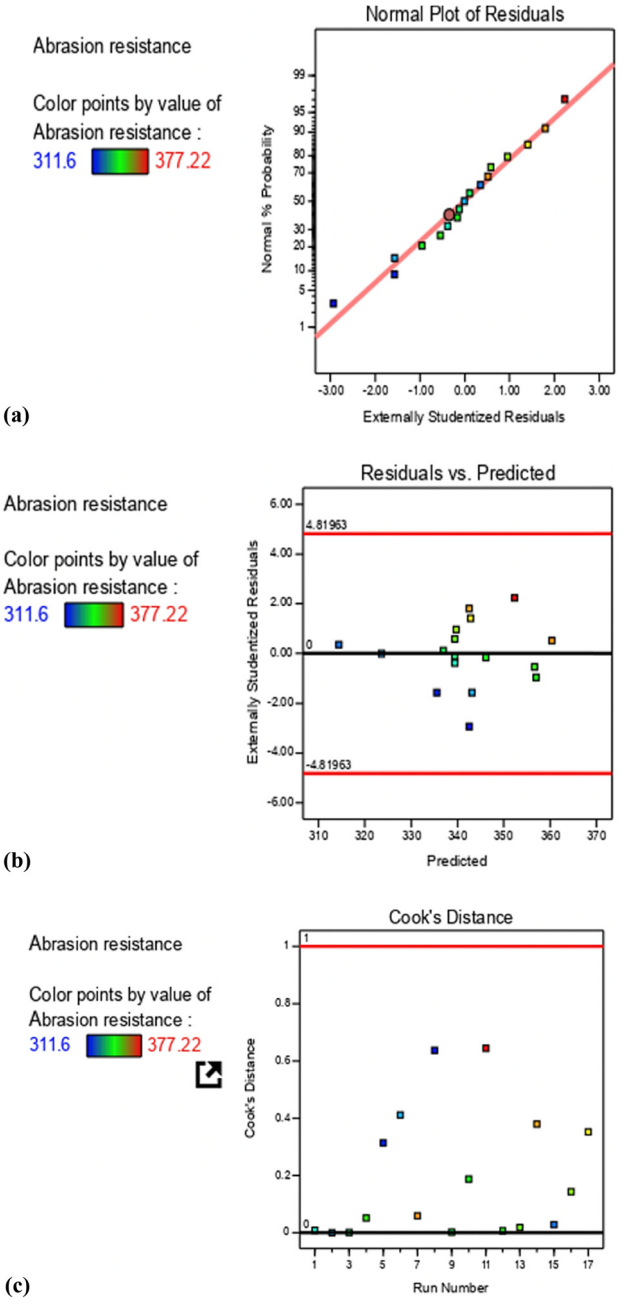

Figure 24: (a) Normal percent probability graph for abrasion resistance. (b) Residual *vs* predicted graph for abrasion resistance. (c) Residual *vs* run graph for abrasion resistance.

Table 16: Fit statistics for abrasion resistance

Std. dev.	4.23	R^2	0.9781
Mean	123	Adjusted R^2	0.9173
CV%	3.26	Predicted R^2	0.8843
		Adeq precision	21.9860

The fitted model was confirmed to ascertain its adequate resemblance to the actual measured values. Till the model exhibits a suitable fit, optimizing the fitted response surface is expected to yield inadequate as well as deceptive outcomes [42–47]. The diagnostic graphs, like anticipated against actually obtained experimentation data, validated the model's appropriateness or viability. The charts demonstrated a correlation among expected, and observed values. Figure 24(b) illustrates the analytic diagnosis diagrams of the response characteristics like abrasion resistance. The dataset values on this chart reclined significantly closer to the straight line suggesting that the real facts and the evidence presented from the models were in excellent accordance. As per the findings, the models employed throughout this investigation were liable for predicting process operational conditions for the production of leather buffing dust-reinforced recycled EVA polymeric composites.

The analytical diagnosis charts of multiobjective optimization of compression molding-based process-operating parameters on abrasion resistance are shown in Figure 24(a)–(c) to further evaluate the adequacy and validity of the regression D-optimum modeling framework for the predictive model. The empirical outliers had an excellent distribution within the specified desired spectrum, as shown in Figure 24(c). The anticipated projected abrasion resistance values of the compression molding were contrasted and evaluated with the observed empirical values to determine the accuracy of prediction (Figure 24(c)). The findings indicate that the experimentation-based observed and forecasted values accord significantly and are evidenced notably by all spots positioned meticulously closer to the diagonal axis line [42–47].

Figure 24(a)–(c) represents the normality test probability distributions for residuals as well as the relationship between an actual and predicted abrasion resistance of leather buffing dust/recycled EVA polymer composites. A standard normality probability distribution curve for residuals evaluated the model's adequacy by examining the abrasion resistance data used throughout the model.

The interaction effects of molding time, molding pressure, and molding temperature against the abrasion resistance were investigated using plotting surface curves. The input parameters are represented by the primary and secondary horizontal axis, while the measured output parameter was an abrasion resistance, which was represented by the vertical axis. The interactions of these factors generate 3D surface curves (3D) as well as contour plots (2D).

Figure 25(a)–(c) demonstrates the dependency of abrasion resistance on molding time, molding pressure, and molding temperature. The abrasion resistance consistently decreases with the increase in molding time and continuously increased with raising molding pressure, whereas an effect of molding temperature can be seen constant.

3.2.1.15 Abrasion resistance response-based numerical optimization

To ensure the proposed model's validity and efficacy, the experimental trials were performed out and under standardized optimal settings, and the average value of the empirically scientific observations was correlated to the anticipated prediction results. Figure 26 shows the ramp function graph, which indicates that the optimum value of abrasion resistance (343.068 mm^3) is obtained with molding temperature (90°C), molding time (40 min), and molding pressure parameters (7 tons) with desirability of 1. Besides, the confirmation experiment was also carried out. Abrasion resistance of leather buffing dust/recycled EVA polymer composites developed at an optimum combination of parameters was found to be 341.10 mm^3. The results revealed that the error between the developed model and experimental results was only 0.5736%. This proved the applicability and potential feasibility of the proposed derived mathematical models for efficiently optimizing the abrasion resistance of leather buffing dust reinforced, recycled EVA polymeric composites.

In another relevant research, Govindaraju and Jagannathan [44] optimized the mechanical behavior of polypropylene polymer matrix composite, which was reinforced with silk fibers. The composites were developed as per the CCD of the experiments, and process parameters in the form of compression temperature, compression time, and compression pressure were chosen. The authors suggested the compression temperature of 180°C, compression time of 7 min, and compression pressure of 35 bar as best settings to obtain better mechanical properties [46].

3.2.1.16 ANOVA and model-fitting for adhesion strength

As depicted in Table 17, the model F-value of 102.27 indicates that the proposed model is statistically significant. An F-value of this magnitude has a 0.01% probability of occurring as a result of noise. Model terms with P-values lower than 0.0500 are significant. Throughout this context, A, AB, A^2, and C^2 are considerable significantly model terms. If the value is higher than 0.1000 then, the model terms are not significantly relevant. If the model has a lot of insignificant terms, then model

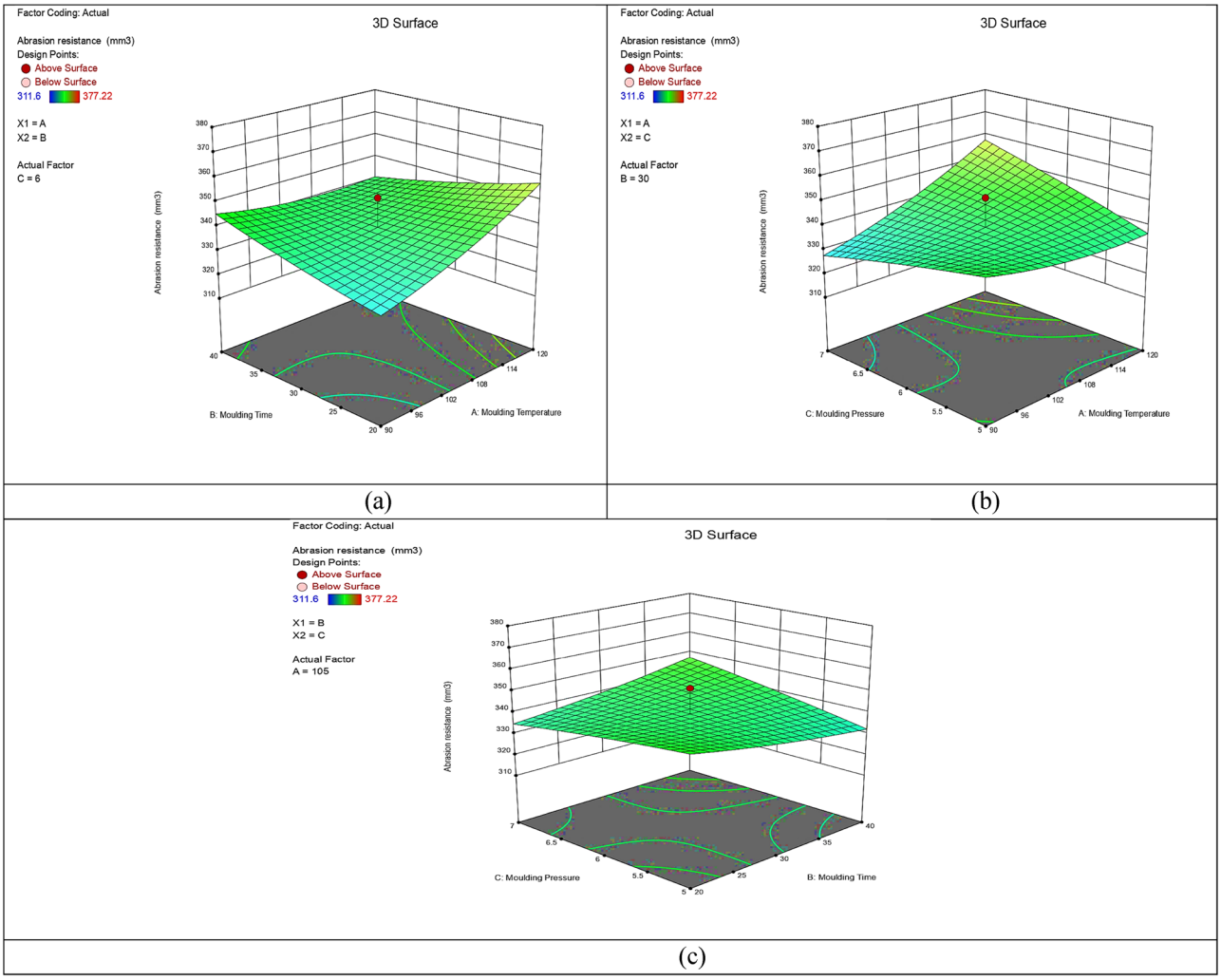

Figure 25: (a–c) 3D interaction plots for abrasion resistance of leather buffing dust reinforced recycled EVA polymer composites.

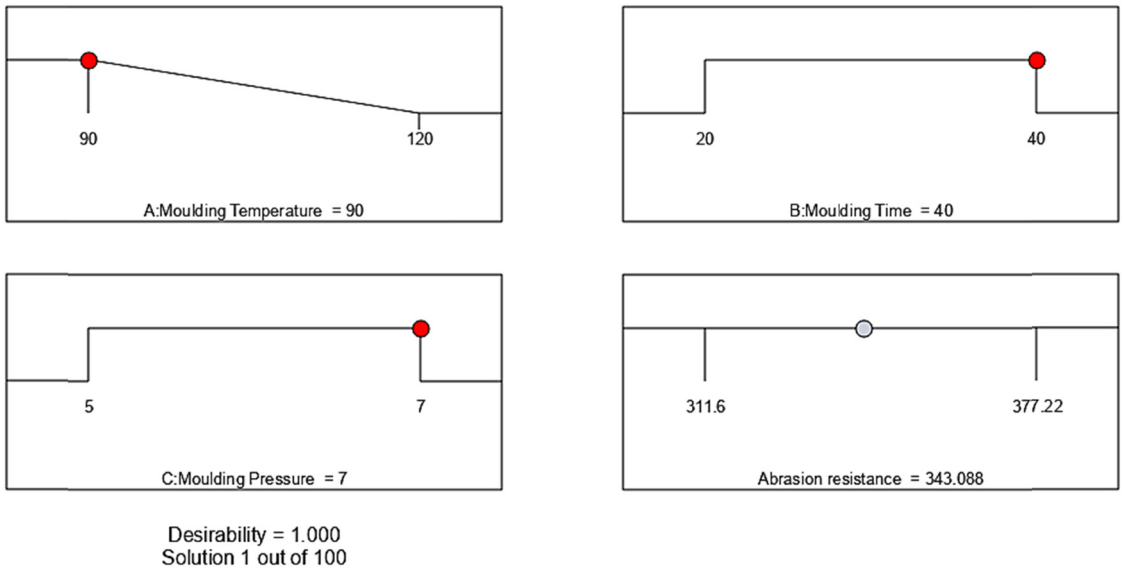

Figure 26: Ramp function graph for abrasion resistance.

Table 17: ANOVA for adhesion strength

Source	Sum of squares	DOF.	Mean square	*F*-value	*P*-value	
Model	488.32	9	84.56	102.27	<0.0001	Significant
A-Molding temperature	88.94	1	88.94	139.63	<0.0001	
B-Molding time	10.57	1	10.57	5.44	0.3883	
C-Molding pressure	6.48	1	6.48	8.22	0.1608	
AB	71.14	1	71.14	88.21	<0.0001	
AC	10.39	1	10.39	8.42	0.3941	
BC	56.12	1	56.12	5.93	0.1296	
A^2	178.71	1	178.71	204.54	<0.0001	
B^2	112.47	1	112.47	162.23	<0.0001	
C^2	65.51	1	65.51	8.47	0.3641	
Residual	5.37	7	0.104			
Lack of fit	0.68	5	0.1293	3.05	0.2652	Non-significant
Pure error	5.41	2	0.042			
Cor total	503.29	19				

reduction can ameliorate the model (not considering those needed to assist and facilitate hierarchy).

The R^2 (adjusted) of 0.9667 is fairly comparative or equivalent to the R^2 (predicted) of 0.9542, and therefore, the disparity/variation is less than 0.2. The signal-to-noise ratio was computed by Adeq precision. A signal-to-noise ratio of 32.412 implies that the signal is adequately effective, and one can utilize this model to navigate the design and model layout space as depicted in Table 18.

Table 18: Fit statistics for adhesion strength

Std. dev.	0.87	R^2	0.9763
Mean	11.52	Adjusted R^2	0.9667
C.V.%	3.61	Predicted R^2	0.9542
		Adeq precision	32.412

3.2.1.17 Evolution of mathematical model from ANOVA for adhesion strength

The quadratic regression mathematical models developed based on RSM for correlating the adhesion strength in terms of coded values and actual values with hot-press processing parameters after eliminating the non-significant terms is specified as follows:

$$\begin{aligned}\text{Adhesion strength} = &-17.49804 + 0.184824\ \text{moulding temperature} \\ &+ 0.057528\ \text{moulding time} \\ &+ 2.70492\ \text{moulding pressure} \\ &+ 0.001408\ \text{moulding temperature} \times \text{moulding time} \\ &- 0.006917\ \text{moulding temperature} \times \text{moulding pressure} \\ &- 0.019625\ \text{moulding time} \times \text{moulding pressure} \\ &- 0.000904\ \text{moulding temperature}^2 \\ &- 0.001327\ \text{moulding time}^2 \\ &- 0.104397\ \text{moulding pressure}^2.\end{aligned} \tag{12}$$

The data analysis was done to further affirm that perhaps the residual distributions were becoming normal. Figure 27(a) reveals that the residuals' data are normally distributed using a normality distribution plot. The residuals depict the variation among the actual measured value of a response as well as the values predicted by the theoretical mathematical model. The presence of a minimal residual value implies that the modeling predictions are satisfactorily acceptable [42–47]. Figure 27(a) exhibits the datasets, which are substantially remarkable and relatively closer toward the straight-line position. Considering normal observations, a few scatter had also been discerned, signifying that now the dataset findings are normally distributed.

The fitted model was affirmed to ascertain its adequate resemblance to the actual measured values. Till the model exhibits a suitable fit, optimizing the fitted response surface is expected to yield inadequate as well as deceptive outcomes [42–47]. The diagnostic graphs, like anticipated against actually obtained experimentation data, validated the model's appropriateness or viability. The charts demonstrated a correlation between expected and observed values. Figure 27(b) illustrates the analytic diagnosis diagrams of the response characteristics like adhesion strength. The dataset values on

this chart reclined significantly closer to the straight line suggesting that the real facts and the evidence presented from the models were in excellent accordance. As per the findings, the models employed throughout this investigation were liable for predicting process operational conditions for the production of leather buffing dust-reinforced recycled EVA polymeric composites. The analytical diagnosis charts of multiobjective optimization of compression molding based process-operating parameters on adhesion strength are shown in Figure 27(a)–(c) to further evaluate the adequacy as well as the validity of the regression D-optimum modeling framework for the predictive model. The empirical outliers used to have an excellent distribution within the specified desired spectrum, as shown in Figure 27(c). The anticipated projected adhesion strength values of the compression molding were contrasted and evaluated with the observed empirical values to determine the accuracy of prediction (Figure 27(c)). The findings indicate that the experimentation-based-observed and forecasted values accord significantly and notably evidenced by all spots positioned meticulously closer to the diagonal axis line [42–47].

Figure 27(a)–(c) represents the normality test probability distributions for residuals as well as the relationship between an actual and predicted adhesion strength of leather buffing dust/recycled EVA polymer composites. A standard normality probability distribution curve for residuals evaluates the model's adequacy by examining the adhesion strength data used throughout the model.

The interaction effects of molding time, molding pressure, and molding temperature against the adhesion strength are investigated by plotting surface curves. The input parameters are represented by the primary and secondary horizontal axis, while the measured output parameter is an adhesion strength, which is represented by the vertical axis. The interactions of these factors generate 3D surface curves (3D) as well as contour plots (2D).

Figure 28(a)–(c) demonstrates the dependency of adhesion strength on molding time, molding pressure, and molding temperature. The adhesion resistance has consistently decreased with the increase in the molding pressure, and molding temperature but remains constant with the increased molding time.

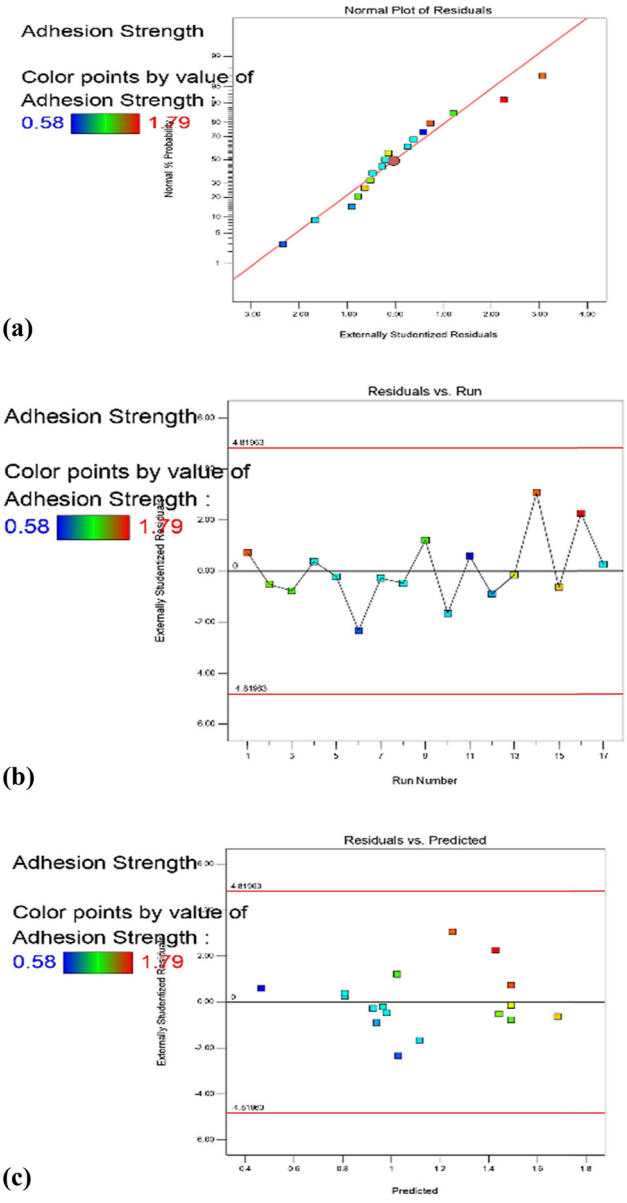

Figure 27: (a) Normal percent probability graph for adhesion strength. (b) Residual *vs* predicted graph for adhesion strength. (c) Residual *vs* run graph for adhesion strength.

3.2.1.18 Adhesion strength response-based numerical optimization

To ensure the proposed model's validity and efficacy, the experimental trials were performed out and under standardized optimal settings, and the average value of the empirically scientific observations was correlated to the anticipated prediction results. Figure 29 shows the ramp function graph, which indicates that the optimum value of adhesion strength (0.925121 N/mm) is obtained with molding temperature (120°C), molding time (20 min), and molding pressure parameters (7 tons) with desirability of 1. Besides, the confirmation experiment was also carried out. The adhesion strength of leather buffing dust/recycled EVA polymer composites developed at an optimum combination of parameters was found to be 0.9575 N/mm. The results revealed that the error between

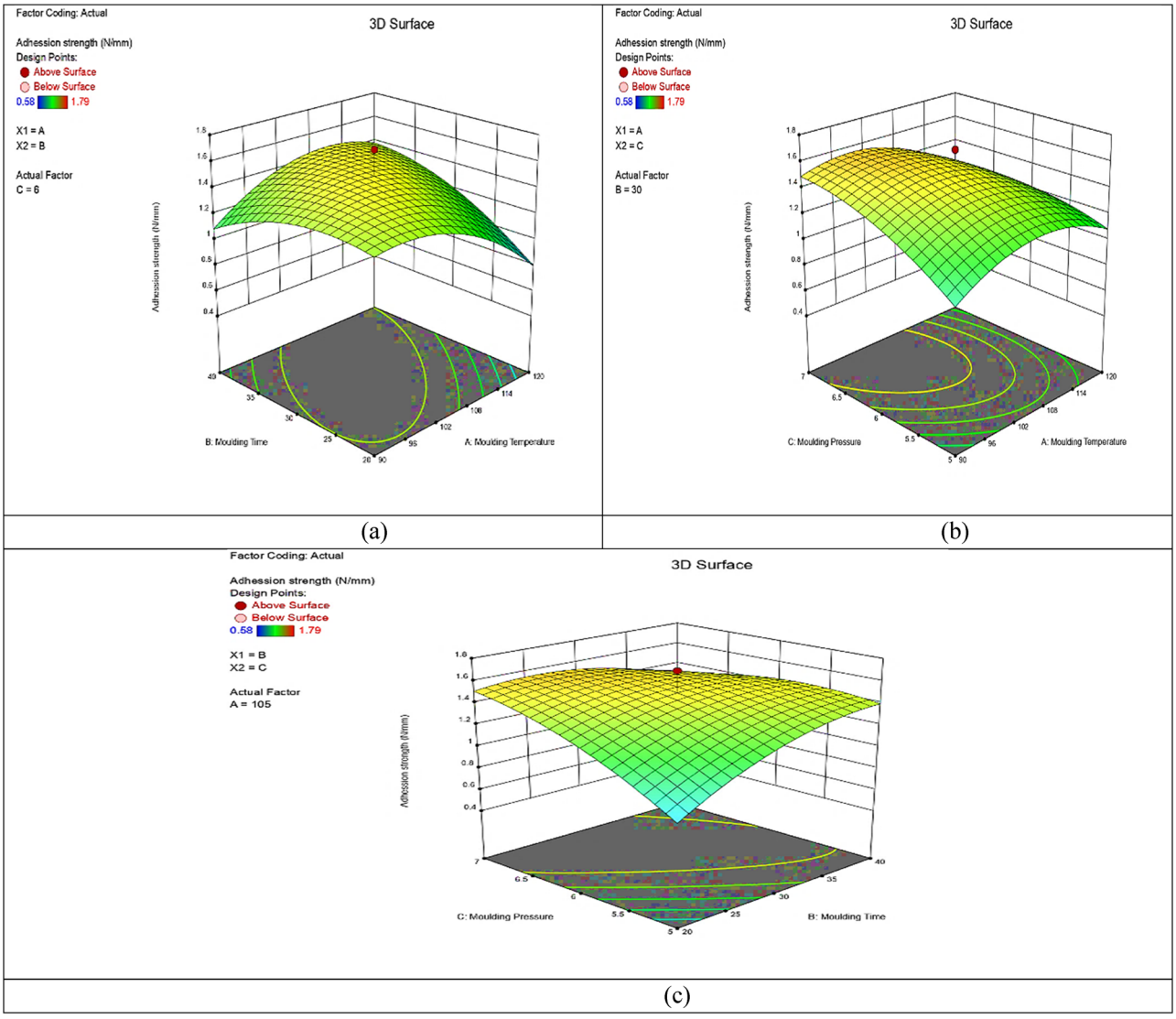

Figure 28: (a–c) 3D interaction plots for adhesion strength of leather buffing dust reinforced recycled EVA polymer composites.

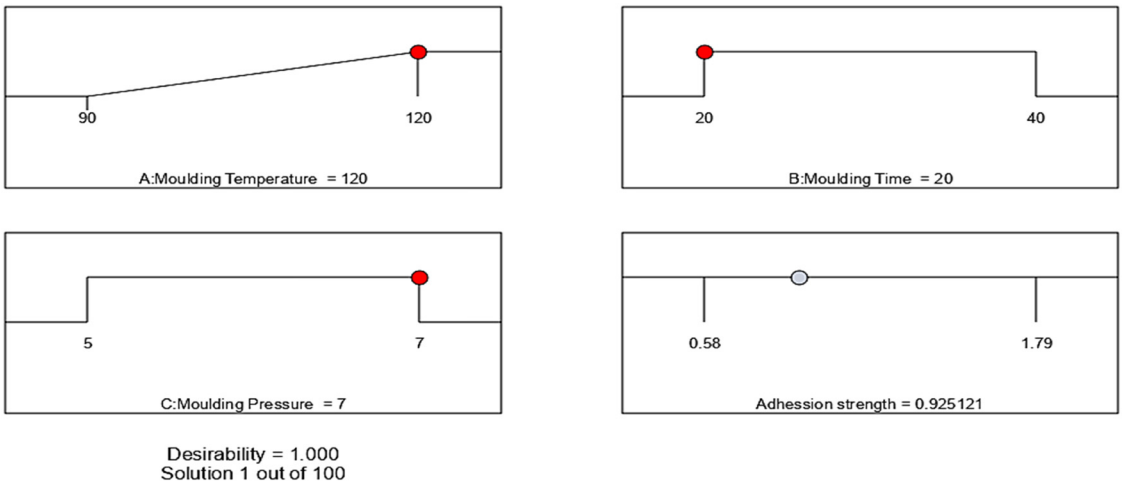

Figure 29: Ramp function graph for adhesion strength.

the developed model and experimental results is only 3.3816%. This proved the applicability and potential feasibility of the proposed derived mathematical models for efficiently optimizing the adhesion strength of leather buffing dust-reinforced recycled EVA polymeric composites.

The related research was being reported by Kale and Jadhav [45] who utilized waste leather as reinforcement in epoxy polymer polymeric matrix composites (PMMCs) and explored their effect on the composite properties. TGA, DMA, and SEM were used to characterize newly developed composites. Optimization was also performed, and the best set of input parameters was suggested. TGA results illustrated that base epoxy is less stable than PMMCs. Also, an increase in leather contents improved interfacial bonding, resulting in better compatibility. DMA results indicated a lower elastic modulus (EM) of epoxy than its composites. SEM images visualized uniform dispersion of leather, resulting in improved mechanical properties. Maximum tensile and flexural strength of 20.58 and 45.27 MPa, respectively, together with the highest impact energy, are obtained at 30% leather composition with 7.5 mm composite thickness. Similarly, for maximum EM, 30% leather and 2.5 mm thickness is required. ANOVA revealed that fiber composition is significant for all output parameters and composite thickness, and interactions between fiber composition and composite thickness are significant for EM and flexural modulus (FM). The interaction of fiber composition with itself is significant for FM and impact energy (IE). Similarly, the interaction of composite thickness with itself is significant for FM. Tensile strength of 19.9 MPa, the EM of 1.57 GPa, the flexural strength of 42.1 MPa were obtained after the application of the optimization technique [47].

3.3 Experimental results

3.3.1 Physicomechanical characteristics

3.3.1.1 Tensile strength

The tensile slabs for the assessment of physicomechanical characteristics were molded using a hydraulic press with electrically heated platens operating at 110°C and a pressure of 6 tons. The compounded sheet, approximately 3.54 mm thickness, was placed in the mold, and the platens were closed under pressure.

The physicomechanical characteristics of the solid leather wastes/recycled polymer composites were fervently affected by the percent leather buffing dust as fiber concentrations. The tensile strength of the neat recycled EVA polymer was found to be 12.295 MPa. However, the average tensile strength of leather buffing dust as a reinforced fiber in recycled EVA polymer composites is found to be 9.485 MPa. This conduct was ascribed to compelling interfacial bonding or adherence strength, and the fact that, with a 1:1 weight fraction of leather waste and recycled EVA matrix, the fiber agglomerations were closer to each other. As a result, the recycled EVA polymer might have served as an adhesive agent amongst the coalescence agglomerations and distributed the stress from one aggregate to another. Thus, it is indicated that an increase in the ductility, and decrement in the elongation at break of the polymer matrix with the incorporation of leather buffing dust as fiber.

In general, improved interfacial strength results if sufficient adhesion exists between the matrix and the fiber. If the interfacial strength is higher than the matrix cohesion force, then the internal resisting force to split the specimen is regulated by the stress concentration throughout the region of the nanofillers reinforcing particulates. Under these conditions, a rise in the modulus, a drastic reduction at the elongation at break, and a rise in tear strength are observed. Tensile strength values do not generally indicate any particular trend since its variation depends on the loading, type of the fiber, and the nature of the matrix. Tensile strength values of composites even lower than that of the unfilled matrix are obtained when the fiber concentration is below the critical volume fraction [48]. However, mechanical properties improve as the fiber concentration increases above the critical volume fraction.

The percent elongation at break reveals the elasticity of the composite materials. The leather buffing dust/recycled EVA polymer composites exhibited lower percentage elongation at break of 34.08% compared to the control sample, that is, neat recycled EVA polymer, which is found to be significantly higher (192.16%) as displayed in Figures 30 and 31. When leather fibers were added to the recycled EVA polymer matrix, they become stiffer, as seen from the very low elongation at break values. The failure process becomes more brittle as the leather loading in the polymer increases.

The low elongation at break values could be attributed to the formation of crevasses, deformations, perforations, tiny cracks encircling the fillers, and the emergence of void cavities caused by a localized detachment of the recycled EVA matrices from the leather fabrics. The elongation at break values is reduced considerably as the composites approach brittle failure. At high filler loading of 1:1, voids were formed, which destroyed the integrity of

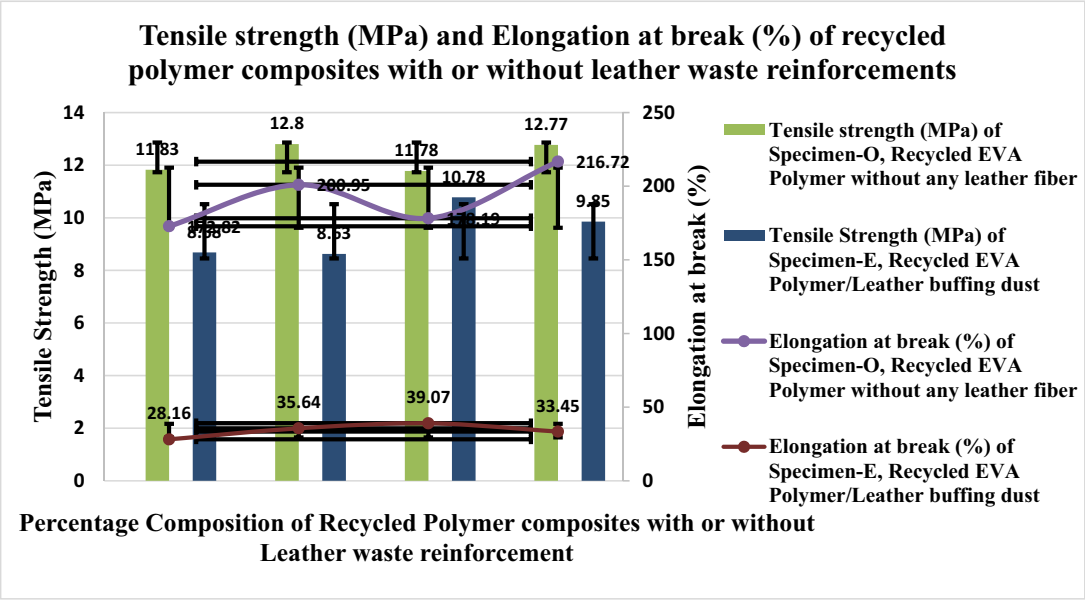

Figure 30: comparison of the tensile strength of neat recycled EVA polymer composites and leather buffing dust/recycled EVA polymer composites.

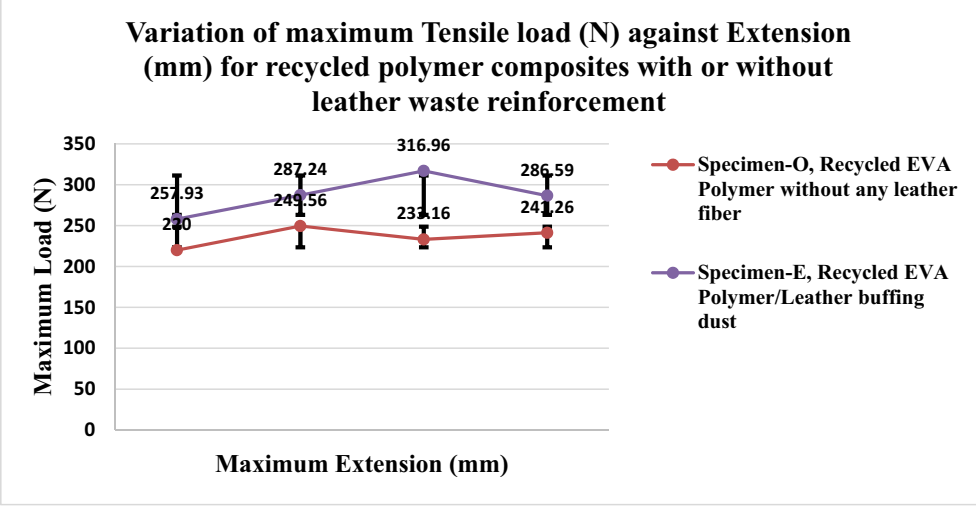

Figure 31: Variation of tensile load (N) against extension (mm) of recycled EVA polymer composites with or without leather buffing dust.

the composites. As the voids grew, they interacted with each other, resulting in the separation of the matrix from the fiber. The increased interaction between the neighboring voids overweighed the reinforcing effect of the leather fibers. In addition, under tensile load, normal stresses are applied to each filler particle. The points at which such stresses are maximum are the most vulnerable as separation of the recycled EVA matrix from the leather fiber is most likely to start there. As the loading increase and reaches up to 1:1, the leather fibers could also form a cohesive network preferentially between themselves, resulting in a weak interface with the recycled EVA matrix leading to poor mechanical properties. Even though, compared with the properties of these composites with the previous findings, the leather buffing dust reinforced recycled EVA polymer composites still exhibit an excellent remarkable physicomechanical strength.

With the mobility and resilience of the leather fibers and the plastic recycled EVA matrix, the agglomerates of leather fibers could be brought closer, exhibiting an

inextricable bond, and the leather buffing dust can be intertwined as well as entangled as the maximum fiber content. The interconnected aggregates covered in the recycled EVA matrix could strongly increase the rigidity, elasticity, stability of the composites and the elastic module as reported by Ambrosio *et al.* [47].

According to Dodwell, a fashionable aesthetic and convenient footwear could have been formed from leather boards with a tensile strength of 5.5 MPa while expensive and light footwear could have been manufactured from leather boards with a tensile strength of 4.0 MPa [50].

Figure 31 further displays a broad spectrum of behavior possibilities on a specific stress–strain curve varying from hard, brittle to ductile, with a yield-point comparable to that of a thermoplastic polymer once exposed to mechanically-agitations (stresses) [51].

The reinforcement's rigidity was already effectively transmitted into the matrix. According to Covington, the amorphous nature of HDPE90/Chrome tanned wastes10 once cooled from melt afterward processing could be accounted for the higher-modulus at 10% waste content [52].

Figure 32(a) and (b) depicts the tensile-fractured micrographs of a pure recycled EVA polymer sample. The surface is typically lined and filled with bulged, twisted, and elongated materials, which appeared to be an indication of such a lateral pressure bearing strength. Substantial deformation capacities, as might be anticipated for relatively flexible recycled EVA copolymer, also substantiated with the enormous strains as measured through experimental studies with a tensile strength of 12.295 MPa and percent elongation at a break of 192.17% as the comparable behaviors were reported by Stael *et al.* [51].

Besides collagen fibrils bundles, Figure 33(a) and (b) displays some perforations, fractures, crevices, cavities, and voids in the recycled EVA polymer surface. This may be attributable to leather buffing dust fibers being pulled out afterward the tensile testing as depicted in Figure 33(a) and (b). The source or location of fiber rupture or deformation was easily detected nearby pull-out openings, implying a poor adherence among leather buffing dust fibers and recycled EVA polymer. Nevertheless, improving the volume of leather buffing dust fibers

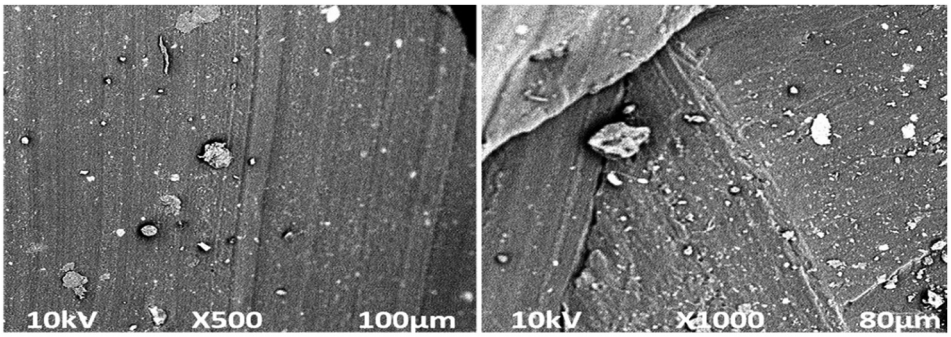

Figure 32: SEM tensile-fractured micrographs of Neat recycled EVA polymer without leather fibers at a magnification of (a) 500×; (b) 1,000×.

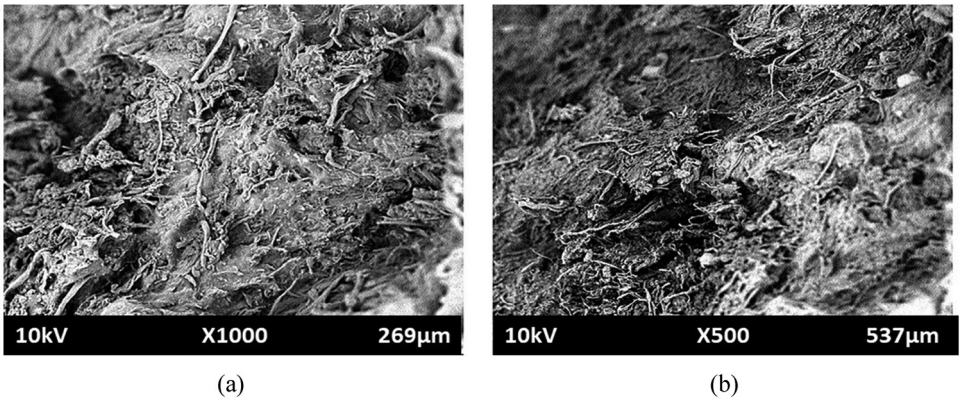

Figure 33: SEM tensile-fractured micrographs of leather buffing dust/recycled EVA polymer composites at a magnification of (a) 1,000×; (b) 500×.

throughout composites ameliorated the permeability, bonding, and interfacial adherence of leather buffing dust fibers to recycled EVA polymer. Indeed, as shown in Figure 33(a) and (b) at 50/50 wt% leather buffing dust fibers/recycled EVA polymer composites, the leather buffing dust fibers distribution was quite fervent. They seemed to shrink in size, indicating that the leather fibers bundle were split into a mere individual fiber. As a result, each fiber throughout the recycled EVA polymer matrices may efficiently shift and reorient, culminating in reasonable leather buffing dust fibers distribution. Nevertheless, whenever the volume of leather fibers was raised, a drop in fiber-fiber interaction significantly enhanced the region of a stress relaxation gradient curvature. Furthermore, the firm bonding between leather buffing dust fibers and recycled EVA polymer demonstrates the significant remarkable improvement in physicomechanical characteristics of leather buffing dust/recycled EVA composites.

3.3.1.2 Compressive strength

The average compression modulus of the representative specimen, leather buffing dust/recycled EVA polymer composite, is higher and found out to be 76.71 MPa. In comparison, the average compression modulus of neat recycled EVA Polymer without fiber content was found to be 66.695 MPa, as demonstrated in Figure 34. Though the compression modulus measures the material's stiffness, higher is the compression modulus which leads to stiffer in the polymer composites.

The compressive strength tends to increase slightly for leather buffing dust/recycled EVA polymer composite (9.95 MPa) as compared to the neat recycled EVA polymer (9.87 MPa), as shown in Figure 35.

The stress–strain curve is nonlinear, which is consistent with the stress–strain profile of thermoplastic polymers. Since the filler has not tempered the ductility, the strain of the control (high-density polyethylene (HDPE)) was higher than its composites, as reported by Musa *et al.* [52]. At minimal waste content (within a 10–20 wt% of fiber), the stiffness and brittle quality of a filler have inculcated its rigidity to some of the most ductile matrix (HDPE), resulting in decreased strain. Outcomes also show that the HDPE90/chrome-tanned waste at 10% composite mixture has higher stress and strain than the control (HDPE) as NR was present, affecting the strain (acting as an extender) and facilitated filling dispersion in the matrix. Thus, HDPE90/chromium-tanned waste with 10% loading had become more ductile and tough as a result.

3.3.1.3 Tear strength

The tear strength of the solid leather waste/recycled EVA composites also indicated the dependence of this property on the leather waste as maximum fiber concentration in the recycled EVA polymer composites. However, the average tear strength with leather buffing dust as reinforcement fibers were found to be around 7.5425 N/mm. While for the neat recycled EVA Polymer, average tear strength was found to be 9.48 N/mm, as displayed in Figure 36, and Figure 37. The maximum leather fiber content leads to greater tear resistance, as reported by

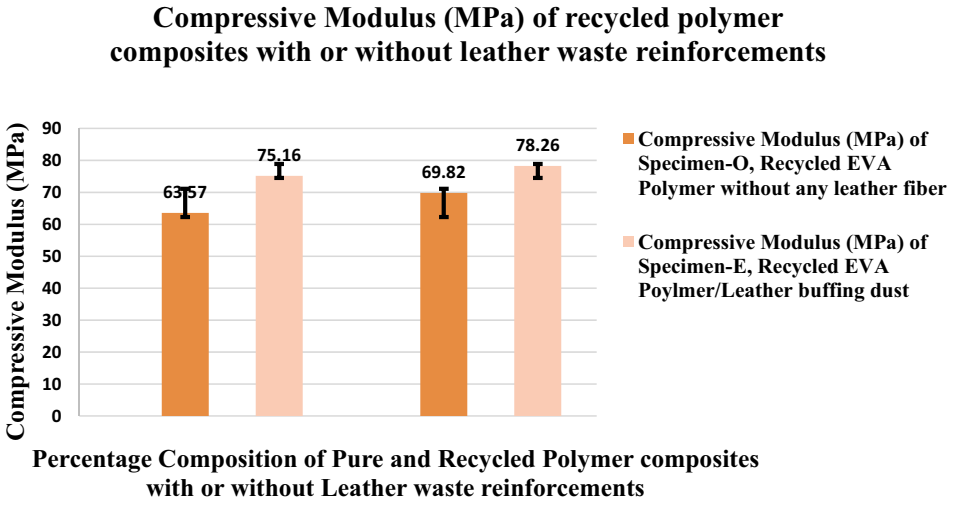

Figure 34: Comparison of compression modulus (MPa) of recycled EVA polymer composites with or without leather buffing dust.

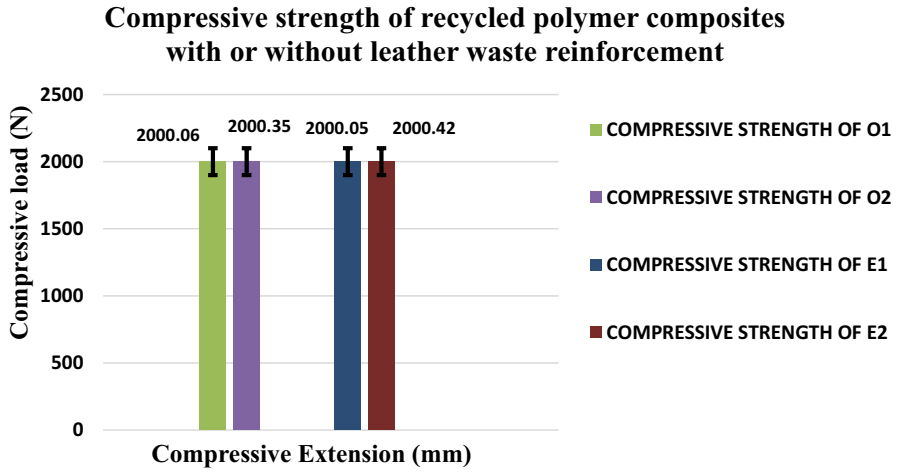

Figure 35: Comparison of compressive strength (MPa) of recycled EVA polymer composites with or without leather buffing dust.

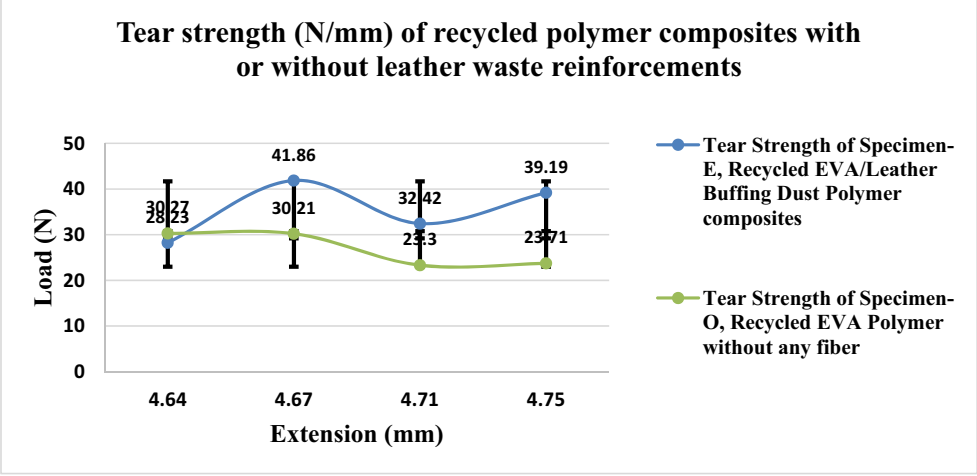

Figure 36: Variation of tear load (N) against extension (mm) of recycled EVA polymer composites with or without leather buffing dust.

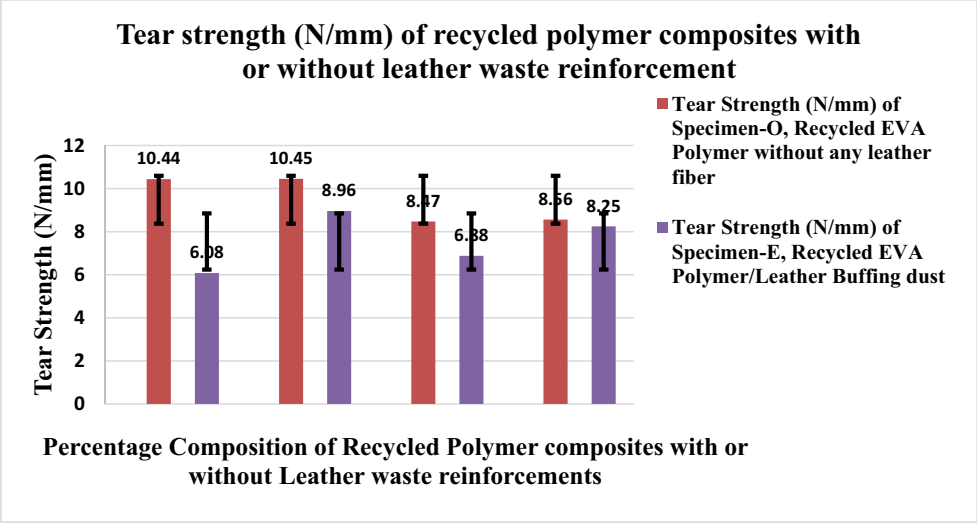

Figure 37: Comparison of tear strength (N/mm) of recycled EVA polymer composites with or without leather buffing dust.

Madera-Santana *et al.* [17]. This is because of the morphological nature of the leather buffing dust in powdery form as incorporated (uniformly dispersed/blended with matrix) in the recycled EVA matrix.

According to Ambrósio *et al.* and Musa *et al.*, the inclusion of additives strengthened the fiber distribution in HDPE matrix, allowing for superior compatibility and interaction among the waste fibers as well as matrix [49,54]. The additives served mostly as a chemical group, forming an interface between the fiber surface and the matrix, enabling efficient stress transfer. Insufficient wetting surface results in significantly lower stress transfer through the interface and may comprehend deterioration at higher waste content

Ravichandran and Nmg reported that the NBR/PVC blends filled with treated leather fibers had exhibited significant improvements in mechanical properties [55]. The addition of leather fibers increases the modulus of elasticity of the blends. Considerable improvement in the tensile strength and tear strength was obtained with ammonia-treated leather shavings. Efficient vulcanization characteristics coupled with the strong polymer-leather interaction could be attributed to the improved modulus and lower elongation at break values. It is also known that the effective surface fracture energy for a composite was always higher than the unfilled polymer. Dispersed leather fibers make the crack propagation path longer or the process delayed. They also absorb a portion of the energy, thereby delaying the deformation of the matrix. This process is more evident from the improved tear strength of the leather-filled composites. This is in general agreement with the fact that the addition of short fibers improved the tear strength of elastomers. The low elongation at break values could be attributed to the formation of crevasses, deformations, perforations, tiny cracks encircling the fillers, and the emergence of void-cavities caused by a localized detachment of the matrices from the fibers [55].

3.3.1.4 Adhesion strength

Figures 38 and 39 have revealed that the average peel strength (anti stripping performance from polymers to the leather/adhesive bonding strength or peel test is carried out to examine the strength of a bond by estimating how much force was required to peel apart the fused materials) between the polymer to leather for leather buffing dust as fiber in recycled EVA matrix was found to be lower than around 0.9575 N/mm. This is due to a small specific surface area of leather buffing dust obtained after milling, decreasing the interfacial interaction between recycled EVA and buffing dust. In contrast, the adhesion peel strength of neat recycled EVA was found to be around 0.675 N/mm.

The test results for neat recycled EVA Polymer show the poor adhesion of upper-to-sole combination, and here, separation or breakdown of adhesive film at the surface was noticed. This may also be for inadequate roughing, poor surface preparation, and inappropriate drying time.

Results were evident that the surface upper leather failure occurs in the neat recycled EVA polymer composites while testing the adhesion between recycled EVA polymer to solid leather waste as displayed in Figure 39. At the same time, Adhesion to upper leather failure occurs

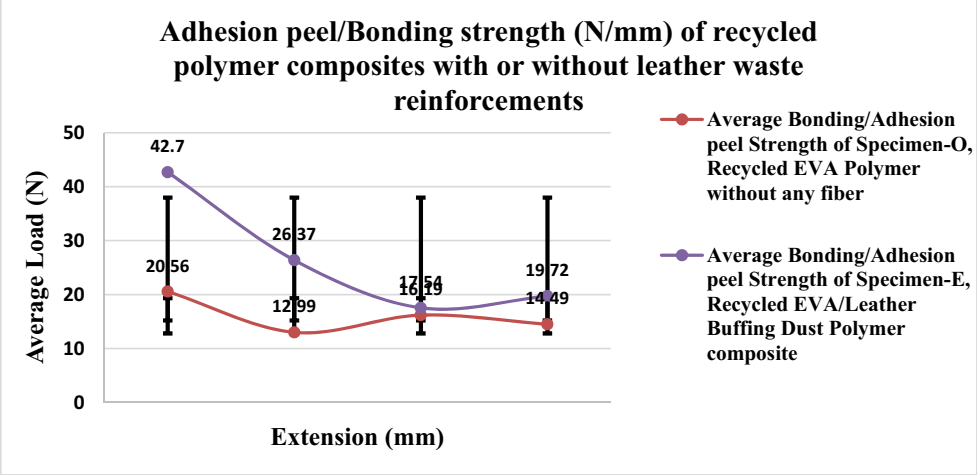

Figure 38: Comparison of average peel load (N) against extension (mm) of recycled EVA polymer composites with or without leather buffing dust.

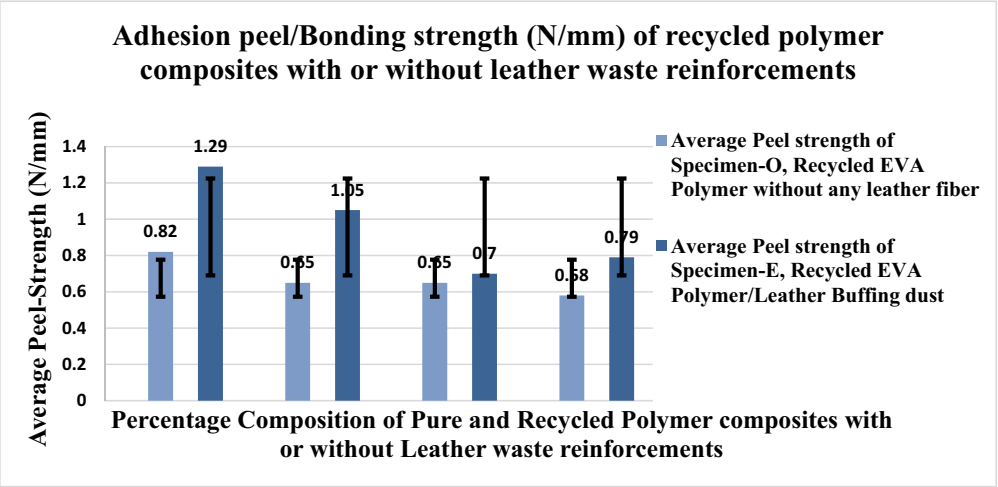

Figure 39: Comparison of adhesion peel strength (N/mm) of recycled EVA polymer composites with or without leather buffing dust.

in the leather buffing dust/recycled EVA Polymer composites during the investigation.

According to Ali Shaikh *et al.*, collagen hydrolyzates were derived from chrome-shaving dust during the initial phase [56]. It was a slightly pale-yellowish or cream-colored, viscid, often stickiness, odorless gel-like product with a pH of 8.15. This solvent-based material was widely employed throughout the leather industry and apparel industries as a result of its fervent interfacial bonding strength. Due to the obvious existence of adhesive, the time for the drying process is relatively shorter (10–15 min), which would be advantageous toward subsequent improvement, efficacy, and functionality. Thus, the research was conducted to develop solvent-borne adhering agents, and there was a reasonable probability of achieving spectacular findings. The investigators carried out experiments on the four samples, incorporating PVA (1–6%) and polyvinyl acetate in varying (1–16%) proportions. All of the aforementioned four samples had an average adhesiveness, including bonding capabilities. The bonding strength was determined once introducing the adherent to a leather sample by utilizing the SATRA-TM416 test. Findings reported that the average peel strengths of the samples were 0.00312, 0.00325, 0.00295, and 0.0025 N/m, respectively [56].

3.3.1.5 Compression and resilience

Compressional resilience is influenced by leather fabric thickness, and the hot-press/rolling mill processing technique, which is aimed at improving the finish, is likely to enhance the handle. Softer the fiber and lesser will be the compressional resilience.

The CRT of the recycled EVA polymeric composites was evaluated to find out the compressional deformation properties of neat recycled as well as leather waste/recycled EVA polymer composites, and results illustrated that the compressional deformation property for leather buffing dust as fiber in the recycled EVA matrix was higher of around 7.7% as compared to the neat recycled EVA matrix which was around 1.42% as presented in Figure 40. This CRT test deliberately signified the resilience energy and load compression properties of the leather buffing dust/recycled EVA composites as satisfactorily better in comparison to the neat recycled EVA polymer composites. The lower the compression set, the better was the elastic recovery of the composite materials. The higher the compressional energy values, the more the fullness and the compressibility of buffing dust leather fibers.

With the increase in the thickness values, the compressional energy values increase. The linearity of the compression–decompression curve could be considered as a measure of softness. The lower linearity of the compression corresponds to leather fiber with a softer handle. Therefore, it was logical to characterize the softness of solid leather fiber wastes using the linearity of the compression and compressional energy values. It was found that both linearity of the compression and compressional energy values show an increase with the increase in solid leather waste as a fiber thickness.

It is a prerequisite to avoid chain slips to boost CRT. The chemical-bonded polymer, as well as organically modified nanoclays, may be used to reduce chain slipping (organo-clay). Park *et al.* had analyzed that the

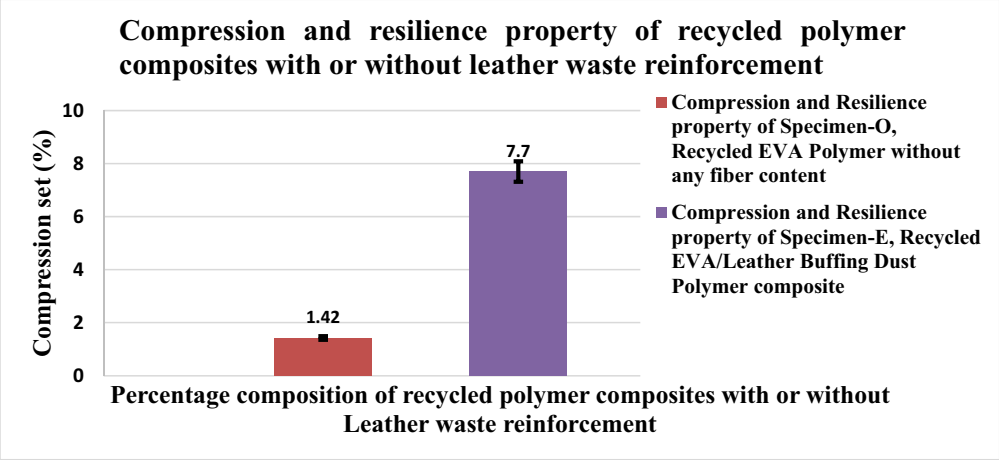

Figure 40: Comparison of compression and resilience (%) of recycled EVA polymer composites with or without leather buffing dust.

lower molecular-mass tri-methoxy-silyl-modified poly-butadiene (silicon hydride) could be furthermore utilized to chemically bind polymer and organo-clay [57]. By utilizing peroxide, silane can be grafted to the poly(ethylenevinyl-acetate) copolymer and ethylene, polymer with 1-butene [58–63]. Polymer with 1-butene radicals was formed as a result of peroxide reactions with poly(ethylenevinyl-acetate) and ethylene, and these developed radicals may respond with poly-butadiene of silicon hydride, as reported by Park *et al.* [57]. As a result, silicon hydride-grafted poly(ethylenevinyl-acetate) and ethylene polymer with 1-butene were developed [57]. The silanol groups of silicon hydride can react with organoclay hydroxyl groups. Although CRT is one such significant characteristic for foam applications, the poor compression-set property of poly(ethylenevinyl-acetate)/ethylene, polymer with 1-butene foams with clay addition should be improved [57]. Since the dissipation of energy contributing *via* the polymeric-backbone chains slip across the clay-surface was claimed to be the cause of the poor elastic recovery, chemical bonded polymers and organo-clays by silicon hydride was being used by Park *et al.* in his research to curtail chain slip across the clay-substrate material [57]. As a result, at a relatively similar density, poly(ethylenevinyl-acetate)/ethylene, polymer with 1-butene/methyl tallow bis(2-hydroxyethyl) quats-nanoclays/silicon hydride-foams either with or without cis-butenedioic anhydride-grafting poly(ethylene-vinyl-acetate)/ethylene and poly(ethylenevinyl-acetate)/ethylene, a polymer containing 1-butene polymeric foams has quite a lower compression set than poly(ethylene-vinyl-acetate)/ethylene, a polymer comprising, 1-butene foams [57]. As per the CRT results, methyl tallow bis(2-hydroxyethyl) quats-nanoclays are more effective than di(hydrogenated tallow)di-methyl-ammonium-chloride quats-nanoclays for enhancing compression set since throughout the inclusion of hydroxyl groups within the organo-clay layer, the hydroxyl groups of an alkyl-ammonium-ion existing within that active layer of methyl tallow bis(2-hydroxyethyl) [57]. Predicated on an absence of the large pinnacle at 3,398 cm^{-1} for poly(ethylenevinyl-acetate)/ethylene, polymer with 1-butene/methyl tallow bis(2-hydroxyethyl) quats-nanoclays/silane and poly (ethylenevinyl-acetate)/ethylene, polymer with 1-butene/di(hydrogenated tallow)di-methyl-ammonium-chloride quats-nanoclays/silicon-hydride foams in the ATR-FTIR spectrum, it can also be inferred that perhaps significant promising chemical-reactions among a residual silanol (Si–O–H) groups of silicon-hydride and the hydroxyl groups of methyl tallow bis(2-hydroxyethyl) quats-nanoclays and di(hydrogenated tallow)di-methyl-ammonium-chloride quats-nanoclays as concluded by the Park *et al.* [57].

3.3.1.6 Abrasion resistance

Wherever durability is important, such as with automotive and upholstery leathers, abrasion resistance is an important criterion. The physicomechanical characteristics and dimensions of the leather particulates are significant for abrasion. The kind of leather, fineness or flowability of leather, and the length of the fiber are the major pivotal factors that influence abrasion. Fibers possessing higher elongation, fatigue strength, strain rate, elastic recovery, and work-of-rupture or breakage have a good ability to endure/sustain the frequent repetitive repeated distortions, leading to a higher degree of abrasion-resistance is achieved.

The fabric mass for every square meter and fabric thickness that are the significant structural characteristics of fabrics profoundly influence abrasion resistance. Relatively larger abrasion resistance is ascertained *via* improved values of these parameters. leather-filled samples exhibit higher weight loss and thus low abrasion. The high surface area maximizes the contact points with the matrix and, as a result, gives improved abrasion resistance.

The abrasion resistance property of solid leather waste/recycled EVA composites using leather sole rotating drum type abrasion tester. Results revealed that the volumetric wear loss for the leather buffing dust as fiber in the recycled EVA matrix was higher at around 341.10 mm^3 compared to neat recycled EVA polymer composites as displayed in Figure 41. As the wt% of leather was raised, the fibrillary-like filaments throughout the composite were subjected to wear in almost the similar proportions as their content, which revealed the substantiated linear increase in wear rate as reported by Ambrósio *et al.* [49]. While volumetric wear loss for the neat recycled EVA composites was found to be around 101.75 mm^3 as a result of high elongation, work fracture, and elastic recovery.

The reduction of wear resistance, tensile strength, percentage elongation, as well as flexing resistance with rising waste fillers inclusion might be evidenced by a shape, structure, and type of additive elements and the ensuing discontinuities in the matrices. Abrasion, tension, and stretch cause the void-cavities can proliferate in shape, magnitude and interrelate with one another, culminating in materials debonding as well as fracture/rupture failure.

3.3.1.7 Hardness

The penetrating of an indenter driven to composites is employed for the hardness testing. The hardness indent is inversely proportionate to a penetrating value and therefore is influenced by the modulus of elasticity, and viscoelastic characteristics of materials.

Results revealed that the shore A hardness strength for leather buffing dust as fiber in the recycled EVA matrix was found to be around 87.5, as exhibited in Figure 42.

Whereas the hardness strength for neat recycled EVA was found to be significantly lower at around 60 as compared to the leather buffing dust/recycled EVA polymer composites. The Shore A hardnesses of the recycled EVA/solid leather waste composites increase significantly with the incorporation of wt% of leather fibers. This increasing trend of hardness emanates as tannery-processed; leather filaments have such a higher hardness than that of the plasticized polyvinyl butyral matrices as reported by Ambrósio *et al.* [49].

However, the improvement in modulus and hardness indicates a certain extent of interaction among the polymer and the leather fibers. Together with the high hardness values of these blends, these properties could be attributable to the homogenous dispersion of the leather fibers.

The composite's resistance to elastic deformation on its surface had enhanced as the composition of chrome-tanned wastes improved from 0 to 40% loading before reducing as the chrome-tanned waste content increased [54].

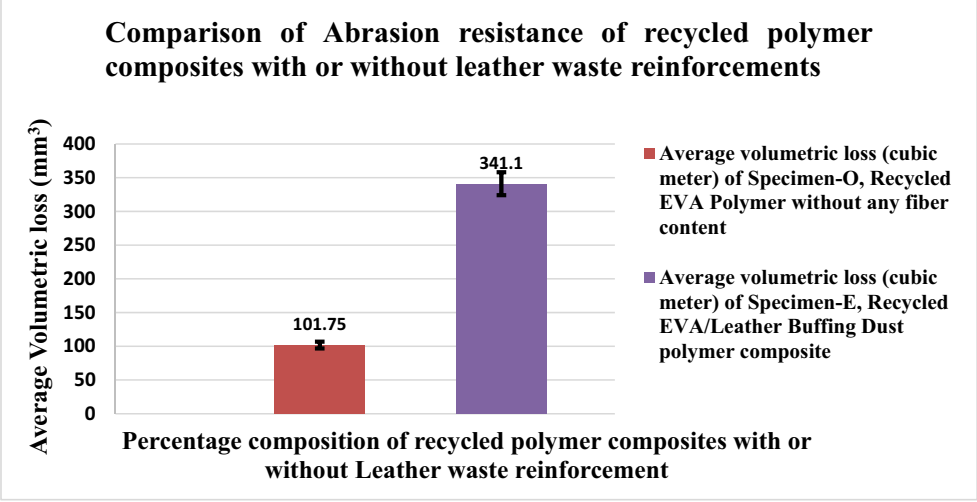

Figure 41: Comparison of abrasion resistance (mm^3) of recycled EVA polymer composites with or without leather buffing dust.

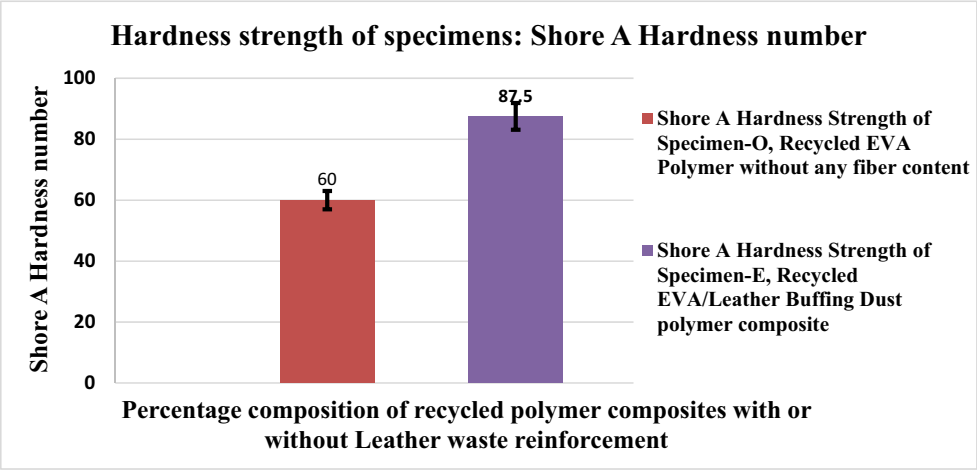

Figure 42: Comparison of hardness (shore A) of recycled EVA polymer composites with or without leather buffing dust.

3.3.1.8 Water absorption

In general, the amount of water absorption is largely influenced by the density and void contents of composites. The greater the length of the fiber, the significantly higher is the water holding capacity. As a result, it is undeniable that the rate of water uptake improves as fiber loading increases, and leather buffing dust possesses a high percent water absorption of around 4.54% as compared to neat recycled EVA polymer composites of 1.56%, as presented in Figure 43.

As the ratio of leather buffing dust loading increases to 1:1, the water absorption of composite increases, which is an obvious behavior because leather fibers are hydrophilic. This property is of commercial significance in the footwear and clothing industry.

The percent water uptake rises as the volume of chrome-tanned wastes significantly increase; however, a higher percentage of water uptake has been revealed in the chrome-tanned wastes/HDPE composites [54]. This implied that indeed additives are responsible for the formation of more micro gaps and deformities, abnormalities, irregularities, and other imperfections in the composites. This could also comprehend the lower tensile modulus, as reported by Musa *et al.* [54].

3.3.1.9 Density

The density of leather buffing dust/recycled EVA polymer composites is higher and found out to be around 1.1845 g/cm^3 in comparison with the neat recycled EVA polymer

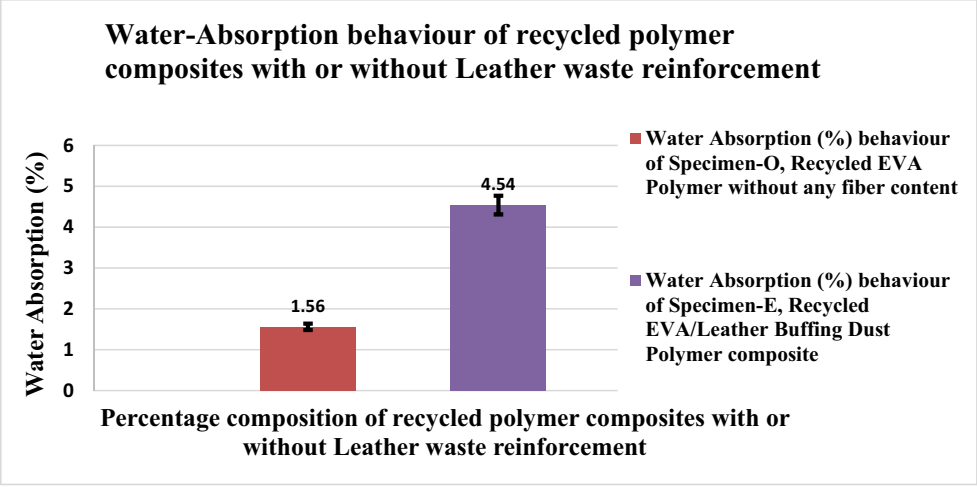

Figure 43: Comparison of water absorption (%) of recycled EVA polymer composites with or without leather buffing dust.

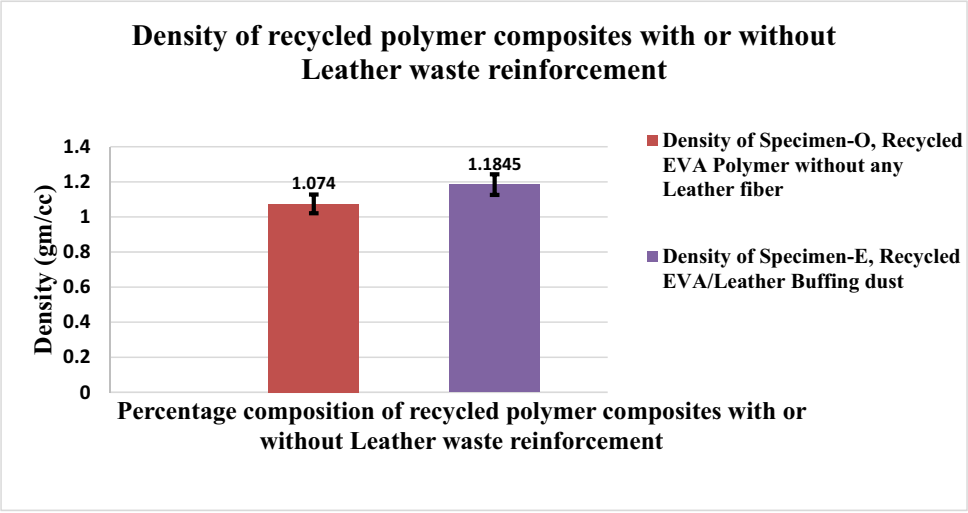

Figure 44: Comparison of density (g/cm^3) of recycled EVA polymer composites with or without leather buffing dust.

composites as illustrated in Figure 44. The incorporation of leather fibers and other additives in the recycled EVA matrix increased the cross-linking density of the solid leather waste reinforced recycled EVA polymer composites as compared to the neat recycled EVA matrix with a density of 1.074 g/cm^3.

3.4 Confirmatory experiments for physicomechanical characteristics

Finally, confirmatory experiments are conducted to validate the optimal parametric combination. The three confirmatory experiments for tensile strength, tear strength, compression modulus, adhesion strength, abrasion resistance, and hardness are conducted at their optimal set process parameters, and their average value is compared with their corresponding estimated mean optimal value. Table 19 shows the results of the confirmatory experiment for tensile strength, tear strength, compression modulus, adhesion strength, abrasion resistance, and hardness produced by CCD in RSM. Confirmation experiments show that results of the trial at optimal conditions have shown improvement when compared with the results of trials at the chosen initial setting of control parameters.

3.5 Thermal studies

3.5.1 TGA

Leather filaments primarily constitute collagenous protein, which itself is comprised of lengthy amino acid chains, chromic oxide, and other biochemical compounds which are incorporated into leather for ensuring chemical stability, appropriate surface texture, and resistance to deterioration/decomposition by fungus and microorganisms/microbes throughout usage. Thermal properties of

Table 19: Results of a confirmatory experiment for tensile strength, tear strength, compression modulus, adhesion strength, abrasion resistance, and hardness

Physicomechanical characteristics	Predicted optimum value	Predicted confidence interval at 95% confidence level	Experimental values	Percentage error
Tensile strength (MPa)	9.68335	A-120; B-40; C-7	9.485	2.048
Tear strength (N/mm)	7.49252	A-120; B-20; C-5	7.5425	0.6670
Compression modulus (MPa)	76.1649	A-120; B-20; C-5	76.71	0.7156
Adhesion strength (N/mm)	0.925121	A-120; B-20; C-7	0.9575	3.3816
Abrasion resistance (mm^3)	343.088	A-90; B-40; C-7	341.10	0.5736
Hardness (shore A)	86.0759	A-120; B-20; C-5	87.5	1.65

the composites were evaluated by TGA and DSC, respectively. The temperature corresponding to 5% weight loss in the TGA thermogram is considered as a minimum weight loss of the sample.

Accordingly, the minimum weight loss of all the samples was found to be in the range 211–289°C, showing that the fabricated composites are quite thermally stable, at least up to 211°C. The thermogravimetric curves demonstrate that the leather fibers investigated hereunder contain a high proportion of water because they exhibit enormous mass loss at temperatures about 100°C.

TGA revealed that the leather particulates are very hygroscopic and showed significant weight loss occurs (99.09318%) after 213.47°C for neat recycled EVA polymer composite specimen as the weight of specimen remains constant up to this temperature *i.e.* 99.09%, which also indicates that the specimen is thermally stable up to 213.47°C, and weight loss occurs (95.71011%) after 211.3°C for leather buffing dust/recycled EVA Polymer composite as the weight of specimen remains constant up to this temperature *i.e.* 95.71%, which also indicates that the specimen is thermally stable up to 211.3°C, respectively, as displayed in Figure 45(a) and (b).

The first mass loss step is due to the release of acetic acid. In the second mass loss step, acetic acid has already been released. The first weight loss (213.47–300°C for neat recycled EVA; and 211.3–347.24°C for leather buffing dust/recycled EVA polymer composite) is due to the where the emission of gaseous acetic acid and development of C═C all along the core-polymeric framework structure appeared. The second mass loss (300–460°C for neat recycled EVA; and 347.24–495°C for leather buffing dust/recycled EVA polymer composite) was due to the oxidization and volatilization of hydrocarbon compounds resulting from the disintegration/degradation of the recycled EVA copolymer network structure.

Similar findings also revealed that level one degradation corresponds to the deacylation of the vinyl acetate group with the elimination of acetic acid. Further, level two degradation of vinyl polyethylene chains formed in level one. In the second stage of degradation, there will be a rapid weight loss with an increase in temperature. The degradation in the range of 100°C shows the loss of water molecules. The thermal degradation behavior of collagen hydrolysate has three main stages of weight loss, as revealed by Tegegn [62]. The first stage was observed between 46.05 and 220.24°C, there was a loss of 9.67% by weight, which can be due to loss of gelatin moisture. The second stage of weight loss was beginning at the temperature of 220.2–350.98°C, and it was the highest weight loss (38.84%) due to the degradation of proteins. Collagen hydrolysate degradation started at 220.2°C, this result is higher slightly than those found by Camila de Campo *et al.*, [63], which showed the initial degradation temperature was observed at 200°C. The third stage of weight loss occurs between the temperature range of 350.98 and 431.35°C. With a weight loss of 12.89% and for a temperature range of 431.4–587.06°C, a corresponding weight loss was 7.24%. It has a residual mass of 30.45% at 587.06°C. The weight loss was highest at 311.75°C, which was 0.766%/°C [64].

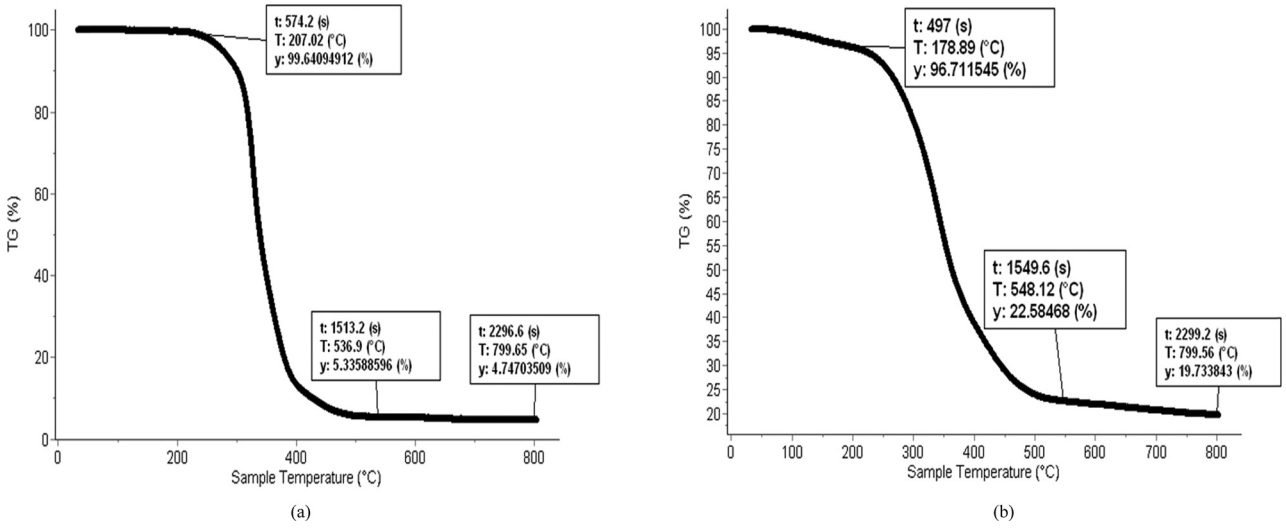

Figure 45: (a) TGA curve of the neat recycled EVA polymer without any leather fibers; (b) TGA curve of the leather buffing dust/recycled EVA polymer composites.

When leather particles are combined with scrap rubber and consolidated at high temperature under pressure, the structure of leather is bound to change as the free and bound water is removed, as stated by Ravichandran *et al.* [64]. Moreover, the decomposition products of leather, including the trivalent chromium, are likely to accelerate the degradation of the scrap rubber matrix. The degradation of scrap rubber vulcanizates containing leather was extensively discussed [66]. Furthermore, the degradation studies using TGA of the vulcanizates under an inert and oxidizing atmosphere and the decomposition products were enumerated in their studies.

Moreover, to understand the role of leather on the thermal stability of NR vulcanizates, TGA of leather samples was investigated between 0 and 400°C in a nitrogen atmosphere [66]. The thermograms of untreated and treated leather have exhibited two stages of degradation below 400°C. The first stage, weight loss that occurs below 100°C, is attributed to loss of entrapped water, and the second weight loss that lies between 200 and 400°C for all samples, to the decomposition of leather. Since all leather samples decomposed nearly at the same temperature between 200 and 300°C, it could be expected that they might have the nearly same influence on the thermal stability of the parent NR scrap rubber vulcanizates. The fragments produced during this stage of decomposition have influenced the decomposition of the NR vulcanizates.

The TGA of NR vulcanizates, which was carried out between 50 and 400°C in a nitrogen atmosphere, is undertaken to explore the role of untreated, sodium–hydrogen–carbonate processed, azane processed, and carbamide processed leather particles on the thermal stability of latex reclaimed rubber vulcanizates [66]. The findings of the respective thermograms depicted better the thermal stability of latex reclaimed rubber vulcanizates in the absence of leather up to 350°C. Although the pattern of decomposition for the vulcanizates containing untreated and treated leather is similar, a reduction in their thermal stability can be observed compared to the vulcanizate in the absence of leather as reflected in the thermograms. It may, therefore, be concluded that the NR vulcanizates without leather are more thermally stable than those containing leather particles. To compare the weight loss between 50 and 400°C, for the untreated and treated leather NR scrap rubber vulcanizates, the percentage weight was monitored in steps of 50°C for all the samples. The outcomes of TGA have indicated the weight that remains for every 50°C rises in temperature for all the samples. The comparison of the data illustrated retainment of more than 92% weight in the latex reclaimed rubber vulcanizates comprising untreated leather up to 350°C. But the data corresponding to all the latex reclaimed rubber vulcanizates comprising processed leather samples showed retainment of about 92% weight only above 300°C. This 50°C decrease in temperature for the treated leather NR scarp rubber vulcanizates in their thermal stability supported the view [66].

Furthermore, a weight loss at 400°C under isothermal conditions was monitored for 46 min in steps of 4 min to compare the rates of degradation for all the samples. The measured weights for all the samples under isothermal conditions, at 400°C, had shown that though the rate of degradation corresponding to latex reclaimed rubber vulcanizates comprising untreated leather appears to be similar to the vulcanizates containing treated leather, there was a slight increase in the rate of degradation in the former compared to the latter. It was also evident, as enumerated by Ravichandran *et al.*, that there is a steep weight loss at a relatively higher temperature for latex-reclaimed rubber vulcanizates without any leather compared to that of latex-reclaimed rubber-vulcanizates comprising leather-particulates [66]. Nearly 50% weight loss had been observed for all the samples at 400°C, under isothermal conditions [66].

The results of the TGA analysis of NR vulcanizates comprised of reclaimed rubber alone (without leather), carried out between 0 and 600°C in the air [66]. The analysis is undertaken to know the influence of untreated leather on the thermostability of NR-scrap rubber vulcanizates. The material does not seem to hold any water in the matrix as there was no weight loss below 150°C. The effluents of TGA analysis for vulcanizates containing no leather are subjected to the *in situ* FTIR at different time intervals [66]. The four spectra appear nearly superimposable to the respective spectra of untreated leather-loaded samples. The results of the TGA of latex reclaimed rubber vulcanizates comprising un-treated leather particulates, was carried out between 0 and 600°C in air.

Previous findings unveiled that the thermogram appeared through the onset of the release of water and the associated rate of decomposition of the rubber matrix appeared to be different in the present case [66]. There is less rate of degradation for the vulcanizate without any leather than the untreated leather-loaded sample. In addition, the final residue of the leather-loaded sample occurs below 500°C in the thermogram. This difference in behavior might be attributed to its untreated leather. The time-dependent water loss observed to occur up to 200°C may be attributed to the structural water present in leather

that takes time to come out of leather due to the possible structural changes in leather as stated by the Ravichandran *et al.* [66].

The TGA trace has indicated the onset of weight loss even below 100°C as a result of loss of weakly adsorbed-water [66]. But the decomposition of the material follows immediately. There is a minute quantity of weight loss (around 18%) between 220 and 350°C, followed by two more stages between 350 and 500°C. The total weight loss in this temperature range corresponded to approximately 42 %. The final residue exhibits a very rapid weight loss starting at 50°C. Since the TGA trace does not reach 100% weight loss, there must be thermally stable residue, certainly inorganic oxide of chromium, as chromium is a common element observed in leather [66].

The TGA results of sodium bicarbonate treated leather vulcanizates showed a continuous release of water below 200°C, and the vulcanizates started their decomposition at 240°C. So, from this, it could be concluded that the influence of sodium bicarbonate treated leather vulcanizates would be similar to untreated leather vulcanizates on the thermal characteristics of latex reclaimed rubber matrix [66].

The TGA results of latex reclaimed rubber vulcanizates contained azane processed leather was similar to urea treated leather vulcanizates [66]. There was no change in the released water and the start of the decomposition of the rubber matrix. The decomposition of the residue at 500°C occurred in two stages. This observation illustrated that degradation of latex-reclaimed rubber vulcanizates contained azane processed leather would have almost similar behavior as that of urea treated leather [66].

The TGA results of urea treated leather composites illustrated similar features in comparison to the composites contained unprocessed leather, differences can be very well observed [66]. The decomposition of the residue occurred in two stages – at 500 and 540°C – in this material which established the influence of urea treated leather on the thermal stability of NR scrap rubber matrix. The release of water was evident below 200°C and the decomposition of rubber matrix immediately after water release (240°C) was also clearly evident as with the composites comprised of unprocessed leather. The second stage decomposition of the vulcanized contained carbamide-processed leather at 540°C may be attributed to the high level of mixing and interaction between the matrix and leather, leading to a co-operative degradation that can take place only at a high temperature [66].

3.5.2 DSC

The thermal properties of adhesives have been examined by employing DSC. The testing was carried out by utilizing a DSC2A-00837 (192.168.1.11) with standardized aluminum crucible pans and lid coverings. Nitrogen was injected or pumped into the cell's environmental surroundings. The initial specimens were tested at room temperature, then cooled to –20°C before even being heated to 400°C at a rate of 10°C/min, and held there for 2 min. Such specimens then were chilled to –20°C and scanned at 10°C/min to 400°C. The first heating operation eliminated the material's manufacturing background; re-crystallization and melting temperatures were computed employing heat-flow indicators obtained throughout the cooling as well as second subsequent heating cycles. The DSC curves generated during the second heating cycle were being used to ascertain the glass-transition temperature (T_g).

A glass transition was indeed a second-order endothermic transformation that occurred as a stepwise progressive changeover shift in subsequent heating graphs of DSC thermograms. As a result of alterations in chain mobility, the physicomechanical characteristics of a polymeric transition have appeared from elastic to brittle at such a point. The T_g values for the neat recycled EVA were discovered to be about –20°C and to be independently of the vinyl-acetate-content and crosslink densities. The T_g of leather buffing dust/recycled EVA polymer composites was found out to be around –21°C, as displayed in Figure 46(a) and (b).

During the rapid cooling, a large exothermic peak appears at about 215°C (for neat recycled EVA polymer composites) and 210°C (for leather buffing dust/recycled EVA polymer composites) due to exothermic crystallization. A melting temperature (T_m) is a first-order transformation that could be seen as an endothermic peak maximal in DSC heating graphs. The T_m of neat recycled EVA found to be around 88.5°C. While the T_m of leather buffing dust/recycled EVA polymer composites was found to be around 110°C.

The lower result in endothermic transitioning could be attributed to specimens with higher water as well as volatile substances in the gradual progressing heating than that of the control board. The endothermic values of leather buffing dust have higher (T_{m1}) as compared to the neat recycled EVA polymer composites. This could be because all the fibers were very evenly distributed throughout the leather matrices, inducing their melting phase to shift toward an elevated temperature. The second, as well as third endothermic peak values of

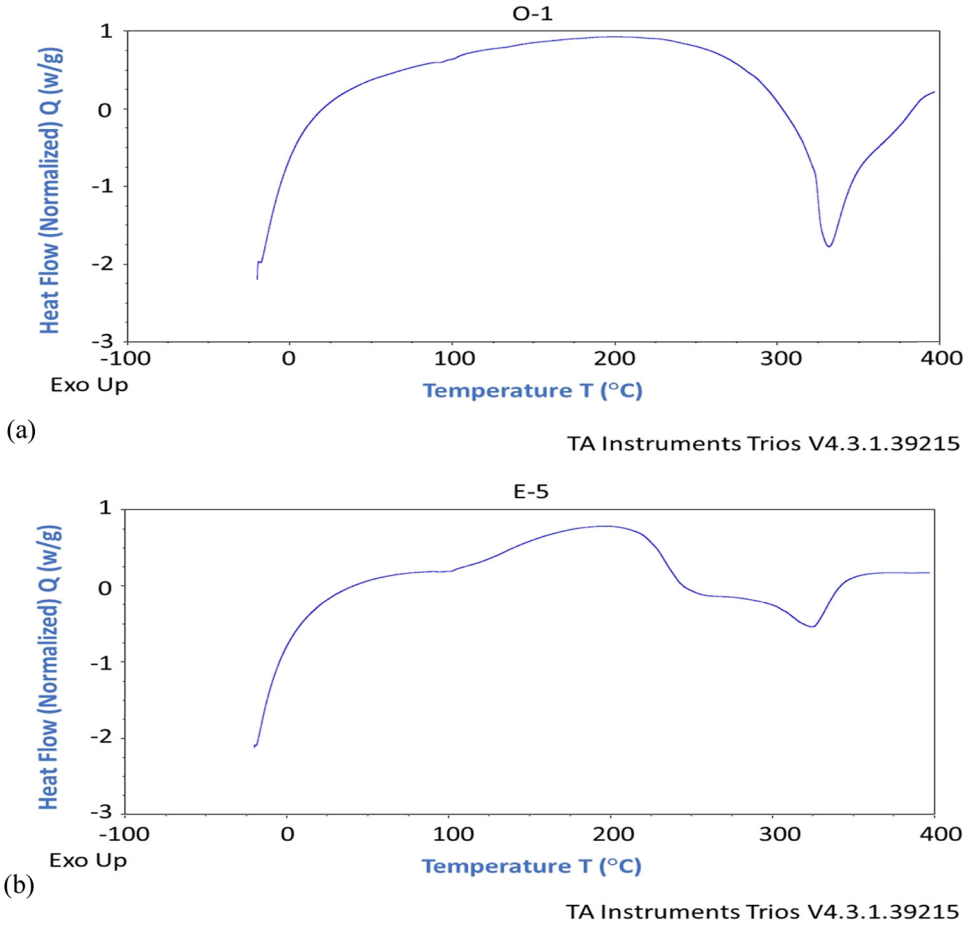

Figure 46: (a) DSC thermograms for neat recycled EVA polymer without any leather fibers. (b) DSC thermograms for leather buffing dust/recycled EVA polymer composites.

such composite, is likewise transitioned to extremely high temperatures owing to the structural heterogeneity of leather, including remnant tanned elements, which can cause interactions among fibrous filaments and leather.

Regardless of the occurrence of leather, the stability and uniformity of the polymeric chain's arrangement is disrupted. The inclusion of a plasticizer inside polymers enhances the motility of the polymer chains, thereby affecting the T_g of polymer.

Furthermore, the DSC study revealed water loss from of the solid leather fibers using an endothermic transition of about 100°C, thermostability up to 211°C, as well as the commencement of collagenous decomposition at 332.56°C for neat recycled EVA sample, and 327.23°C for leather buffing dust/recycled EVA polymer composites samples respectively. Glass transition temperature (T_g) of fabricated composites were also measured and found to be in the range of –16 to 30°C, which is a useful characteristic for understanding the processing parameters as measured by using DSC. The mass loss persisted somewhere between 130 and 150°C and was ascribed to unstable, volatile compounds like lubricants (oils) and low molecular weight greases observed throughout the leather fibrils from the leather preparatory operation around 325 and 500°C, a substantial mass loss appeared owing to protein loss and calcination of a material.

The comparable outcomes for the DSC melting thermograms have exhibited that there was no melting peak for the pure leather sample, which further concluded that the leather waste was completely amorphous, as stated by Joseph *et al.* [65]. For a pure polycaprolactone (PCL) sample, a significant melting peak had observed at 57.14°C. For other compositions containing leather and PCL, only one peak was observed, which corresponds to the melting of PCL also, there was no shift in the position of the peak. This result had also confirmed that there was no interaction between PCL and leather wastes. The intensity of the peak decreases proportionately to the increase in leather content. There was a negligible effect of leather

on the melting temperature of composites. The melting temperature ranges from 56.6–58.2°C.

The crystallization thermograms had shown the effect of leather content on crystallization temperature of composite. By incorporating leather wastes in the PCL matrix, the crystallization temperature was increased by 2–34°C. This property furthermore can be beneficial for processing this composition by extrusion or injection molding in final products, as it will reduce the cooling time and so overall cycle time [67].

Similar outcomes have also been unveiled in the case of the DSC analysis of latex-reclaimed rubber vulcanizates without any leather, and with leather, samples are carried out between 0 and 400°C, at a heat-rate of 20°C/min underneath N_2 atmospheric surroundings have illustrated that the DSC trace of latex reclaimed rubber vulcanizates without leather, untreated leather, and urea treated leather samples as showed by the Ravichandran *et al.* [66]. The slight endothermic elevations up to 200°C for NR reclaimed rubber vulcanizates in the absence of leather and also for all the leather treated samples are ascribed to the release of entrapped water. There is an endothermic hump observed between 200 and 250°C for vulcanizates containing urea, sodium–hydrogen–carbonate, and azane-treated leather and also for vulcanizates without any leather [66]. This hump can be attributed to the endothermic chain disentanglement of the polymer chains. Subsequent endothermic hump between 200 and 300°C in almost all the samples can be attributed to minute decomposition. This decomposition was not well resolved in the thermograms for leather and latex reclaimed rubber-vulcanizates contained leather [66].

Above 300°C, there was a major endothermic elevation in the DSC traces of all the samples and was seemed to coincide very well with the decomposition stage of latex reclaimed rubber vulcanizates contained with and without leather samples. A careful examination of the origin of the major endotherm of all the samples has illustrated more stability for NR scrap vulcanizates in the absence of leather than the latex reclaimed rubber vulcanizates comprised leather, as the origin of the endotherm of the former lies above the latter [66].

3.6 FTIR

Interfacial interaction verification of the samples has been conducted by FTIR (FT/IR-4700 type A Serial Number C016661788). FTIR has been carried out in a humidity-free atmosphere at room temperature in transmission mode. Spectra have been taken from 4,000–600 cm^{-1} for powdered sample. Solid samples have been analyzed by ATR.

The ATR-FTIR monograph shows surface layer changes in recycled EVA polymer are studied relative to the absorption regions O–H (3,100–2914.88 cm^{-1}), which increased in intensity under humidity conditions due to hydrogen bonding interaction between the carbonyl group in vinyl acetate and water, stretching vibration of C═O due to the terminal trans-vinylene double bond (1701.87–1736.58 cm^{-1}), C═C and due to the methylene stretch (1432.85–1466.6 cm^{-1}), CH_3 (1371.14 cm^{-1}), C═O (1296.89 cm^{-1}) and band is ascribed to C–O–C stretch mode at 1123.33 cm^{-1} which are examined in comparison with the CH_2 group deformation bands (1,464 cm^{-1}). This band can be used as an integral standard to monitor the functional groups of EVA with VA content in it. The main absorption band of the acetate function appears at 1,739 cm^{-1}, as displayed in Figure 47(a).

These peaks attribute to alcohols, phenols, and carboxylic acid groups of EVAs that are mainly responsible for the strength behavior of the material. The spectra of the neat recycled EVA copolymers show absorption peaks around 2917.77 and 2869.56 cm^{-1} that correspond to the C–H asymmetric and symmetric stretching of the methylene group ($-CH_2-$), respectively of EVA copolymers. The characteristic absorption peaks of the VA groups are as follows: 1732.73 cm^{-1} attributed to the stretching vibration of the –C═O band; 1130.08–1104.05 cm^{-1} attributed to the asymmetrical stretching vibration of the C–O band; 996.053 cm^{-1} attributed to the symmetric stretching vibration of the C–O–C band; 810.92 cm^{-1} attributed to the inner rocking vibration of a methylene group. The observed absorption peaks around 1379.82 cm^{-1} are largely attributed to the contributions from both VA and ethylene ($-CH_2$) units. The intensities of the absorption peaks at 810.92, 996.053, 1130.08–1104.05, 1379.82, 2869.56, and 2917.77 cm^{-1} seem to increase with an increase in the VA content, which is to be expected.

The ATR-FTIR results were obtained for solid leather wastes/recycled EVA composites processed after a combined two roll mill and hot press. The recycled EVA was obtained from the reaction of (vinyl acetate) with polyethylene. The curve compares the spectra of recycled EVA composites processed after a combined two roll mill and hot press.

While in ATR-FTIR monograph, the molecular structure of leather buffing dust/recycled EVA composites can be observed as the 3314.07 cm^{-1} band corresponding to the vinyl alcohol –OH group; 2849.31–2916.81 cm^{-1} is due to the $-CH_2$, $-CH_3$ groups inside chains and terminal

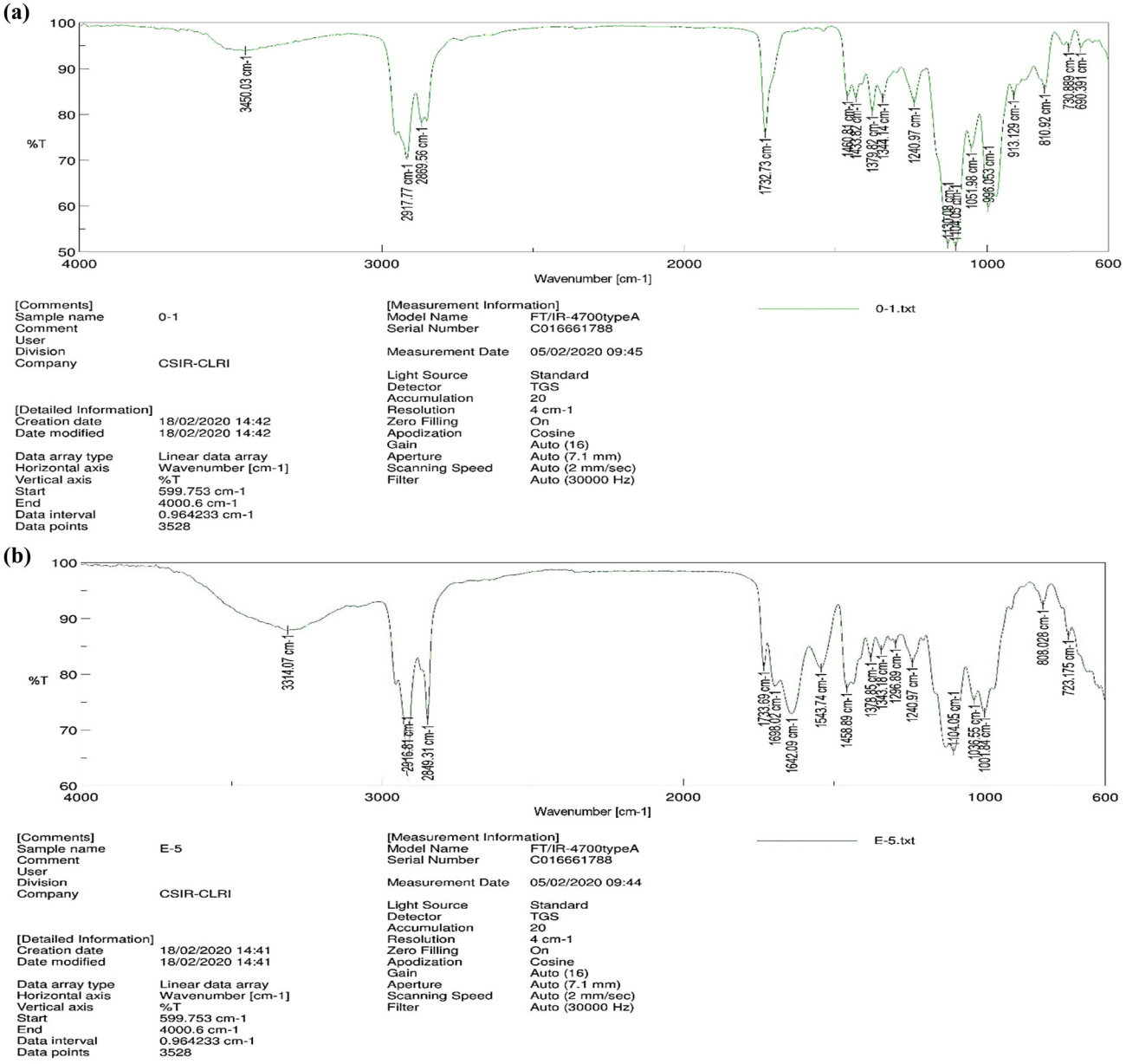

Figure 47: (a) FTIR spectra of neat recycled EVA polymer without any leather fibers and (b) FTIR spectra of leather buffing dust/recycled EVA polymer composites.

groups and below 723.175–600 cm^{-1} is due to Cr–O bonds. Although, the presence of fatty substances has been observed in the spectrum of leather buffing dust/recycled EVA polymer composite at 1,700–1,800 cm^{-1}, as demonstrated in Figure 47(b).

The spectra of two roll mill processed solid leather waste and recycled EVA seem to be comparable, implying that there have been no alterations in absorbance and also that the copolymer chains of the reprocessed EVA and the plasticizers/additives do not lead to improvements in their molecular interaction geometries after manufacturing by the combined processing effect of the two roll mill and hot press, as similarly reported by Ambrósio *et al.* [49].

The past findings unveiled that in leather–PCL composites, the intensity of these peaks increases as the leather content increases, as revealed by Joseph *et al.* [67]. There are no other peaks than that of characteristics peaks for leather and PCL in leather–PCL composite, which confirmed that there was no chemical interaction between leather and PCL as previously affirmed by the DSC results as analyzed by Joseph *et al.* [67].

An analogy outcome had been reported by Tegegn for the FTIR spectra (which was used to examine chemical

property) of the gelatin-starch cross-linked film with KBr pellet by using Shimazu IR affinity-IS spectrometer [64]. The FTIR spectrum of gelatin/starch/PVA/glutaraldehyde cross-linked composite film from the leather wastes was characterized by amide: A (3254.05 cm^{-1}) no significant change in the absorbance of band amide A, it was (3252.12 cm^{-1}) associated with NH stretching, and amide B (2922.28 cm^{-1}) band inextricably correlated with stretching vibration of CH_2 bonds it was 2920.35, 1645.35, 1543.12, and 1238.35 cm^{-1} inextricably correlated with amide: I, II and III correspondingly, as well as amide I associated with C═O stretching, slight shift shown in amide: I (1649.21–1645.35 cm^{-1}) and amide: II and III are associated with CN stretching and NH bonding. A slight shift has happened in amide: III (1238.35–242.21 cm^{-1}) similar change happened due to cross-linking of leather wastes reinforced composite polymer interaction [68]. A 1411.95 and 1097.54 cm^{-1} band was associated with CH_2 bending and C–O–C stretching [65].

The comparable literature effects have also been disclosed to understand the nature of decomposition, *in situ* FTIR analyses of the decomposition products for vulcanizates that contained untreated leather were performed between 500 and 4,000 cm^{-1} at different time intervals as reported by Ravichandran *et al.* [66]. The spectra obtained for different time intervals were illustrated the IR spectrum of the decomposition products recorded between 0 and 23 min. The release of hydrocarbon waste fragments during thermal analysis has been shown by a very less intense peak just below 3,000 cm^{-1}. The release of water was partly evident around 3,500 cm^{-1} due to –OH stretch, and the release of CO_2 was evident by its stretching vibration at 2354.5 cm^{-1}. Its bending mode was also evident at 666.7 cm^{-1}. These observations have established the combustive degradation of the materials in the said time interval. The IR spectrum for the products released between 24 and 46 min has carried more intense peaks and further illustrated the release of more fragments and the oxidized products, namely CO_2 and water [66]. It may be ascribed to more activation as the temperature was increased.

The IR spectrum of the released products between 46–52 min has illustrated that the peaks due to the above fragments were much more intense compared to those between 24 and 46 min [66]. In addition, the release of water and CO_2 was very well evident by their characteristics peaks just above 3,500 and 2354.3 cm^{-1}, respectively. Again, the high temperature might be the cause of such intense peaks as there could be more oxidation [66].

Due to the released products between 52 and 60 min, the IR spectrum showed that the number of released hydrocarbon fragments and water had exhibited a decrease in the intensity for CO_2 vibration at 2354.3 cm^{-1} [66]. An observation to mention with this spectrum was the release of less amount of water which was evident by the decrease in the intensity of the peak above 3,500 cm^{-1}. This observation has illustrated the residue that has undergone decomposition at this particular stage might be of less quantity as most of the decomposition was already complete.

The *in situ* FTIR spectra of combustion products released for vulcanizates containing sodium bicarbonate treated leather at different time intervals have shown more release of CO_2, and water than organic fragments as per the Ravichandran *et al.* [66]. There was an enhanced release of CO_2 and water between 46 and 52 min, hence the range of temperature corresponded to this decomposition may be more suitable to combustion, more of the rubber matrix. There is also a decreased release of CO_2 and water illustrated the less amount of cross-linked matrix residue for combustion between 52 and 60 min [66].

The *in situ* FTIR analysis of the combustion products for vulcanizates containing ammonia-treated leather, carried out at different time intervals, has illustrated more release of CO_2, hydrocarbons, and water. It might be due to higher temperature between time intervals of 30 and 50 min. The spectra have also illustrated the release of lesser amounts of all these combustion products exhibited more thermal stability for the resulting residue. But in some parts of spectra, the outcomes have illustrated the release of more amounts of CO_2 and water and less volume of organic fragments [66]. So, there was a requirement for more thermal energy for the residue near the completion of combustion. The FTIR analysis of the combustion products for vulcanizates containing urea treated leather for different time intervals was illustrated, the release of CO_2, hydrocarbon fragments, and water as reported by the Ravichandran *et al.* [66]. This was verified by inflections in the spectrum just above 3,500 cm^{-1} due to –OH stretch of water, just below 3,000 cm^{-1} due to C–H stretch of organic fragments, and at 2354.3 cm^{-1} due to CO_2. The spectra have illustrated the well resolved, more intense peaks for CO_2 at 2363.6 cm^{-1}, hydrocarbon at 2927.6 cm^{-1}, and water at 3,600 cm^{-1}. The other spectra have illustrated the more release of CO_2 and water but less release of organic fragments. This might be due to a well-fused combination of the cross-linked structure of the rubber matrix with the residue of the leather [66].

3.7 SEM with EDAX

The EDAX studies revealed the elemental composition and confirmed the distribution of entrapped solid leather fibers at the molecular level. The SEM images have illustrated that the particles are in the uniformly-dispersed and of spherical structural morphology while EDAX explores the stoichiometric compounds as well as percent chemical purity of the specimens to ascertain the occurrence/existence of chemical elemental compositions.

An image of the surfaces of recycled EVA polymer with leather buffing dust fibers shows a structure whose EDAX analysis exhibits the major elements (sulfur and oxygen). The EDX of the neat recycled EVA matrix reveals that the surface contains S, Cl, C, O, P (Figure 48(a)). Similar outcomes were also unveiled by Saikia *et al.* [67]. The EDX of leather buffing dust/recycled EVA polymer composite surfaces (Figure 48(b)) reveals that some of the chemical elements like S and Cl were removed away due to the incorporation of leather fibers and additives during the processing of the combined effect of rolling as well as hot-press compression molding.

3.8 SEM morphological analysis

Figure 49(a) and (b) shows micrographs of the neat recycled EVA composites, whereas Figure 49(a) and (b) depicts the microstructures, as well as cryogenics, ruptured interfaces in the leather buffing dust/recycled EVA composites; whereby leather fiber agglomeration tends to be adequately dispersed throughout the recycled EVA matrix. Even though there exist certain crevasses, openings, and voids in the surface morphology, apparently attributable to defibrillation and extraction of the leather fiber aggregates, the uniformity or compatibility of leather fibers agglomerates within the recycled EVA matrix reveals an excellent interfacial bonding strength. Figure 49(a) and (b) signifies locations of interfacial-layer interaction adherence or bonding with interface consistency or cohesion. Owing to the physicochemical disparities among hydrophilic fibers (constituted of collagenous macromolecules) as well as the hydrophobic thermoplastic matrix, it's indeed generally hard to accomplish strong compatibility, better bonding, excellent stability, strong adherence binding between the thermoplastic matrices and leather fibers. Utilizing stabilizers, additives, binding, or compatibilization agents, including cis-butenedioic anhydride on polypropylene blends for finely powdered wood is a certain approach to strengthen interfacial bonding strength, biocompatibility, miscibility, and produce uniform contiguous surface-areas within thermoplastic-composites with natural fabrics [49,66,70]. The micrographs of the recycled EVA/leather buffing dust composite with 50% leather fiber are shown in Figure 50(a) and (b). An agglomeration of leather fibers is encapsulated throughout a recycled EVA skin in Figure 50(a). Such recycled EVA skin has, demarcated which, implied strong-compatibility, interfacing-adherence, or intimate-contact among the leather fiber as well as the recycled EVA matrix, including the possibility that indeed interphase seems to be fervent than the aggregates of leather fibers. The higher-magnification representation of a leather fabric coalesces, or agglomerate in Figure 50(b) (symbolized *via* agglomerations throughout Figure 50(a)) illustrates the structural layout of leather-fibers including micro-fibrils of size less than 1 μm [49].

Figure 50(b) depicts recycled EVA residues trace-fragments on the layer of a leather fabric aggregates, confirming that the recycled EVA is binding the agglomeration as well as that the recycled EVA and the leather fibers possess firm, reasonable interfacial bonding and adherence strength. Therefore, in this context, the composites cryogenically fracturing or deformation/rupture would have existed inside the coalescing amalgamates rather than through the interfacial framework, indicating the interface's potential to pass matrices stress to the leather-fibrils coalescence. The leather fibrous aggregates appear to be quite relatively near and contact with each other as the composition of leather particles within the recycled EVA matrix increases, as shown in Figure 50(a). The grooves, discontinuities as well as voids in the microstructure in Figure 50(a) and (b), which were caused by defibrillation and isolated/detached, might be alleviated if the leather-particulates were appropriately filled by recycled EVA matrix. Even though the blending using a combined influence of two roll milling and hot-press compression molding processes was effective, the blend formulation can be ameliorated by combining in a twin-screw extruder. A twin-screw extrusion or injector including conveying/kneading blocks is desirable for dissipating and diffusing leather-fibrous agglomerations and then uniformly/homogenously/scattering the leather buffing dust fabrics throughout the recycled EVA matrix.

SEM has been used to study the degree of fiber alignment, uniformity of fiber dispersion, and the extent of fiber elastomer adhesion [71,72]. SEM studies have revealed excellent fiber orientation in cellulose fiber rubber composites. The fibers are very nearly parallel [73]. Among the short fibers such as glass, carbon, aramid and nylon, and cellulose, the degree of fiber alignment

(a)

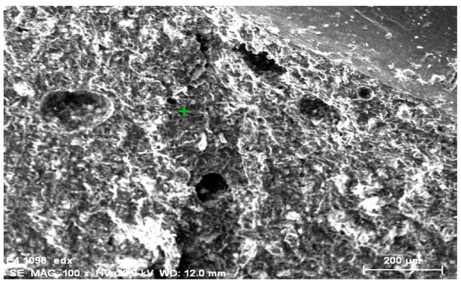

E4 1098Date:9/15/2020 3:55:00 PMImage size:600 x 450Mag:100xHV:20.0kV

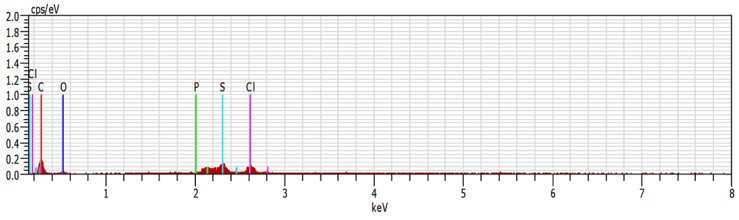

Spectrum: O2 1235 Date:9/15/2020 3:55:23 PM HV:20.0kV Puls th.:0.23kcps

El	AN	Series	unn. C [wt.%]	norm. C [wt.%]	Atom. C [at. %]	Error [wt.%]
O	8	K-series	4.16	40.25	58.49	1.5
S	16	K-series	3.01	29.09	21.09	0.2
Cl	17	K-series	2.84	27.44	18.00	0.2
P	15	K-series	0.33	3.22	2.42	0.1
C	6	K-series	0.00	0.00	0.00	0.0
Total:			10.33	100.00	100.00	

(b)

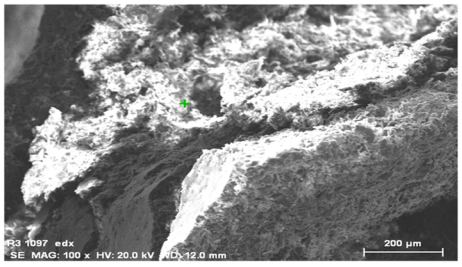

R3 1097Date:9/15/2020 3:50:46 PMImage size:600 x 450Mag:100xHV:20.0kV

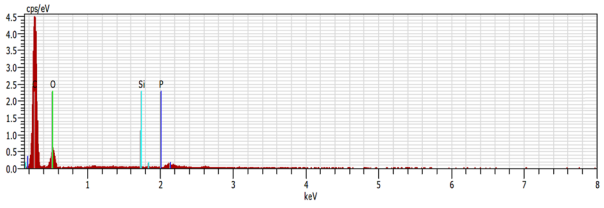

Spectrum: E4 1234 Date:9/15/2020 3:51:08 PM HV:20.0kV Puls th.:0.60kcps

El	AN	Series	unn. C [wt.%]	norm. C [wt.%]	Atom. C [at. %]	Error [wt.%]
O	8	K-series	93.49	93.49	96.42	19.1
P	15	K-series	4.57	4.57	2.43	0.5
Si	14	K-series	1.95	1.95	1.14	0.3
C	6	K-series	0.00	0.00	0.00	0.0
Total:			100.00	100.00	100.00	

Figure 48: (a) SEM–EDAX of the surface of neat recycled EVA polymer without any leather fibers. (b) SEM–EDAX of the surface of leather buffing dust/recycled EVA polymer composites.

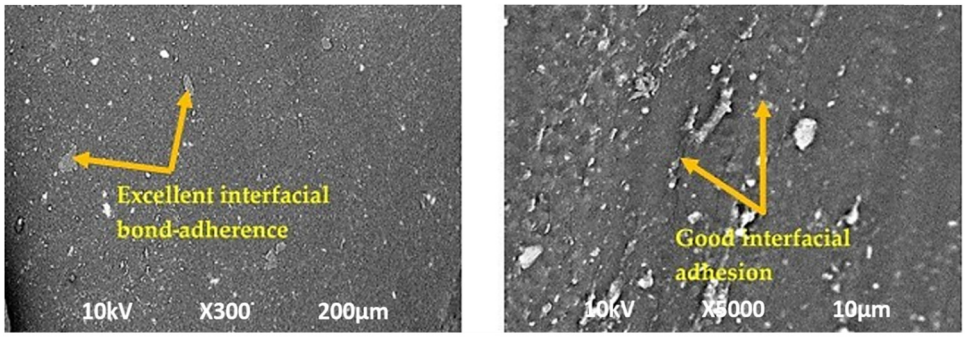

Figure 49: Micrographs of neat recycled EVA polymer without leather fibers at a magnification of: (a) 300× and (b) 5,000×.

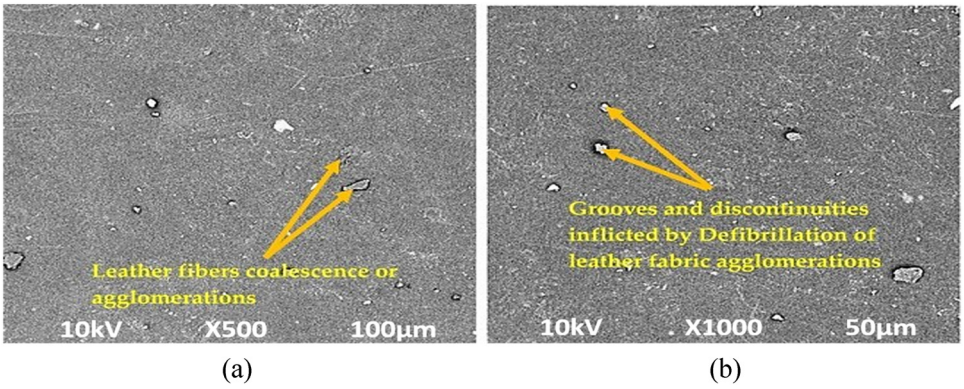

Figure 50: Micrographs of leather buffing dust/recycled EVA polymer composites at a magnification of (a) 500× and (b) 1,000×.

and fiber-elastomer adhesion is found to be poor with nylon and aramid fibers [74]. Cellulose fibers have exhibited good dispersion as well as good adhesion to the elastomer matrix. The improved adhesion between cellulose fibers and elastomers could be partly attributed to specific interactions between the constituents. Leather is a highly polar material that could also exhibit similar interactions when used with polar polymers such as nitrile rubber and its blends with PVC. It should also be noted that the cohesive strength of the leather is very high when compared to its adhesive strength with the matrix.

The SEM micrographs are shown in Figures 49 and 50(a) and (b) revealing that the cut-section of the neat recycled EVA matrix is smooth, and even-surfaced while the leather buffing dust fibers were well distributed over the surface and had an inadequate binding, bonding, and compaction of leather buffing dust to the recycled EVA matrix in some portions. In smaller amounts, contiguous separated leather fibers are evident, this may be due to sheer plucking or twisting forces exerted during the combined effect of rolling and hot press composition. As the volume of fibers increases, more amalgamation, fragmentation, and entrapment of leather fibers are seen. The penetration of recycled EVA matrix through entanglement is observed, which is responsible for physical adhesion between matrix and fibers, thus improved tensile strength around a maximum content of 1:1 of leather content is obtained.

The addition of leather buffing dust to recycled EVA composite was led to an increase in collecting the fibrillar of recycled EVA matrix, as well as, the volume of fibrillar-interaction structures tended to be higher in volume (1:1) by leather buffing dust incorporation, which was observed in micrographs at magnification 5,000×. In addition, the lower magnification at 300× shows that the leather buffing dust particles are homogeneously distributed and complex structured, which show as fully covered with fibrillar structures of recycled EVA matrix. This indicates a strong binding and adhesion between recycled EVA matrix and leather buffing dust as fibers.

Leather is a closely knitted structure of collagen fibers. SEM has been used to study the degree of adhesion between leather buffing dust fibers and recycled EVA blends. Morphology of recycled EVA polymer mixed

with leather buffing dust fibers at high temperatures has been found to exhibit a highly diffused interface between the fibers, and the matrix. The matrix completely covers the fibers, and extensive fusion of the fibers with the matrix has been observed as they are incorporated in the matrix at high temperatures [41]. In this study, though leather buffing dust is employed in particulate form, it is expected to be an integral part of the recycled EVA polymer.

Figure 50(a) and (b) shows the morphological features of leather buffing dust as obtained in fibrous form. The closely knitted fibrous leather is dispersed so easily as such into an EVA matrix, especially in large quantities of recycled EVA polymer.

An identical outcome has been reported for the effect of untreated as well as neutralized leather particle morphology of NR vulcanizates contained 500 parts of a scrap of the same particle size (200–300 μm) to micrographs had been taken for cryogenically fractured vulcanizates as unveiled by Ravichandran *et al.* [53,55,66]. The morphology of scrap rubber vulcanizates contained untreated leather particles wherein the leather appears to existed a co-continuous stage across with the matrices with clear boundaries separated two phases. This was a direct result of the rigid and closely knitted structure of untreated leather particles. The morphology of processed leather particulates had found to have a loose-bounded structure for leather which is otherwise a closely knitted fibrous material [55,66]. The treated leather particles appear to occurs like a continuous stage in the rubber matrices with varying degrees of interfacial adhesion with the rubber matrix depending on the type of treatment [55,66]

The comparable identical SEM micrograph findings had revealed that the leather fibers were well distributed over the surface as well as a weak-adherence, bond-strength, and permeability of buffing dust to the polycaprolactone matrix as revealed by Joseph *et al.* [67]. At smaller contents, a confined, separated, secluded fiber could be noticed, this may be attributable to shear stresses loads exerted during the extruder process of composition. The aforementioned composition of fibers was increased, thereby resulting in the further accumulation, amalgamation, and entrapment of fibers. The penetration of PCL matrix through entanglement was observed, which was responsible for physical adhesion between matrix and fibers, thus improved tensile strength around 20% of leather content was obtained [67].

Comparable insights regarding relevance with existent materials' physicomechanical, thermostability, morphologies, and multiobjective optimization of process/operating parameters are explored by Huang *et al.* [73] developed PLA and PBS mixtures with the help of melt blending approach, which was compounded with various composition of HDI. The goal of this study was to analyze the influence of HDI composition on the morphology and characteristic characteristics of the mixture. From the SEM results, the authors observed that the size of PLA and PBS was reduced with an increase in the HDI contents. Also, PBS accelerated the crystallization rate of the PLA. Moreover, due to better interface bonding between PLA and PBS, the toughness of the newly developed composites significantly improved. Pan *et al.* [74] presented a review article on the utilization of various catalyst substances during the catalytic pyrolysis of waste materials like plastics (such as PP, PE, PS, and PVC) and waste materials from petroleum industries (petroleum mud). The authors studied the use of molecular sieves, carbons, oxides of metals, and M-series catalysts to treat petroleum waste and plastic waste materials. The mechanism, challenges, and future progress of CP were also presented in the review article. The authors concluded that it is required to prepare systematic planning to reuse the plastics, and petroleum industries' waste materials, and needed to pay more attention to it. Sun *et al.* [75] evaluated the tribological behavior of epoxy-based composites, which include metal microcapsules (MMCs) and polymer microcapsules (PMCs). The authors observed that MMCs possess more compressive strength, wear loss, and modulus than PMCs under normal conditions. The friction coefficient of PMCs was lower than that of MMCs. Moreover, the friction value was reduced with an increase in the concentration of microcapsules in PMCs, however, MMCs show the opposite results. Prabhu *et al.* [76] evaluated the influence of nano clay in the glass fiber-reinforced PMCs. Hybrid polyester-based PMCs were developed using the resin infusion method under vacuum, in which the composition of clay was varied from 1 to 55 by weight in steps of 1. Mechanical and machining behavior were analyzed using various standard testing techniques. TEM, tensile test, impact test, SEM, and fracture test were performed to characterize the newly developed composites. Machining behavior was carried out using the drilling process. The authors observed that tensile strength increased with increasing the clay contents. A composite contacting 3% clay contents possessed better mechanical characteristics, among others. This composite exhibits lower delamination at a high feed rate, as observed in microstructure analysis. Also, fracture toughness and strain energy obtained in hybrid composites were more than the conventional composites. Gopinath *et al.* [77] developed glass and jute fibers

reinforced vinyl ester polymer matrix composites using the hand lay-up method. Different deck configurations were examined, and results were validated using ANSYS and FEM. The authors observed that the appropriate location and shape of stiffeners performed better in the alteration of responses. The stiffener deck configuration in "V" shape and combination of "V" and "U" shape possessed better results than others. Also, the addition of stiffener at the web joint provided better results than other locations with the least deflection and strain. Guo *et al.* [78] developed HDPE-based polymer matric composites, which were reinforced with wood and glass fibers. The authors followed the injection molding technique during the fabrication of PMCs. The mechanical behavior and water absorption capacity of the newly developed composites were carried out. The authors observed that under the same conditions, hybrid composites possessed 40 and 253% more tensile strength and modulus, respectively, than the woof-fiber-reinforced composites. Fiber swelling and weakening of interface bonding is the drawback resulting from more water absorption by WPCs. Also, the addition of glass fibers significantly improved the mechanical properties of the PMCs as compared to WPC. Ma *et al.* [79] fabricated nHA reinforced PEEK polymer matrix composites using the 3D braiding self retention hot-pressing technique. The composition of the nHA was varied as 6.5% and 14.5% by weight. The authors observed that modulus, hardness, and strength obtained in the PMC containing 6.5% nHA were 8.3 GPa, 3.34 GPA, and 155.32 MPa, respectively, which was much more than the base matrix. Also, the toughness was increased up to 54.9% with the addition of 6.5% HA, whereas a reduction of 23.6% was observed with the addition of 14.5%. This reduction was due to poor interfacial bonding obtained due to the increase of the nHA contents. Mei *et al.* [80] developed glass fiber, Kevlar-Fiber, and carbon fiber (CF) reinforced nylon polymeric matrix composites and evaluated their influence on the characteristics of the base matrix. The fiber was used in the form of rings and layers during fabrication. The newly developed composites were analyzed using SEM and tensile tests. The authors observed that CF reinforced composites possessed better tensile strength (110 MPa) and modulus (3,941 MPa), among others. The mechanical behavior was improved with an increase in the concentration of fiber rings and layers. Pan *et al.* [81] reviewed different techniques to recycle the plastics waste materials to discard plastics waste. The authors also reviewed the advantages and disadvantages of the methods used to recycle and dispose of plastic waste materials. The authors suggested that there is a necessity to establish new techniques to dispose of or recycle plastic waste materials to reduce air pollution and to protect human life.

4 Applications of the developed leather waste/recycled EVA polymer composites

The scientometric analysis has been performed using the Vos-viewer analytical tool to investigate recent applications, and advancements in the domain of leather buffing dust reinforced recycled EVA polymer composites. The database used for analysis has been extracted from Scopus and Web of Science for the last twenty-two years. The network of keywords has been displayed in Figure 51(a) which indicates the extensive implementation of leather wastes technologies for the production of composites with superior properties for a wide range of usages such as footwear, leather ancillaries, automotive, transportation, and packaging applications. The approach toward making useful products from waste material would be a synergetic effect on environmental impact as well as to create value addition to the wastes generated from the leather, and polymer industry, respectively. The implementation of other leather wastes and recycled polymers are also studied.

Figure 51(b) plots the network analysis of leather wastes utilization with various domains studied related to recycled and virgin polymers. The novel class of fabricated composites can find numerous multifunctional applications including, composite sheets, footwear, and clothing industries, leather-like personal goods, floorings, personal safety goods, decorative furniture applications, leather boards, low-cost adsorbents, activated carbon, energy recovery, and energy generation, pigments for ceramic glazes, Adhesives in woodworking industries, biogas generation, polymer films, biodegradable materials, biofertilizers agriculture applications, poultry feeds, cosmetics, biomedical applications, biocomposites, and to microencapsulate-drugs, construction, and buildings materials, automotive interior-trim molding parts, thermal, and acoustical insulation panels, cushioning boards, shoe soles, floorcovering, and moldings with quite-outstanding physical characteristics, air permeance, and desirable aesthetics.

Similar findings following the pragmatic implantation of the existing materials were investigated by Qin *et al.* [82] developed acrylate resin-based cotton fabric

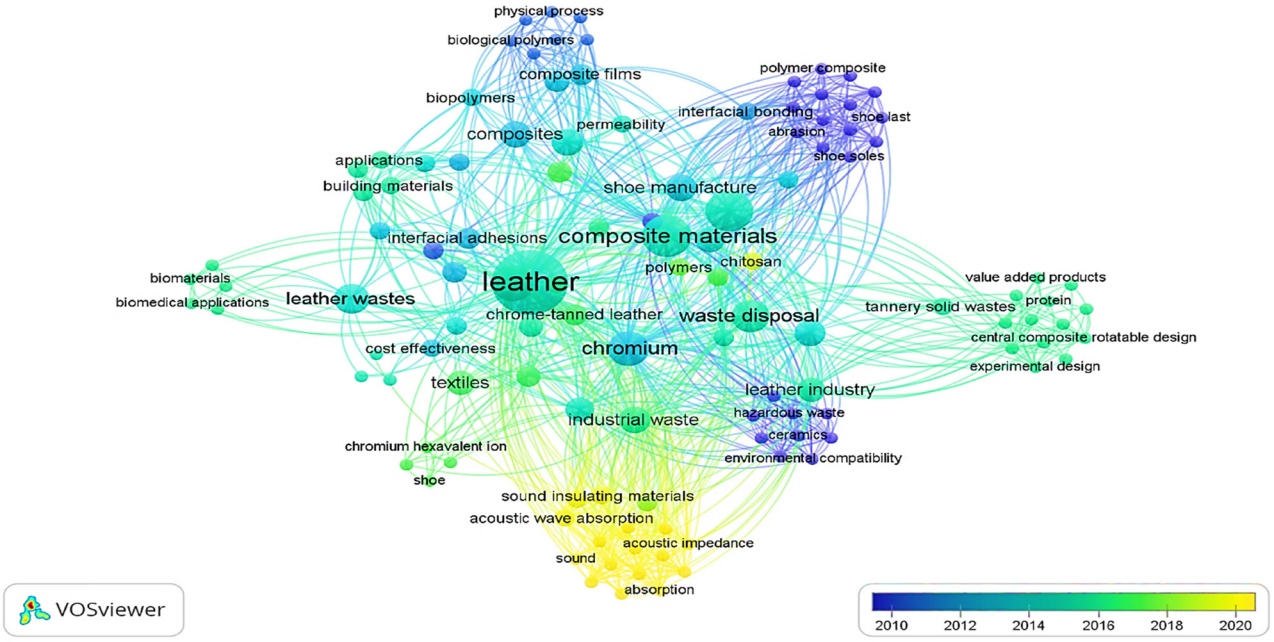

(a)

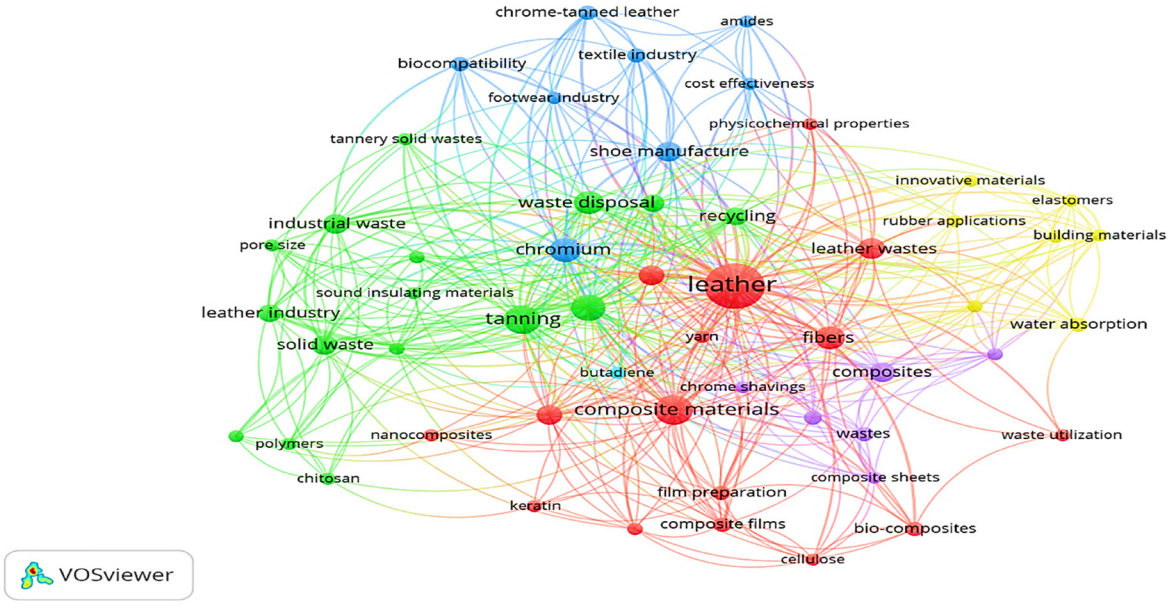

(b)

Figure 51: (a) Scientometric analysis and (b) network analysis exhibiting the comprehensive, diversified applications of leather buffing dust reinforced recycled EVA polymer composites.

composite materials by adding $Mg(OH)_2$ fluids in trimethylolpropane triacrylate (TPT). The fabrication route was followed by cotton fabrics coating using photopolymerization. The cast-composited were characterized using standard testing techniques. The authors observed that the tensile strength and modulus of the newly developed composite were 46 and 1,440 MPa, respectively, which were much more than the base matrix. Also, the addition of $Mg(OH)_2$ in TPT reduced its water vapor transmission rate significantly. Rudresh *et al.* [83] evaluated

the combined effect of micro, and nano size fillers of glass, and carbon on the various characteristics of the PTFE-based PMCs. The fabrication was involved melt mixing through extrusion followed by injection molding. The authors observed that the use of mixed nano and microfibers caused impaired in tensile strength and flexural strength. Nano-sized fibers indicated significant improvement in the impact strength but with the loss of stiffness. Also, the thermal stability was reduced with the addition of microfibers. Sengwa *et al.* [84] developed polymer matrix composites in which a mixture of poly(ethylene-oxide) and poly(methyl-methacrylate) (in ratio 1:1) was chosen as the matrix, and nanofillers of alumina were selected as reinforcement phase. Composites were fabricated through solution casting techniques, and constituents of alumina were varied as 0, 1, 3, and 5% by weight. The newly developed composite layer was characterized using SEM, XRD, FTIR, and dielectric relaxation spectroscopy techniques. The authors analyzed the influence of alumina nanofillers on the spherulite and porous morphology, extent of crystallinity, interface interactions, dielectric permittivity, electrical conductivity, and structural dynamics. The authors observed that crystallinity and dielectric permittivity were reduced with the addition of alumina in the base matrix. Also, the further increase in reinforcement contents up to 5% caused irregular alteration in the polymer dynamics. This study was very helpful in designing nano alumina fillers reinforced polymer nanocomposites for the advanced technology.

Sun *et al.* [85] produced nanoplatelets of PA66 based matrix, which was reinforced with ZrP using a simple melting process. SEM results revealed that 1.33 μm ZrP platelets having an aspect ratio (AR) of 3.8 were dispersed in the base matrix. However, 230 nm ZrP platelets containing AR of 6.2 were formed large-scale aggregates even at 1% of ZrP contents. The tensile test revealed that large size ZrP platelet reinforced PMCs possessed better properties than small size ones. The addition of 3% ZrP in the PA66 matrix possessed a 14% enhancement in strength and 10% in modulus value as compared to the unreinforced matrix. Also, large ZrP platelet-based composites exhibited 43 and 59% reduction in friction coefficient, and wear when tested under similar conditions respectively. Ashok *et al.* [86] presented a review article that described the feasibility, and suitability of various natural fibers with different types of matrices materials and reviewed the impact of these fibers on the dynamic-mechanical-behavior of the natural fiber-reinforced composites (NFRCs). The authors concluded that NFRCs are the best alternates of conventional materials in many engineering applications. Almost all types of natural fibers can be embedded in the matrix materials. DMA is the best route to analyze the characteristics of NFRCs. Dynamic properties are influenced significantly for the input parameters such as fiber-contents, fiber-shape/sizes/orientations, and stacking sequences of the natural composites. Das *et al.* [87] presented a review article on the preparation, and development of carbon fiber-reinforced PMCs because these materials possess many applications in aerospace, sports, and automobile industries. This article also presented various aspects of characteristic properties and applications of the carbon fiber-reinforced PMCs. Liu *et al.* [88] used nucleophilic substitution to synthesize (AMPBA)-PPG and cross-linked polymer(CLP)-boroxine. Thereafter CLP-boroxine was added to WPU to fabricate (AMPBA)-PPG/WPU-composites. The outcomes of this study indicated that a boroxine/WPU composite containing 5 wt% CLP possessed around 94% efficiency when simulated with water for 4 h at normal temperature. Furthermore, the (AMPBA)-PPG/WPU composite performed more impressively than neat-WPU leather in context with the wear-resistance. Moreover, this composite, when coated with leather, possessed better wear resistance. These outcomes are attributed to H_2 Bonding among the constituents. Xu *et al.* [89] used three different catalytic were utilized for the combustion and thermolysis of polyethylene. The authors used a cone calorimeter, tubular thermolysis furnace together with a mass spectrometer in this study. Catalytic also reduces the possibility of fire risk. Combustion efficiency was enhanced with increasing catalytic pore size. Among the available catalytic, HZSM-5 was a highly influencing catalyst due to its strong acidic nature [90–98]. This research is useful to design processes for plastic recycling [99–147]. Thus, it can be deduced from a present scientometric investigation that leather wastes utilization for value-addition diverse multifarious applications to reduce the environmental issues and to provide a sustainable solution and other allied can be further explored.

5 Concluding remarks

The utilization of tannery solid wastes, especially chrome buffing dust, has become a necessity for leather manufacturers. It serves partly as a measure of improving the value of the raw material and partly to implement the growing environmental regulations. Efforts are being made continuously to seek more efficient methods to

utilize these fibrous materials. The work reported in the current investigation is such an attempt to efficiently utilize the chrome buffing dust in recycled EVA polymer.

The leather itself is a polymer that is highly polar and cohesive, while recycled EVA polymer has been used in this work as matrix materials to ensure a degree of compatibility. In this study, leather Buffing dust and recycled EVA was converted into flexible composite sheets using two roll mills followed by a combined effect of two roll milling and hot-press compression molding. When leather fibers are used with high wt% content of 1:1 in recycled EVA matrices, the first important consideration is the uniform blending. As a biopolymer, leather would undergo denaturation during vulcanization at high temperatures.

a) This novel research discovered that the scrap/discarded leather wastes could be utilized to develop the leather buffing dust/recycled EVA polymer composites with high weight percent content of leather wastes with 1:1. With the leather loading of 1:1, the findings have concluded that the physicomechanical strength of the composite is escalating dramatically.
b) The SEM micrographs have revealed that the leather buffing dust adhered to the recycled EVA polymer matrix is quite reasonable with superior interfacial bonding and adherence strength. With such a substantial proportion of loading, the thermal characteristics of composites were discovered to be peculiar. It is undoubtedly anticipated that such experimental insights would make a significant contribution to it and also facilitate the deployment of leather buffing dust reinforced recycled EVA polymer composites throughout the fabrication of groundbreaking as well as cost-efficient contemporary modernistic composites with desirable physicomechanical strength, thermostability, and cushioning.
c) The leather fibrous loading with the composition of 1:1 seemed to have a substantial massive impact on the physicomechanical characteristics of recycled EVA/leather buffing dust composites. The composite's tensile strength was considerably lesser than that of neat recycled EVA. When the quantity of leather buffing dust within composites has been increased up to 1:1, then the tensile strength tends to strengthen marginally. This phenomenon was ascribed to superior interfacial bonding as well as adherence strength and the fact that the fiber agglomerations become relatively closer to each other as the weight percent of leather buffing dust significantly increases. The modulus of elasticity of composites improved massively as the volume of leather fibrous throughout the composites increased. This behavior was attributable to the assertion that the leather fiber aggregate-based conglomerate clusters are quite proximate to one another, providing the prospect of entangled.
d) The physicomechanical and viscoelastic characteristics of the recycled EVA/leather buffing dust composites were considered satisfactory or promising and illustrated the predicted behaviors for this novel emerging class of hybrid composites. The compressional resilience is prominent due to its importance in contributing to the hand of the fabric. Compressional properties play a very significant role in the handle and comfort characteristics of fabrics. The compressional deformation properties of neat recycled, as well as leather waste/recycled EVA polymer composites and results, illustrates that the compressional deformation property for leather buffing dust as fiber in the recycled EVA matrix was found out to be higher of around 7.7% as compared to the neat recycled EVA matrix was found to be around 1.42%. This demonstrates that the irregularity of the fabric surface is very considerable.
e) Results revealed that a volumetric wear loss of the leather buffing dust as fiber in the recycled EVA matrix was higher at around 341.10 mm^3 compared to neat recycled EVA polymer composites which come around 101.75 mm^3. This indicates that the leather buffing dust/recycled EVA composites have an enormous potential to endure/sustain the frequent repetitive repeated distortions leading to a higher degree of abrasion resistance.
f) Results revealed that the shore A hardness strength for leather buffing dust as fiber in the recycled EVA matrix was found out to be around 87.5 which undoubtedly has been reported to be more superior compared to neat recycled EVA composites which come around 60. This implies that the leather buffing dust/recycled EVA composites possess a remarkable modulus and strength than neat recycled EVA composites.
g) SEM microimages have illustrated that the leather particulates are uniformly dispersed and of spherical structural morphology within recycled EVA matrices. Whereas EDAX revealed that the surface of leather buffing dust/recycled EVA composites shows a structure that exhibits the major elements (sulfur and oxygen). The EDX of the neat recycled EVA matrix unveiled that the surface contains S, Cl, C, O, and P elements. Whilst, the EDAX for leather buffing dust/recycled EVA composite surfaces divulges that some of the chemical elements like S and Cl were removed away due to the incorporation of leather fibers and additives during the processing of the combined-

effect of rolling as well as hot-press compression molding.

h) The adhesion test of recycled EVA and adhesive for different uppers and soles joining are examined. Results revealed that the average peel strength between the polymer to leather (for leather buffing dust as fiber) in recycled EVA matrix was found to be around 0.9575 N/mm. Here, it is clear that most of the upper-to-sole joints gained sufficient bond strengths for footwear bonding but a few provided with poor performances, which may have been influenced by any of the reasons like incompatibility of adhesive with the materials, improper halogenations, cohesively weak layers of the materials or inadequate roughing.

i) The multiobjective optimization for hot-press, compression molding processing variables to manufacture a new class of leather buffing dust/recycled EVA polymer composites was exhibited by employing the CCD experimental research paradigm in RSM. The optimal variables for tensile strength, tear-strength, compressive-modulus, adhesion-strength, abrasion resistance, and hardness are 9.68335 MPa, 7.49252 N/mm, 76.1649 MPa, 0.925121 N/mm, 343.088 mm^3, and shore A of 86.0759. The optimal values have been evaluated and the optimized results in terms of input parameters were ascertained as follows, molding temperature of 120°C; time of 20 min; and pressure of 7 tons. As a result, the approach has revealed that the model was suitable, and the developed models were deemed significant with efficient, viable, reliable portrayals and standardized prototypical of the scientific findings, illustrating the predictive performance errors of lower than ±5%.

j) The TGA analysis revealed that the leather fibers are quite hygroscopic, with no noticeable substantial weight loss nearly equivalent to 211°C; the recycled EVA polymer was thermostable up to 213.47°C. The DSC findings indicate the release of moisture from the leather buffing dust *via* an endothermic transition about 100°C, thermostability up to 211°C, and the commencement of collagen decomposition at 332.56°C for neat recycled EVA sample; and 327.23°C for leather buffing dust/recycled EVA polymer composites samples, respectively.

k) The ATR-FTIR spectra have explored the surface-interface-layer alterations and abnormalities in recycled EVA copolymer about absorbance bands, O–H (3,100–2914.88 cm^{-1}) that enhanced in intensity under humidity circumstances owing to hydrogen bonding interacting-interface connection among the carbonyl-group in vinyl-acetate as well as water, stretching vibration of C═O attributable to the terminus branched trans vinylene junction based doubled covalent bonding (1701.87–1736.58 cm^{-1}), C═C and due to the methylene stretch (1432.85–1466.6 cm^{-1}), CH_3 (1371.14 cm^{-1}), C═O (1296.89 cm^{-1}) and band-spectrum are attributed to C–O–C stretching-vibrational mode linkage at 1123.33 cm^{-1} that are comparable to methylene grouping distortion predicated deforming-fractured bands at 1,464 cm^{-1}. While in ATR-FTIR monograph, the molecular structure of leather buffing dust/recycled EVA composites can be observed as the 3314.07 cm^{-1} band corresponding to the vinyl alcohol –OH group; 2849.31–2916.81 cm^{-1} is due to the $-CH_2$, $-CH_3$ groups inside chains and terminal groups and below 723.175–600 cm^{-1} is due to Cr–O bonds. However, fatty substances have been observed in the spectrum of leather buffing dust/recycled EVA polymer composite at 1,700–1,800 cm^{-1}. The evidence reported by an FTIR investigation concurred with the other outcomes for recycled EVA polymer composites.

l) The SEM surface morphology analysis of the recycled EVA/leather buffing dust composites has demonstrated that the leather fibrils particulates are widespread existent as conglomerate aggregate clusters and are adequately dispersed or interspersed throughout the recycled EVA matrices. The micrograph findings indicate that the recycled EVA matrix, as well as the leather buffing dust residue particulates, has exhibited multiple interfaces with significant exceptional bonding strength and interfacial interaction. It is also noticed the agglomerations with leather buffing dust fibrils excavated from a central-core section, whereas the fibers in the external surface periphery, in interaction with the recycled EVA matrix, continue to remain unaffected.

m) An addition of leather fibers in recycled EVA polymer matrices with 1:1 composition is generally associated with an increase in the modulus, tear strength and a reduction in elongation at break values. The leather fibers also behaved similarly when used in elastomer composites. Improved physicomechanical properties are obtained with leather buffing dust/recycled EVA polymer composites. As the fiber loading increases, failure of the composite occurs in a brittle manner. The Micrographs have shown diffused interface between the recycled EVA matrix and the leather fibers. This synergism effect might be due to the interfacial adhesion between the leather fibers and the recycled EVA matrix. Water absorption studies reveal that these materials could be used in footwear applications where controlled transport of water is essential for

a long duration. The high-thermostability and absorption properties signify their possible application in insulation materials, fabrication of gaskets, oil-rings, *etc*. Consequently, the current work offers a valuable solution for recycling and managing buffing dust as industrial wastes by efficiently converting them into useful composite materials.

To conclude, it is needless to conclude that these low-cost recycled EVA/leather buffing dust waste composites can be used for multifunctional applications as well as in environmental pollution abatement.

6 Suggestions for future work

The subsequent suggestions were proposed premised on aforesaid experimental outcomes.

a) This study only utilizes leather buffing dust to reuse/reprocess and develop flexible composites. Nevertheless, throughout this research, it's also undoubtedly encouraged that additional future investigations should evaluate the different leather residues in the reutilization and reprocessing method. Modifications can be done to improve mechanical properties and to furthermore increase the application areas of the leather composites reinforced recycled EVA polymer composites by using different cross-linkers. Dechroming of chrome buffing dust waste should be considered.
b) The combination of leather wastes and recycled EVA polymer in a suitable form was found to accelerate the degradation of the TPE phase in the composites. However, more investigation employing model compounds is required to establish the fundamental processes responsible for the accelerated degradation. These fundamental processes cannot be understood exactly with the waste materials like recycled EVA and leather buffing dust. The model compounds could include a combination of virgin EVA polymer with materials such as basic chromium salts, hide powder, or collagen, and possibly with vegetable-tanned leather.
c) Combined TGA-FTIR analysis of such model composition (1:1) would bring light to the exact degradation processes. Sophisticated calorimetric techniques could also be employed to investigate the energy changes involved in the degradation aspects of these model compounds. While such microscopic analysis could lead to more understanding of the basic degradation process, it is equally important to combine recycled EVA polymer with leather wastes in suitable reactors on a large scale and study various processing parameters for their pyrolysis under controlled environments.
d) Though a reduction in particle size and the associated increase in surface area would result in improved reinforcement, an increase in contact points between the constituents might cause extensive degradation to the recycled EVA matrix. Hence, the effect of surface area on the possible degradation of the recycled EVA matrix might be studied. In addition, treatments that would remove chromium from the buffing dust could prevent recycled EVA matrix degradation considerably. If the buffing dust is to be used as such without any pretreatment, it is worth investigating the properties of leather composites based on recycled EVA polymer. In this process, it may be possible to integrate the recycling processes of both recycled EVA polymer and tannery wastes.

Acknowledgments: The author Shubham Sharma wish to acknowledge the Department of RIC, IK Gujral Punjab Technical University, Kapurthala, Punjab, India for providing the opportunity to conduct this research task. The author P. Sudhakara gratefully acknowledges the support from Science and Engineering Research Board (SERB), New Delhi, India. Furthermore, the authors are thankful to the department of CATERS, CSIR-CLRI (CSIR-CLRI Communication no. 1642), Chennai, for providing the testing facilities.

Funding information: This research was supported by the Ministry of Education, Youth and Sports of the Czech Republic and the European Union (European Structural and Investment Funds-Operational Programme Research, Development and Education) in the frames of the project "Modular platform for autonomous chassis of specialized electric vehicles for freight and equipment transportation," Reg. No. CZ.02.1.01/0.0/0.0/16_025/0007293.

Author contributions: S.S.: conceptualization, methodology, formal analysis, investigation, resources, supervision, writing – original draft preparation, and writing-review and editing. P.S.: conceptualization, methodology, formal analysis, investigation, resources, writing-original draft preparation, supervision. M.P.: investigation, formal analysis, investigation, resources, writing-review, and editing, project administration, funding acquisition. J.S.: resources, writing-original draft preparation, writing-review and editing. S.R.: investigation, resources, writing-review, and editing, supervision. All authors have accepted

responsibility for the entire content of this manuscript and approved its submission.

Conflict of interest: The authors state no conflict of interest.

References

[1] Choudhury SR, Lane O, Kazerooni D, Narang GS, Jang ES, Freeman BD, et al. Synthesis and characterization of post-sulfonated poly(arylene ether sulfone) membranes for potential applications in water desalination. Polymer. 2019;177:250–61. doi: 10.1016/j.polymer.2019.05.075.

[2] Borjigin H, Stevens K, Liu R, Moon J, Shaver A, Swinnea J, et al. Synthesis and characterization of polybenzimidazoles derived from tetraaminodiphenylsulfone for high temperature gas separation membranes. Polymer. 2015;71:135–42. doi: 10.1016/j.polymer.2015.06.021.

[3] Kanagaraj J, Velappan KC, Babu NKC, Sadulla S. Solid wastes generation in the leather industry and its utilization for cleaner environment. ChemInform. 2006;37(49):541–8. doi: 10.1002/chin.200649273.

[4] Kanagaraj J, Senthilvelan T, Panda RC, Kavitha S. Eco-friendly waste management strategies for greener environment toward sustainable development in leather industry: a comprehensive review. J Clean Prod. 2015;89:1–17. doi: 10.1016/j.jclepro.2014.11.013.

[5] Jiang H, Liu J, Han, W. The status and developments of leather solid waste treatment: a mini-review. Waste Manag Res. 2016;34(5):399–408.

[6] Sundar VJ, Raghavarao J, Muralidharan C, Mandal AB. Recovery and utilization of chromium- tanned proteinous wastes of leather making: a review. Crit Rev Environ Sci Technol. 2011;41(22):2048–75. doi: 10.1080/10643389.2010.497434.

[7] Newhall H. South essex sewerage district. Personal c~munication with J. Margolis. Massachusetts, United States: JRB Associates; 1982.

[8] Cabeza LF, Taylor MM, Dimaio GL, Brown E, Marmer WN, Carrió R, et al. Processing of leather waste: Pilot scale studies on chrome shavings. Isolation of potentially valuable protein products and chromium. Waste Manag. 1998;18:211–8. doi: 10.1016/S0956-053X(98)00032-4.

[9] Krecke ED. Process for the production of leather base material. US Pat No. US4536430; 1982.

[10] Waite E, Franklin FB, Massachusetts B. Improvement in fabrics from waste leather. Utility (Process) Patent. Letters Patent No. 114373; 1871.

[11] Ostberg AJ. Method of manufacturing substitutes for leather-board. US976827A Patents. Victoria, Australia; 1909.

[12] Mathieu N. Improvement in manufacture of leather paste-board and paper. US20020A Patents. Paris, France, New York, N.Y.; 1858.

[13] Suzuki M, Sasaki M. Synthetic resin leather. US20030190438A1. United States; 2004.

[14] Adams. Flexible-leather-board composition. US1188600A; 1916.

[15] Albert Clapp L. Fibrous material and method of making the same. US1269905A; 1918.

[16] Wyler A. Process for bonding leather to leather. US5028285A; 1991.

[17] Madera-Santana TJ, Aguilar-Vega M, Marquez A, Moreno F, Richardson M, Machin J. Production of leather-like composites using short leather fibers, II. Mechanical characterization. Polym Compos. 2004;23:991–1002.

[18] Andreopoulos A, Tarantili P. Waste leather particles as a filler for poly(vinyl chloride) plasti-sols. JMS-Pure Appl Chem. 2007;37(11):1353–62.

[19] Garcia NG, dos Reis EAP, Budemberg ER, da Silva Agostini DL, Salmazo LO, Cabrera FC, et al. Natural rubber/leather waste composite foam: a new eco-friendly material and recycling approach. J Appl Polym Sci. 2014;132:1–10. doi: 10.1002/app.41636.

[20] Mari EJJE, Villena Cabangon R. Utilization of spent tea leaves and waste plastics for composite boards. Philippine For Products J. 2013;4:29–36.

[21] Senthil R, Hemalatha T, Kumar BS, Uma TS, Das BN, Sastry TP. Recycling of finished leather wastes: a novel approach. Clean Technol Environ Policy. 2014;17:187–97.

[22] Parisi M, Nanni A, Colonna M. Recycling of chrome-tanned leather and its utilization as polymeric materials and in polymer-based composites: a review. Polymers. 2021;13(3):429. doi: 10.3390/polym13030429.

[23] Ponsubbiah S, Suryanarayana S, Gupta S. Composite from Leather Waste. Int J Latest Technol Eng. 2018;VII:77–80.

[24] Zăinescu G, Deselnicu V, Constantinescu R, Georgescu D. Biocomposites from tanned leather fibers with applications in constructions. Leather Footwear J. 2018;18(3):203–6. doi: 10.24264/lfj.18.3.4.

[25] Shanmugam V, Mensah RA, Försth M, Sas G, Restás Á, Addy C, et al. Circular economy in biocomposite development: state-of-the-art, challenges and emerging trends. Compos Part C: Open Access. 2021;5:100138. doi: 10.1016/j.jcomc.2021.100138.

[26] Reports on waste and climate change: Global trends and strategy framework, UNEP; 2010.

[27] Official method of analysis. Society of leather technologist and chemist; 1996.

[28] IULTCS Chemical Test method: Determination of Chromium VI Content. 1997;81:109.

[29] Cochran WG, Cox GM. Experimental designs. New York, USA: John Wiley and Sons, Inc; 1992.

[30] Montgomery DC. Design and analysis of experiments. New York: John Wiley; 2012.

[31] Draper NR. On the experimental attainment of optimum conditions, breakthroughs in statistics. New York, USA: Springer Series in Statistics (Perspectives in Statistics); 1951.

[32] Myers RH, Khuri AI, Carter WH. Response surface methodology. 1966–1988. Technometrics. 1966;31:137–57.

[33] SATRA Tm137, Tensile properties of plastics and rubbers. June, 1995.

[34] Standard Test Method for Compressive Properties of Polymer Matrix Composite Materials with Un- supported Gage Section by Shear Loading, ASTM D3410/D3410M-16e1; 2016.

[35] SATRA Tm-218, Tear strength of rubbers and plastics – trouser method; June 1999.
[36] SATRA Tm 205, A. Shore, Hardness of Others-Soling Materials, Rubber Materials, PU Sole Materials, and Leather Sole; 2016.
[37] SATRA Tm 401, Peel strength of adhesive bonds; 2000.
[38] SATRA Tm 64, Compression Set Apparatus Test Machine/ Equipment (GW-053); 1996.
[39] Natchimuthu N, Radhakrishnan G, Palanivel K, Ramamurthy K, Anand JS. Vulcanization characteristics and mechanical properties of nitrile rubber filled with short leather fibers. Polym Int. 1994;33(3):329–33. doi: 10.1002/pi.1994.210330313.
[40] Kandar MM, Akil HM. Application of design of experiment (DoE) for parameters optimization in compression molding for flax reinforced biocomposites. Procedia Chem. 2016;19:433–40. doi: 10.1016/j.proche.2016.03.035.
[41] Mamoune A, Saouab A, Ouahbi T, Park CH. Simple models and optimization of compression resin transfer molding process. J Reinforced Plast Compos. 2011;30(19):1629–48. doi: 10.1177/0731684411421539.
[42] Xie J, Wang S, Cui Z, Wu J. Process optimization for compression molding of carbon fiber- reinforced thermosetting polymer. Materials. 2019;12(15):2430.
[43] Singh JK, Ching Y, Abdullah L, Ching K, Razali S, Gan S. Optimization of mechanical properties for polyoxymethylene/glass fiber/polytetrafluoroethylene composites using response surface methodology. Polymers. 2018;10(3):338–8. doi: 10.3390/polym10030338.
[44] Govindaraju R, Jagannathan S. Optimization of mechanical properties of silk fiber-reinforced polypropylene composite using Box-Behnken experimental design. J Ind Text. 2018;47(5):602–21.
[45] Kale RD, Jadhav NC. Utilization of waste leather for the fabrication of composites and to study its mechanical and thermal properties. SN Appl Sci. 2019;1(10):1–9. doi: 10.1007/s42452-019-1230-9.
[46] Ibarra L, Jorda C. Effect of a diazide as adhesive agent in elastomeric matrix-short polyamide fibers composite. J Appl Polym Sci. 1993;48:375–81.
[47] Ambrósio JD, Lucas AA, Otaguro H, Costa LC. Preparation and characterization of poly(vinyl butyral)-leather fiber composites. Polym Compos. 2011;32(5):776–85. doi: 10.1002/pc.21099.
[48] Dodwell G. Components—guidelines and characteristics opportunities. In: Leao AL, Carvalho FX, Frollini E, editors. SATRA Bull; 1989. p. 208–209.
[49] Ebewele RO. Polymer science and technology, 1st ed. Boca Raton: CRC Press. doi: 10.1201/9781420057805.
[50] Covington AD, Chemis T. The science of leather. UK: Royal Society of Chemistry; 2009.
[51] Stael G, Rocha M, Menezes S, Almeida JR, Ruiz NMDS. Analysis of the mechanical properties and characterization by solid state 13C NMR of recycled EVA copolymer/silica composites, Materials Research-ibero-american. J Materials-Mater Res-Ibero-Am J Mater. 2005;8:269–73.
[52] Musa ET, Hamza A, Ahmed AS. Investigation of the mechanical and morphological properties of high-density polyethylene (HDPE)/leather waste composites. IOSR J Appl Chem. 2017;10(1):48–58. doi: 10.9790/5736-1001014858.
[53] Ravichandran K, Natchimuthu N. Vulcanization characteristics and mechanical properties of natural rubber-scrap rubber compositions filled with leather particles. Polym Int. 2005;54(3):553–9. doi: 10.1002/pi.1725.
[54] Aftab M, Shaikh A, Deb AK, Akter E, Ferdous T, Abu M, et al. Resource addition to leather industry: adhesive from chrome shaving dust. J Sci Innovative Res. 2017;6(4):138–41.
[55] Park KW, Kim GH, Chowdhury SR. Improvement of compression set property of ethylene vinyl acetate copolymer/ethylene-1-butene copolymer/organoclay nanocomposite foams. Polym Eng Ing Sci. 2008;48(6):1183–90.
[56] Shieh YT, Tsai TH. Silane grafting reactions of low-density polyethylene. J Appl Polym Sci. 1998;69:255.
[57] Shieh YT, Liu CM. Silane grafting reactions of LDPE, HDPE, and LLDPE. J Appl Polym Sci. 1999;74:3404.
[58] Parent JS, Geramita K, Ranganathan S, Whitney RA. Silane-modified poly(ethylene-co-vinyl acetate): influence of comonomers on peroxide-initiated vinylsilane grafting. J Appl Polym Sci. 2000;76(8);1308–14. doi: 10.1002/(sici)1097-4628(20000523)76:8<1308:aid-app11>3.0.co;2-7.
[59] Sirisinha K, Meksawat D. Comparison in processability and mechanical and thermal properties of ethylene-octene copolymer crosslinked by different techniques. J Appl Polym Sci. 2004;93(3):1179–85. doi: 10.1002/app.20554.
[60] Kuan H-C, Kuan J-F, Ma C-CM, Huang J-M. Thermal and mechanical properties of silane- grafted water crosslinked polyethylene. J Appl Polym Sci. 2005;96(6):2383–91. doi: 10.1002/app.21694.
[61] Sirisinha K, Meksawat D. Preparation and properties of metallocene ethylene copolymer crosslinked by vinyltrimethoxysilane. Polym Int. 2005;54(7):1014–20. doi: 10.1002/pi.1800.
[62] Tegegn WB. Preparation of biodegradable film using Gelatin from wet blue shaving dust and starch from tamarind seed. BDU: School of Research and Graduate Studies of Bahir Dar Institute of Technology; 2018.
[63] Campo D, Pagno CH, Costa TMH, de Oliveira Rios A, Flôres SH. Gelatin capsule waste: new source of protein to develop a biodegradable film. Polímeros. 2017;27(2):100–7. doi: 10.1590/0104-1428.2371.
[64] Ravichandran K, Natchimuthu N. Natural rubber: leather composites. Polímeros. 2005;15(2):102–8. doi: 10.1590/s0104-14282005000200008.
[65] Joseph S, Ambone TS, Salvekar AV, Jaisankar SN, Saravanan P, Deenadayalan E. Processing and characterization of waste leather based polycaprolactone biocomposites. Polym Compos. 2017;38(12):2889–97. doi: 10.1002/pc.23891.
[66] Srinivasan MV, Ramachandran RK, Gopinath A, Madhan B, Saravanan P. Sustainable packaging materials from tannery trimming solid waste: a new paradigm in wealth from waste approaches. J Clean Prod. 2017;164:885–91. doi: 10.1016/j.jclepro.2017.06.200.
[67] Saikia P, Goswami T, Dutta D, Dutta NK, Sengupta P, Neog D. Development of a flexible composite from leather industry waste and evaluation of their physico-chemical properties. Clean Technol Environ Policy. 2017;19(8):2171–8. doi: 10.1007/s10098-017-1396-z.

[68] Oksman K, Clemons C. Mechanical properties and morphology of impact modified polypropylene- wood flour composites. J Appl Polym Sci. 1998;67(9):1503–13. doi: 10.1002/(sici)1097-4628(19980228)67:9<1503:aid-app1>3.0.co;2-h.
[69] Chakraborty SK, Setua DK, De SK. Short jute fiber reinforced carboxylated nitrile rubber. Rubber Chem Technol. 1982;55(5):1286–307. doi: 10.5254/1.3535930.
[70] Setua K, De SK. Short silk fiber reinforced natural rubber composites. Rubber Chem Technol. 1983;56(4):808–26. doi: 10.5254/1.3538156.
[71] Coran AY, Boustany K, Hamed P. Short-fiber – rubber composites: the properties of oriented cellulose-fiber – elastomer composites. Rubber Chem Technol. 1974;47(2):396–410. doi: 10.5254/1.3540449.
[72] Connor JE. Short-fiber-reinforced elastomer composites. Rubber Chem Technol. 1977;50:945–58.
[73] Huang J, Zou W, Luo Y, Wu QB, Lu X, Qu J. Phase morphology, rheological behavior, and mechanical properties of poly (lactic acid)/poly(butylene succinate)/hexamethylene diisocyanate reactive blends. ES Energy Environ. 2021;12:86–94.
[74] Pan D, Su F, Liu H, Liu C, Umar A, Castañeda L, et al. Research progress on catalytic pyrolysis and reuse of waste plastics and petroleum sludge. ES Mater Manuf. 2021;11(2):3–15.
[75] Sun D, Yan J, Ma X, Lan M, Wang Z, Cui S, et al. Tribological investigation of self-healing composites containing metal/polymer microcapsules. ES Mater Manuf. 2021;14:59–72.
[76] Prabhu P, Iqbal SM, Balaji A, Karthikeyan B. Experimental investigation of mechanical and machining parameters of hybrid nanoclay glass fiber-reinforced polyester composites. Adv Compos Hybrid Mater. 2019;2(1):93–101.
[77] Gopinath R, Poopathi R, Saravanakumar SS. Characterization and structural performance of hybrid fiber-reinforced composite deck panels. Adv Compos Hybrid Mater. 2019;2(1):115–24.
[78] Guo G, Finkenstadt VL, Nimmagadda Y. Mechanical properties and water absorption behavior of injection-molded wood fiber/carbon fiber high-density polyethylene hybrid composites. Adv Compos Hybrid Mater. 2019;2(4):690–700.
[79] Ma J, Li ZJ, Xue YZB, Liang XY, Tan ZJ, Tang B. Novel PEEK/nHA composites fabricated by hot-pressing of 3D braided PEEK matrix. Adv Compos Hybrid Mater. 2020;3:1–11.
[80] Mei H, Ali Z, Ali I, Cheng L. Tailoring strength and modulus by 3D printing different continuous fibers and filled structures into composites. Adv Compos Hybrid Mater. 2019;2(2):312–9.
[81] Pan D, Su F, Liu C, Guo Z. Research progress for plastic waste management and manufacture of value-added products. Adv Compos Hybrid Mater. 2020;3:1–19.
[82] Qin Y, Yu Q, Yin X, Zhou Y, Xu J, Wang L, et al. Photo-polymerized trifunctional acrylate resin/magnesium hydroxide fluids/cotton fabric composites with enhancing mechanical and moisture barrier properties. Adv Compos Hybrid Mater. 2019;2(2):320–9.
[83] Rudresh BM, Kumar BR, Madhu D. Combined effect of micro- and nano-fillers on mechanical, thermal, and morphological behavior of glass–carbon PA66/PTFE hybrid nano-composites. Adv Compos Hybrid Mater. 2019;2(1):176–88.
[84] Sengwa RJ, Choudhary S, Dhatarwal P. Investigation of alumina nanofiller impact on the structural and dielectric properties of PEO/PMMA blend matrix-based polymer nanocomposites. Adv Compos Hybrid Mater. 2019;2(1):162–75.
[85] Sun H, Fang Z, Li T, Lei F, Jiang F, Li D, et al. Enhanced mechanical and tribological performance of PA66 nanocomposites containing 2D layered α-zirconium phosphate nanoplatelets with different sizes. Adv Compos Hybrid Mater. 2019;2(3):407–22.
[86] Ashok RB, Srinivasa CV, Basavaraju B. Dynamic mechanical properties of natural fiber composites – a review. Adv Compos Hybrid Mater. 2019;2(4):586–607.
[87] Das TK, Ghosh P, Das NC. Preparation, development, outcomes, and application versatility of carbon fiber-based polymer composites: a review. Adv Compos Hybrid Mater. 2019;2:1–20.
[88] Xu D, Huang G, Guo L, et al. Enhancement of catalytic combustion and thermolysis for treating polyethylene plastic waste. Adv Compos Hybrid Mater. 2021;5:113–29. doi: 10.1007/s42114-021-00317-x.
[89] Liu C, Yin Q, Li X, et al. A waterborne polyurethane–based leather finishing agent with excellent room temperature self-healing properties and wear-resistance. Adv Compos Hybrid Mater. 2021;4:138–49. doi: 10.1007/s42114-021-00206-3.
[90] Etaati A, Pather S, Cardona F, Wang H. Injection molded noil hemp fiber composites: Interfacial shear strength, fiber strength, and aspect ratio. Polym Compos. 2014. doi: 10.1002/pc.23172.
[91] Kabir MM, Wang H, Lau KT, Cardona F. Chemical treatments on plant-based natural fiber reinforced polymer composites: an overview. Compos Part B Eng. 2012;43:2883–92. doi: 10.1016/j.compositesb.2012.04.053.
[92] Ku H, Wang H, Pattarachaiyakoop N, Trada M. A review on the tensile properties of natural fiber reinforced polymer composites. Compos Part B Eng. June 2011;42(4):856–73.
[93] Liu C, Zhang T, Luo Y, Wang Y, Li J, Ye T, et al. Multifunctional polyurethane sponge coatings with excellent flame retardant, antibacterial, compressible, and recyclable properties. Compos Part B Eng. 2021;215:108785.
[94] Lu T, Liu S, Jiang M, Xu X, Wang Y, Wang Z, et al. Effects of modifications of bamboo cellulose fibers on the improved mechanical properties of cellulose reinforced poly(lactic acid) composites. Compos Part B Eng. 2014;62:191–7. doi: 10.1016/j.compositesb.2014.02.030.
[95] Siakeng R, Jawaid M, Asim M, Saba N, Sanjay MR, Siengchin S, et al. Alkali treated coir/pineapple leaf fibers reinforced PLA hybrid composites: evaluation of mechanical, morphological, thermal and physical properties. eXPRESS Polym Lett. 2020;14:717–30. doi: 10.3144/expresspolymlett.2020.59.
[96] Ra S, Karayil J, Sanjay MR, Siengchin S, Parameswaran Pillai JK. A review on the extraction of pineapple, sisal and abaca fibers and their use as reinforcement in polymer matrix. eXPRESS Polym Lett. 2020;14:309–35. doi: 10.3144/expresspolymlett.2020.27.
[97] Sanjay MR, Siengchin S. Exploring the applicability of natural fibers for the development of biocomposites. eXPRESS Polym Lett. 2021;15:193. doi: 10.3144/expresspolymlett.2021.17.
[98] Sharma S, Patyal V, Sudhakara P, Singh J, Petru M, Ilyas RA. Mechanical, morphological, and fracture-deformation behavior of MWCNTs reinforced (Al-Cu-Mg-T351) alloy cast nanocomposites fabricated by optimized Mechanical milling and

Powder metallurgy techniques. Nanotechnol Rev. 2021;11:65–85. doi: 10.1515/ntrev-2022-0005.
[99] Chohan JS, Mittal N, Kumar R, et al. Optimization of FFF process parameters by naked mole-rat algorithms with enhanced exploration and exploitation capabilities. Polymers. 2021;13(11):1702.
[100] Ilyas RA, Sapuan SM, Asyraf MRM, et al. Polymer composites filled with metal derivatives: a review of flame retardants. Polymers. 2021;13(11):1701.
[101] Chohan JS, Mittal N, Kumar R, et al. Mechanical strength enhancement of 3D printed acrylonitrile butadiene styrene polymer components using neural network optimization algorithm. Polymers. 2020;12(10):2250.
[102] Singh Y, Singh J, Sharma S, Aggarwal V, Pruncu CI. Multi-objective optimization of kerf-taper and surface-roughness quality characteristics for cutting-operation on coir and carbon fiber reinforced epoxy hybrid polymeric composites during CO2-pulsed laser-cutting using RSM. Lasers Manuf Mater Process. 2021;8(2):157–82.
[103] Sharma S, Singh J, Kumar H, et al. Utilization of rapid prototyping technology for the fabrication of an orthopedic shoe inserts for foot pain reprieve using thermo-softening viscoelastic polymers: a novel experimental approach. Meas Control. 2020;53(3–4):519–30.
[104] Singh Y, Singh J, Sharma S, Sharma A, Chohan JS. Process parameter optimization in laser cutting of coir fiber reinforced epoxy composite – a review. Mater Today Proc. 2021;48:4738–44 (in press).
[105] Chohan JS, Kumar R, Singh TB, et al. Taguchi S/N and TOPSIS based optimization of fused deposition modelling and vapor finishing process for manufacturing of ABS plastic parts. Materials. 2020;13(22):5176.
[106] Prabhakaran S, Krishnaraj V, Sharma S, Senthilkumar M, Jegathishkumar R, Zitoune R. Experimental study on thermal and morphological analyses of green composite sandwich made of flax and agglomerated cork. J Therm Anal Calorim. 2020;139(5):3003–12.
[107] Sharma S, Sudhakara P, Singh J, Ilyas RA, Asyraf MRM, Razman MR. Critical review of biodegradable and bioactive polymer composites for bone tissue engineering and drug delivery applications. Polymers. 2021;13(16):2623.
[108] Sharma S, Sudhakara P, Omran AAB, Singh J, Ilyas RA. Recent trends and developments in conducting polymer nanocomposites for multifunctional applications. Polymers. 2021;13(17):2898.
[109] Jha K, Tyagi YK, Kumar R, et al. Assessment of dimensional stability, biodegradability, and fracture energy of bio-composites reinforced with novel pine cone. Polymers. 2021;13(19):3260.
[110] Kadier A, Ilyas RA, Huzaifah MRM, et al. Use of industrial wastes as sustainable nutrient sources for bacterial cellulose (BC) production: mechanism, advances, and future perspectives. Polymers. 2021;13(19):3365.
[111] Singh Y, Singh J, Sharma S, Lam T-D, Nguyen D-N. Fabrication and characterization of coir/carbon-fiber reinforced epoxy based hybrid composite for helmet shells and sports-good applications: influence of fiber surface modifications on the mechanical, thermal and morphological properties. J Mater Res Technol. 2020;9(6):15593–15603.
[112] Suriani MJ, Ilyas RA, Zuhri MYM, et al. Critical review of natural fiber reinforced hybrid composites: processing, properties, applications and cost. Polymers. 2021;13(20):3514.
[113] Kumar R, Ranjan N, Kumar V, et al. Characterization of friction stir-welded polylactic acid/aluminum composite primed through fused filament fabrication. J Mater Eng Perform. 2021;31:2391–409. doi: 10.1007/s11665-021-06329-4.
[114] Ilyas RA, Zuhri MYM, Norrrahim MNF, Misenan MSM, Jenol MA, Samsudin SA, et al. Natural fiber-reinforced polycaprolactone green and hybrid biocomposites for various advanced applications. Polymers. 2022;14(1):182. doi: 10.3390/polym14010182.
[115] Azlin MNM, Ilyas RA, Zuhri MYM, Sapuan SM, Harussani MM, Sharma S, et al. 3D printing and shaping polymers, composites, and nanocomposites: a review. Polymers. 2022;14(1):180. doi: 10.3390/polym14010180.
[116] Ilyas RA, Zuhri MYM, Aisyah HA, Asyraf MRM, Hassan SA, Zainudin ES, et al. Natural fiber-reinforced polylactic acid, polylactic acid blends and their composites for advanced applications. Polymers. 2022;14(1):202. doi: 10.3390/polym14010202.
[117] Kumar J, Singh D, Kalsi NS, Sharma S, Pruncu CI, Pimenov DY, et al. Comparative study on the mechanical, tribological, morphological and structural properties of vortex casting processed, Al-SiC-Cr hybrid metal matrix composites for high strength wear-resistant applications: Fabrication and characterizations. J Mater Res Technol. 2020;9(6):13607–15.
[118] Dwivedi SP, Saxena A, Sharma S. Influence of nano- CuO on synthesis and mechanical behavior of spent alumina catalyst and grinding sludge reinforced aluminum based composite. Int J Metalcasting. 2021;16:292–303. doi: 10.1007/s40962-021-00597-5.
[119] Muni RN, Singh J, Kumar V, Sharma S. Parametric optimization of rice husk ash, copper, magnesium reinforced aluminium matrix hybrid composite processed by EDM. ARPN J Eng Appl Sci. 2019;14(22):3832–9.
[120] Muni RN, Singh J, Kumar V, Sharma S. Influence of rice husk ash, Cu, Mg on the mechanical behavior of aluminium matrix hybrid composites. Int J Appl Eng Res. 2019;14(8):1828–34.
[121] Dwivedi SP, Saxena A, Sharma S, Srivastava AK, Maurya NK. Influence of SAC and eggshell addition in the physical, mechanical and thermal behavior of cr reinforced aluminium based composite. Int J Cast Met Res. 2021;34(1):43–55.
[122] Saxena A, Dwivedi SP, Dixit A, Sharma S, Srivastava AK, Maurya NK. Computational and experimental investigation on mechanical behavior of zirconia toughened alumina and nickel powder reinforced EN31 based composite material. Materialwissenschaft Werkstofftechnik. 2021;52(5):548–60.
[123] Sharma S, Singh J, Gupta MK, Mia M, Dwivedi SP, Saxena A, et al. Investigation on mechanical, tribological and microstructural properties of Al-Mg-Si-T6/SiC/muscovite-hybrid metal-matrix composites for high strength applications. J Mater Res Technol. 2021;12(21):1564–81.
[124] Dwivedi SP, Agrawal R, Sharma S. Effect of friction stir process parameters on mechanical properties of chrome containing leather waste reinforced aluminium based composite. Int J Precis Eng Manufacturing-Green Technol. 2021;8(3):935–43.

[125] Kumar J, Singh D, Kalsi NS, Sharma S, Mia J, Singh M, et al. Investigation on the mechanical, tribological, morphological and machinability behavior of stir-casted Al/SiC/Mo reinforced MMCs. J Mater Res Technol. 2021;12:930–46.
[126] Aggarwal V, Singh J, Sharma S, Sharma A, Singh G, Parshad J. Empirical modeling of machining parameters during WEDM of inconel 690 using response surface methodology. AIP Conf Proc. 2020;2281:020032. doi: 10.1063/5.0027284.
[127] Aggarwal V, Singh J, Sharma S, Harish K, Garg A, Sharma G, et al. An experimental study of wire breakage frequency on different electrodes during WEDM of Inconel-722. IOP Conf Ser: Mater Sci Eng. 2020;954:12013.
[128] Aggarwal V, Pruncu CI, Singh J, Sharma S, Pimenov DY. Empirical investigations during WEDM of Ni-27Cu-3.15Al-2Fe-1.5Mn based superalloy for high temperature corrosion resistance applications. Materials. 2020;13(16):3470.
[129] Qureshi MN, Sharma S, Singh J, Khadar SDA, Baig RU. Evaluation of surface roughness in the turning of mild steel under different cutting conditions using back propagation neural network. Proc Estonian Acad Sci. 2020;69:109–15.
[130] Islam S, Dwivedi SP, Dwivedi VK, Sharma S, Kozak D. Development of marble dust/waste PET based polymer composite material for environmental sustainability: fabrication and characterizations. J Mater Perform Charact. 2021;10(1):538–52.
[131] Ilyas RA, Sapuan SM, Asyraf MRM, Dayana DAZN, Amelia JJN, Rani MSA, et al. Polymer composites filled with metal derivatives: a review of flame retardants. Polymers. 2021;13:1701.
[132] Sharma S, Sudhakara P. Fabrication and optimization of hybrid AA-6082-T6 alloy/8%Al_2O_3(Alumina)/2%Grp metal matrix composites using novel Box-Behnken methodology processed by wire-sinking electric discharge machining. Mater Res Exp. 2019;6(11):1–16. doi: 10.1088/2053-1591/ab4b97.
[133] Singh H, Singh J, Sharma S, Dwivedi SP, Obaid AJ. Comparative performance of copper, graphite, brass and aluminium/graphite based different tool electrodes for optimizing the material removal rate during die-sinking EDM of stir-casted, Al6061/SiC MMCs for sustainable manufacturing and energy applications. J Green Eng. 2021;11(1):922–38.
[134] Dwivedi SP, Saxena A, Sharma S, Singh G, Singh J, Mia M, et al. Effect of ball-milling process parameters on mechanical properties of Al/Al_2O_3/collagen powder composite using statistical approach. J Mater Res Technol. 2021;15:2918–32. doi: 10.1016/j.jmrt.2021.09.082.
[135] Khare JM, Dahiya S, Gangil B, Ranakoti L, Sharma S, Huzaifah MRM, et al. Comparative analysis of erosive wear behavior of epoxy, polyester and vinyl esters based thermosetting polymer composites for human prosthetic applications using taguchi design. Polymers. 2021;13(20):3607. doi: 10.3390/polym13203607.
[136] Dwivedi SP, Maurya N, Sharma S. Study of CCLW, alumina and the mixture of alumina and CCLW reinforced aluminum based composite material with and without mechanical alloying. J Inst Eng (India): Ser D. 2021;13:1–16. doi: 10.1007/s40033-021-00312-y.
[137] Dwivedi SP, Sahu R, Saxena A, Dwivedi VK, Srinivas K, Sharma S. Recovery of Cr from chrome-containing leather waste and its utilization as reinforcement along with waste spent alumina catalyst and grinding sludge in AA 5052-based metal matrix composites. Part E: J Process Mech Eng. 2021:1–11. doi: 10.1177/09544089211038385.
[138] Dwivedi SP, Maurya M, Saxena A, Sharma S. Synthesis and characterization of spent alumina catalyst and grinding sludge reinforced aluminium based composite material. Part C J Mech Eng Sci. 2021;1–12. doi: 10.1177/09544062211061451.
[139] Dwivedi SP, Sharma S. Synthesis and characterization of Cr, eggshell and grinding sludge reinforced aluminum based metal matrix composites: an ingenious experimental approach. Green Mater (ICE Virtual). 2021;1–10. doi: 10.1680/jgrma.21.00035.
[140] Ilyas RA, Aisyah HA, Nordin AH, Ngadi N, Zuhri MYM, Asyraf MRM, et al. Natural-fiber-reinforced chitosan, chitosan blends and their nanocomposites for various advanced applications. Polymers. 2022;14:874. doi: 10.3390/polym14050874.
[141] Chandel PS, Tyagi YK, Jha K, Kumar R, Sharma S, Singh J, et al. Study of mode II interlaminar fracture toughness of laminated composites of glass and jute fibers in Epoxy for structural applications. Funct Compos Struct. 2021;3:044002. doi: 10.1088/2631-6331/ac376e.
[142] Yeswanth IVS, Jha K, Bhowmik S, Kumar R, Sharma S, Rushdan AI. Recent developments in RAM based MWCNT composite materials: a short review. Funct Compos Struct. 2022;1–9. doi: 10.1088/2631-6331/ac5730.
[143] Kumar R, Chohan JS, Singh S, Sharma S, Singh Y, Rajkumar S. Implementation of Taguchi and Genetic Algorithm techniques for prediction of optimal part dimensions for polymeric biocomposites in fused deposition modeling 2021. Int J Biomater (Hindawi-Wiley). 2022;2022:4541450. doi: 10.1155/2022/4541450.
[144] Kumar R, Chohan JS, Singh S, Sharma S, Babbar A, Singh J, et al. Investigations of process parameters of Plastic Jet Printing of polymeric biocomposites using Genetic Algorithm. Int J Mech Eng. 2022;7(2):230–7. https://kalaharijournals.com/ijme-vol7-issue-feb2022.php.
[145] Chohan JS, Kumar R, Singh S, Sharma S, Rajkumar S. Optimization and dimensional accuracy analysis using Genetic Algorithm of polymeric biocomposite parts fabricated by fused filament fabrication. Int J Mech Eng. 2022;7(2):238–45. https://kalaharijournals.com/ijme-vol7-issue-feb2022.php.
[146] Chohan JS, Kumar R, Singh S, Sharma S, Dwivedi SP, Rajkumar S. Dimensional accuracy analysis of Material extrusion Additive manufacturing process for polymeric biocomposites using Genetic Algorithm: A computational optimization approach. Int J Mech Eng. 2022;7(2):252–60. https://kalaharijournals.com/ijme-vol7-issue-feb2022.php.
[147] Kumar R, Ranjan N, Kumar V, Kumar R, Chohan JS, Piyush AY, et al. Characterization of friction-stir welded poly-lactic-acid/aluminium composite primed through fused filament fabrication. J Mater Eng Perform. 2021;31:2391–409. doi: 10.1007/s11665-021-06329-4.